ASSESSMENT OF AIRCRAFT EMISSIONS IMPACTS ON AIR QUALITY AT MULTIPLE MODEL SCALES

Lakshmi Pradeepa Vennam

A dissertation submitted to the faculty at the University of North Carolina at Chapel Hill in partial fulfillment of the requirements for the degree of Doctor of Philosophy in the Department of Environmental Sciences and Engineering in the Gillings School of Global Public Health.

Chapel Hill
2016

Approved by:

Saravanan Arunachalam

William Vizuete

Rohit Mathur

Jason West

Marc Serre

ABSTRACT

Lakshmi Pradeepa Vennam: Assessment of aircraft emissions impacts on air quality at multiple model scales
(Under the direction of Saravanan Arunachalam and William Vizuete)

Aviation activity has grown steadily, and will likely continue to grow in the future. Aviation-related air pollutants occurring during full-flight (landing and takeoff, as well as cruise) can impact air quality, human health and climate. The overall goal of this dissertation is to study the air quality impacts of aviation at local, regional and global scales. The central hypothesis of this study is that fine scale modeling provides better characterization of aviation emissions impacts on air quality and health. To test this hypothesis, a model-based assessment of aviation emissions impacts was conducted at multiple scales ranging from local (4×4 km^2) to hemispheric (108×108 km^2) scales.

Firstly, we focused on key risk-prioritized Hazardous Air Pollutants (HAPs) and assessed their impacts near a mid-sized U.S. airport using a chemistry-transport model at a fine scale (4×4 km^2). Overall modeled aircraft-attributable HAPs contributions are in the range of 0.5 – 28% near this airport. Second, we concentrated on the full-flight emissions impacts on air quality near surface for O_3 and $PM_{2.5}$ at a resolution of 108×108 km^2, spanning the Northern hemisphere (NH). Including full-flight aviation emissions at the hemispheric scale contributed 1.3% and 0.2% for O_3 and $PM_{2.5}$ at the surface on an annual domain-wide basis. Our comparison of these predictions with 36×36 km^2 application over North America highlighted that the coarse scale resolution was unable to capture non-linearities in chemical processes near airport locations and other major urban areas. Lastly, we conducted a tracer study to understand the role of dynamic

processes on cruise altitude aviation emissions (CAAE) impacts at the surface using a hemispheric scale application. Model predictions indicated that < 0.6% of CAAE tracer in the total atmospheric column was transported to the surface and ~40% was transported to mid-troposphere during all four seasons. This intercontinental tracer-tagging approach provided quantitative evidence that North America and Europe CAAE tracers can impact the surface (~0.5 – 1% of total column burden) near high terrain regions like Tibet Plateau and relatively lower aviation emissions regions such as Middle East, North Africa and South East Asia.

ACKNOWLEDGEMENTS

Firstly I am very grateful to my advisors: Dr. Saravanan Arunachalam and Dr. William Vizuete for their support, patience, cooperation throughout my PhD coursework and research. I owe my appreciation and deepest gratitude to them. My sincere thanks to Sarav for the financial support during all these years under Federal Aviation Administration project funding. I would also like to acknowledge my committee members for being in my committee and for their valuable suggestions.

A simple thanks is very less to my family and friends who gave enormous support throughout my graduate school. Without my Father (V. Naga Malleswara Rao), Mother (V. Padmavathi) and Sister (V.L. Praneetha), I wouldn't have been in this position today. My husband (P.V Ravi Kiran) has been my biggest support and immense strength throughout my graduate school (Masters and PhD) period since 2008 and motivated me from time to time. Since I got married last year (2015) my in-laws are very supportive and helped me focus on my research. Last but not the least my friends in Chapel Hill area are very friendly, helpful, supportive and gave me some social life during weekends.

I want to thank my IE lab mates: Matt, Changsy, and Scott for their wonderful company, more than lab mates they are like my brothers. We shared lot of technical discussions, programming skills and having them around made a huge difference in acquiring knowledge. I want to thank my colleagues at Institute for the Environment (Jeanne (retired), Frank, BH, Jiaoyan) and many others for sharing their expertise. I am also thankful to MAQ/CHAQ lab mates (especially Yuqiang, Yadong) for helping with plotting and analysis questions.

TABLE OF CONTENTS

LIST OF TABLES

LIST OF FIGURES

CHAPTER 1: INTRODUCTION

The association of air pollution to adverse human health has been well established from numerous studies (Lim et al., 2012; Caiazzo et al., 2013; Holliday et al., 2014), and assessing air quality impacts from various sources to develop policy action is needed to protect public health. State-of-art atmospheric modeling evolved as one essential tool to study air quality impacts and undertake measures to mitigate effects from various emission sources. It is also important to improve the modeling applications and evaluate them to better predict emission sources impacts. In recent years, transportation has become one of the major emission sectors contributing to ambient air pollution and health impacts throughout the world.

Aviation is the one of fastest transportation modes whose growth increased tremendously due to commercial travel, worldwide trade, and technology improvements in both developed and developing countries. Steady growth of 5% in passenger and 6% in freight transportation per year has been observed since 1950. It accounts for ~ 10% and 30% of passenger-km traveled and goods traded internationally (Schäfer and Waitz, 2014) in recent years. In future years, the average annual growth rate is predicted to increase around 4.6% per year from 2010 to 2030 (Federal Aviation Administration (FAA), 2010). Till last year, it was one of the single largest green house gas (GHG) emitting transportation sectors that was not subjected to U.S Environmental Protection Agency (EPA) GHG standards. This year both EPA (U.S EPA, 2016) and ICAO (ICAO, 2016) announced a CO_2 standard for new aircraft delivered after 2028; presently work is underway to develop a non-volatile particulate matter standard (Lobo et al.,

2016) for commercial aircraft. These recent regulatory standard implementations show the efforts undertaken by federal agencies to reduce the aircraft emissions impacts on air quality, human health and climate change. Therefore the major focus in this thesis is the aviation sector and to improve modeling of aviation emissions to better characterize their air quality impacts.

Wilkerson et al., (2010) indicated that in 2006, the commercial aircraft fleet flew 31.26 million flights covering 38.68 billion kilometers by burning 188.20 million metric tons of fuel, which contributes to 3% of current global annual fossil fuel usage. The Organization of Petroleum Exporting Countries (OPEC) (Mazraati, 2010) mentioned aviation as second major consumer with 11.2% of total oil demand in transportation sector and projected that fuel consumption will increase from 188 Tg in 2002 to 327 Tg in 2025 (Eyers et al., 2004). Efforts are already underway to use bio-fuels and low emission fuels for automobiles; however, application of these enhanced alternative fuels for aviation industry may present various challenges. There are several ongoing research activities both within and outside the U.S to address these issues. Measurement campaigns such as NASA's Alternative Aviation Fuel Experiment (AAFEX) showed reduction in particulate emissions (Beyersdorf et al., 2014), black carbon (Speth et al., 2015) due to alternative jet fuels and other synthetic jet fuels. Health impact assessments (Morita et al., 2014) concluded that alternative fuels and technology improvements could reduce mortality rate by 72% and 59% respectively when compared with 2050 reference scenario. In recent times, major technological modifications have been made to increase engine efficiency and to reduce fuel consumption, although the projected growth and associated environment impacts can offset those improvements (Masiol and Harrison, 2014). Particularly implementation of these technologies in developing countries in near future will be a key challenge due to limited resources. On the other hand, studies showed consistent (8%) increase in

Asia flight departures (Wasiuk et al., 2016) between 2005 – 2011 and expected to see 10% (Brunelle-Yeung et al., 2014) increase in growth particularly in countries like China and India. Therefore, this growth in aviation activity can implicate aircraft emissions to cause significant air quality, climate and health impacts in coming years worldwide. Aviation is also one of the anthropogenic emissions sources that can affect environment at local scale (air quality near airports, noise), regional scale (air pollution) and global scale (air pollution and climate change) (Schäfer and Waitz, 2014) as shown in Figure 1.1. The areas highlighted in orange color rectangle boxes are the ones related to air quality impacts, which are some of the key interests in this dissertation.

Like any other combustion source, aircraft emits various pollutants including Nitrogen oxides ($NO + NO_2 = NO_x$), Sulfur dioxides (SO_2), Carbon Monoxide (CO), Volatile Organic Compounds (VOC), Carbon dioxide (CO_2), Fine Particulate Matter ($PM_{2.5}$) (particulate matter of size less than 2.5 microns) and other unburnt hydrocarbon related pollutants (Hazardous Air Pollutants) during various stages of flight activity. These emissions are mainly categorized into landing-takeoff (LTO) and cruise altitude aviation emissions (CAAE) based on the engine thrust and flight path. The LTO is further divided into idling, taxing, approach and climb out stages. Different stages of flight path emit different pollutants, for example during idling, unburnt hydrocarbons and CO emissions are high, and during cruising stage NO_x emissions are higher. Dessens et al., (2014) mentioned that on a global scale, aviation NO_x emissions are about 10% of on-road (50% of total traffic) and 20% of shipping NO_x (30% of total traffic) emissions. In the U.S, aviation NO_x is three percent of the total transportation NO_x, but near some major airports like Atlanta (ATL) and New York (JFK) it can contribute ~3% and ~15% to area NO_x and non-road NO_x emissions respectively (Federal Aviation Administration, 2005). These emissions can

undergo various atmospheric transport and chemical changes by interacting with background emissions (from other non-aviation sources) locally near urban areas and in the upper troposphere. These pollutants can even perturb the greenhouse gases such as methane (CH_4) and ozone (O_3), thereby causing local-scale as well as global-scale air quality and climate impacts.

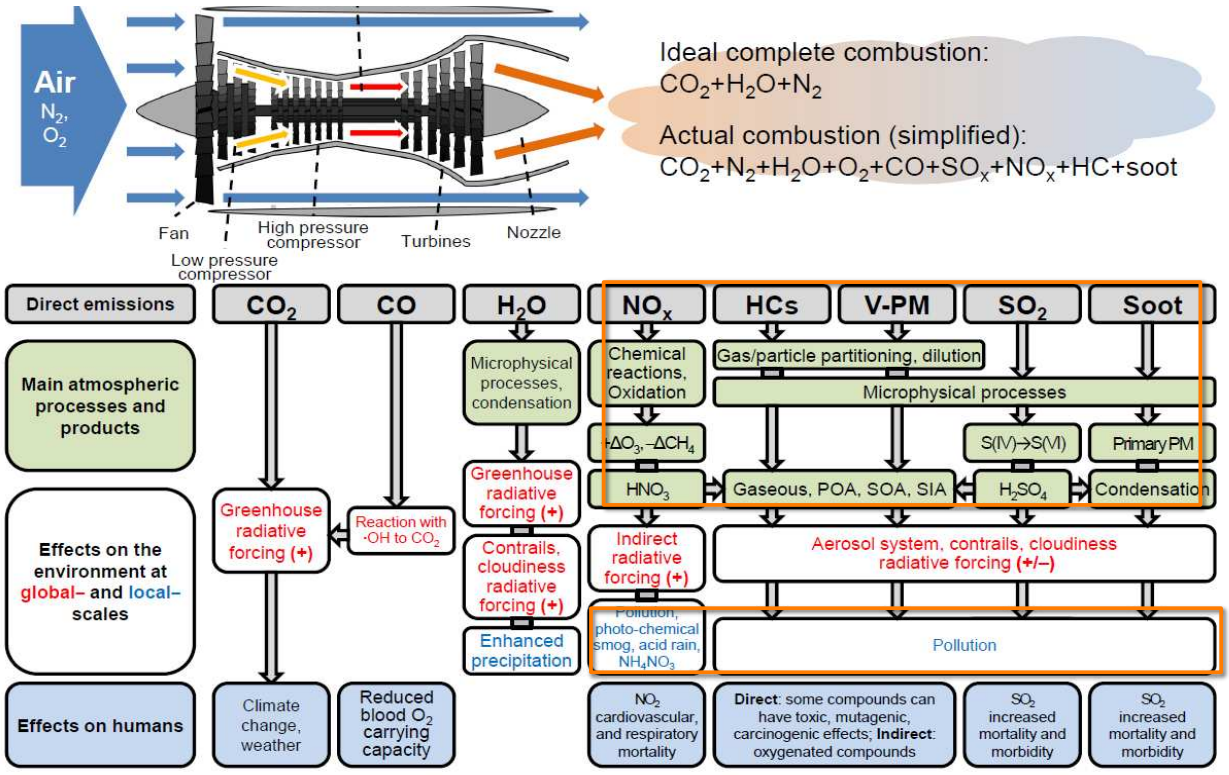

Figure 1.1: Aviation emissions and their environmental impacts (Source: Masiol and Harrison, 2014) and areas highlighted with orange boxes are some of the fields related to aviation air quality impacts.

Early measurement studies (Clark et al., 1983) observed violations of the health-based standards for CO and hydrocarbons (HC), that contributed significantly to the existed photochemical oxidant issues near the airport terminals and runways at some of the major airports. Since then many LTO aviation emissions based modeling studies (Unal et al., 2005; Arunachalam et al., 2011; Woody et al., 2011) and observational studies (Turgut and Rosen,

2010; Nikoleris et al., 2011; Zhu et al., 2011) focused on key pollutants (O_3, $PM_{2.5}$, NO_x , VOC) and their contribution in the vicinity of airports. These studies improved our understanding of air quality impacts from LTO aviation emissions and their sensitivities near urban and airport areas. As stated in Ratliff et al., 2009, almost ~150 airports in U.S are located near urban areas that are in non-attainment (i.e., areas that exceeded NAAQS (National Ambient Air Quality Standards)) for one or more criteria pollutants.

Based on model predicted LTO air quality impacts, Brunelle-Yeung et al., (2014) showed ~ 210 deaths per year in contiguous U.S with ~11 and 39 premature mortalities reductions due to desulfurization and NO_x stringency policy scenarios. Another future year US major airports (99 airports) risk analysis study (Levy et al., 2012) projected a factor of ~6 increase in 2025 mortality when compared to 2005 (~180 deaths per year) due to LTO emissions. Overall these studies indicated consistent air quality (O_3, $PM_{2.5}$, NO_x) and health impacts attributable to LTO aviation emissions for key pollutants. There is, however, no study on model assessment of Hazardous Air Pollutants (such as formaldehyde, acrolein and acetaldehyde) and their impacts near airports using a chemistry transport model. Research performed by Airport Cooperative Research Program (ACRP) (Wood et al., 2008; Herndon et al., 2012) stated the research gaps (such as emission inventories missing low thrust HAPs emissions, emissions dependency with ambient conditions) and ongoing monitoring efforts to study HAPs near airports. These reports also stressed the need for quantifying the aircraft impacts through HAPs modeling near airports. One other known gap was lack of detailed HAPs emissions estimates for aircraft. Therefore, EPA and FAA (FAA, 2009) recently developed an aircraft-specific speciation profile, which is one major update to generate airport-specific HAPs emissions.

Similarly, there are large uncertainties associated with full-flight and CAAE emissions modeled air quality assessments. Globally, CAAE emissions (particularly NO_x) are ~60 – 70% (Olsen et al., 2013) among the total full-flight emissions when compared to LTO emissions. These CAAE are not traditionally incorporated in regional scale modeling for studying air quality, but given the role of intercontinental transport, high convection and deep mixing in transporting pollutants from upper troposphere to surface (Wild and Akimoto, 2001; Parrish et al., 2004; West et al., 2009; Parrish et al., 2010) and vice versa, it is imperative to consider even upper troposphere emission sources in assessing surface air quality impacts of aviation emissions in their entirety. Allen et al., (2012) stated that natural emissions of NO_x from lightning can significantly increase upper tropospheric (20 ppbV) and surface (1.5 – 4.5 ppbV) ozone. Aviation is the only anthropogenic source that emits emissions directly into the upper troposphere, yet knowledge gaps still exists in assessing the magnitudes of CAAE impacts on surface air quality and their associated health impacts. Previous studies showed widely varying full-flight attributable health impacts estimates, ranging from ~ 405 (Morita et al., 2014) to ~ 12,600 (Barrett et al., 2010) premature mortality per year due to aviation-attributable particulate matter. Most of these studies used coupled climate (Jacobson et al., 2011; Morita et al., 2014) and chemistry transport (Barrett et al., 2010) global models with coarse resolutions ($4^o \times 5^o$, $2^o \times 2.5^o$) to arrive at their exposure estimates. This shows that high range of uncertainty is involved with health assessments related to CAAE, that perhaps could be improved through fine scale modeling for better characterization of air quality predictions as mentioned in Jacobson et al., (2011) and Yim et al., (2015). Despite these global models indicating higher mortality due to CAAE, very limited studies (Whitt et al., 2011) have focused on assessing the role of dynamic processes in transporting CAAE to surface and still remains as a process not well understood in

aviation air quality literature. Therefore in this study, for the first time, we have used fine scale model resolutions (108 × 108 km^2, 36 × 36 km^2) to quantify contributions of full-flight emissions on air quality at northern hemispheric and regional scales. We also studied the role of transport processes on CAAE at hemispheric scale.

Overall goal of this thesis dissertation is to study the aviation-attributable perturbations that impact air quality at local, regional and global scales. The central hypothesis of this dissertation is that fine scale modeling provides better characterization (spatial heterogeneity and temporal variability) of aviation emissions impacts on air quality and health. To test this hypothesis, we conducted a model-based assessment of aviation emissions impacts using U.S EPA's Community Multi-scale Air Quality (CMAQ) (Byun and Schere, 2006) modeling framework at multiple scales ranging from local (4 × 4 km^2) to hemispheric (108 × 108 km^2) scale. We used these enhanced modeling applications to address the uncertainties present in three main study areas: aviation-related HAPs, full-flight emissions impacts and transport of cruise altitude emissions to the surface. Investigating these areas will enhance our scientific understanding in modeling aircraft emissions for assessing their impacts on surface air quality, and likely provide an enhanced scientific basis for improved policy-making. The main objectives of the three study areas are:

1. Estimate impacts of risk prioritized aviation-related HAPs near mid-sized airport due to LTO emissions and discuss the model's ability to predict HAPs near an airport at different model resolutions (4 × 4 km^2, 36 × 36 km^2). Improve the model performance by modifying aircraft HAPs emissions during idling, and assess the aviation-attributable HAPs impacts (Chapter 2).

2. Quantify the full-flight (CAAE + LTO emissions) impacts on surface air quality and on overall troposphere at hemispheric scale using the CMAQ model. Compare coarse and fine resolution North America predictions and quantify the changes occurring in aviation-attribution perturbations due to grid resolution (Chapter 3).

3. Assess the transport of cruise altitude emissions to surface at hemispheric scale by using passive tracer based modeling. Additionally, tag the CAAE tracers in individual sub-regions to study the intercontinental transport of aviation emissions and develop source-receptor relationships (Chapter 4).

Finally in Chapter 5, the final conclusions from all three studies were discussed along with the limitations. The future work to further improve the understanding of aviation-related air quality impacts was also highlighted in this chapter.

CHAPTER 2: EVALUATION OF MODEL-PREDICTED HAZARDOUS AIR POLLUTANTS NEAR A MID-SIZED U.S. AIRPORT[1]

2.1 Introduction

Aviation has experienced proliferative growth in the past few decades. Commercial aviation operations are rapidly increasing worldwide, with a growth rate of 61, 40, and 22 percent in large, medium, and small hub airports (FAA, 2011). The average annual growth rate is predicted to increase around 4.6 percent from 2010 to 2030 (FAA, 2010). These quantitative projections clearly indicate substantial aviation growth in future. This growth implicates potential increase in aircraft emitted pollutants such as Nitrogen oxides (NO_x), Sulfur oxides (SO_x), Particulate matter (PM), and Volatile Organic Compounds (VOC) including Hazardous Air Pollutants (HAPs). Thus, there is a need to characterize impact of aviation emissions on local air quality particularly in the vicinity of an airport as a first step to assess their impacts on the environment and human health. Further, stringent emission standards on road transport (US EPA, 2014) will likely increase the relative contributions from aviation emissions that impact local air quality.

Although significant research has been undertaken quantifying the impact of $PM_{2.5}$, NO_x and O_3 near airports, there has been little focus on exposure assessment for HAPs. Airport-related air-quality studies have focused mainly on NO_x (Wood et al., 2008; Timko et al., 2010), $PM_{2.5}$ (Mazaheri et al., 2009) and CO due to their relatively higher contribution to the overall

[1] This chapter previously appeared as an article in *Atmospheric Environment*. The original citation is as follows: Vennam, L. P., Vizuete, W., & Arunachalam, S. (2015). Evaluation of model-predicted hazardous air pollutants (HAPs) near a mid-sized US airport. *Atmospheric Environment*, *119*, 107-117.

airport-related emissions (Schürmann et al., 2007). These studies measured emissions during landing and takeoff conditions (LTO) and showed that these pollutants have significant impact on air quality near the airport. Air-quality modeling studies have reported maximum impacts of O_3 and $PM_{2.5}$ of 56 ppbV and 25 $\mu g/m^3$ near Hartsfield-Jackson airport in Atlanta (Unal et al., 2005). Arunachalam et al., (2011) showed that the LTO emissions could have 28-35% of impacts in $PM_{2.5}$ occurring 300km away from the airport due to secondary formation. Woody et al., (2011) reported that the other background emissions (from non-aviation sources) can have an important role on the aviation-attributable impacts and the $PM_{2.5}$ impacts in the airport grid-cell is approximately twice the national average. These studies show that airport emissions have a significant impact on air quality near airports and suggest that there could be significant exposures of other emitted pollutants like HAPs.

HAPs are a listing of 187 pollutants that are known or suspected to cause serious health effects specifically categorized in the 1990 Clean Air Act (CAA, Section 112). Recent studies (Laurent and Hauschild, 2014) suggested that carcinogenic pollutants like HAPs have not been controlled sufficient enough to protect public health. They reported that some of the key HAPs such as formaldehyde and acrolein contributed only 6% and 0.2% of total NMVOCs (non-methane volatile organic compounds), but account for 90% cancer effects and 89% non-cancer effects respectively. The higher health risk pertaining to HAPs and their chemically reactive nature in the atmosphere calls for more attention in local scale air-quality studies. Prior aviation studies (Herndon et al., 2012) indicated that 15 of the 187 identified HAPs are observed in aircraft exhaust. An aircraft-attributable health study (Levy et al., 2008) found that significant local health effects such as cancer and cardiopulmonary risks were caused from air toxics in spite of their relative low contribution (5–10%) to total aviation emissions. However, they ranked

HAPs as lower in priority compared to both $PM_{2.5}$ and O_3 due to aircraft emissions. Studies have found that when compared to LTO operations there were 80 – 90% higher emissions during idling-taxing, emitting several HAPs including: formaldehyde, acetaldehyde, benzene, ethylene, propene and butenes + acrolein (Anderson et al., 2006; Herndon et al., 2006). Spicer et al., (1996) also reported that these seven pollutants make up ~75% of the volatile organic compound (VOC) emissions that are being detected in aircraft exhaust. According to the Airport System Performance Metrics database (ASPM, FAA), the average taxi time at mid-sized to large-sized airports is reported in the range of 10 – 20 minutes, which is significant amount of time to emit HAPs.

Though idle and taxi activities have the potential to impact air quality near airports, limited studies exist with detailed model-based characterization of HAP emissions. With such limited knowledge of aviation HAPs airport authorities are unable to provide effective guidance to state and local constituencies. One known gap is the lack of detailed HAPs emissions estimates from aircraft during LTO operations. In this study we have attempted to reduce these uncertainties by using new FAA-EPA generated aircraft-specific speciation profiles (FAA, 2009) for Total Organic Gases (TOGs) that estimate individual HAPs and differentiating emissions by aircraft operating modes. To evaluate this model and current HAP modeling approaches we took advantage of field observational data available at the T.F. Green airport (PVD) in Providence, Rhode Island. The detailed modeling and evaluation performed in this study provides an assessment of the tools that help airport regulatory authorities in making any decisions and regulators to evaluate air quality and potential health risk associated with the HAPs in the vicinity of an airport.

2.2 Methodology

We focused on eight major aviation health-risk prioritized (Levy et al., 2008) HAPs: formaldehyde, acetaldehyde, acrolein, 1,3-butadiene, benzene, toluene, xylene and naphthalene. Based on their toxicity levels, (Wood et al., 2008) also ranked these HAPs as important near-airport exposure pollutants.

2.2.1 Air Quality Model (CMAQ)

We used the Community Multi-scale Air-Quality (CMAQ) (Byun and Schere, 2006) model to evaluate the changes in HAPs emissions, as well as their impacts on ambient air quality. Table 2.1 shows the model scenarios description and domain specifications considered in this study. Figure 2.1 shows both 36 × 36 km^2 and 4 × 4 km^2 horizontal resolution model domains whose model results for year 2005 were used for this evaluation.

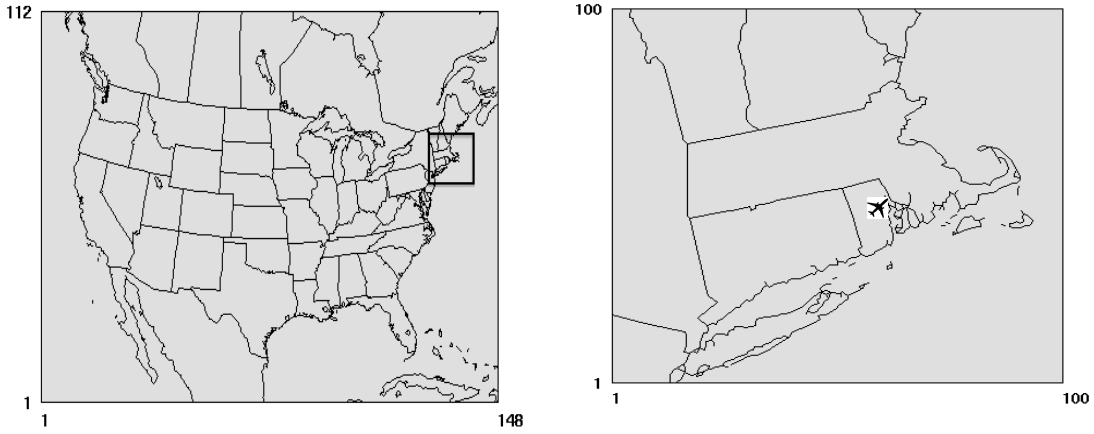

Figure 2.1: 36 × 36 km^2 Continental US domain (left, with black square showing the 4 × 4 km^2 model domain) and 4 × 4 km^2 northeast US (right) domain with location of PVD airport (black aircraft icon).

The CMAQ 4 × 4 km^2 scale resolution simulations were conducted in the Northeast U.S. for 2005 annual year with 100 x 100 horizontal grid cells as shown in Figure 2.1 (black square, left side). Emissions from all sources go up to 22 vertical layers (~ 680 hPa) and aircraft emissions go up to 17 layers (~ 850 hPa, Figure A1) to represent the LTO cycles within the

lowest ~1000 meters (3000 ft). The T.F. Green airport (PVD) in Providence, Rhode Island is labeled in Figure 2.1 with an aircraft icon. CMAQ v5.0.2 model with revised Carbon Bond (CB05) multi-pollutant mechanism (Yarwood et al., 2005; Whitten et al., 2010; CMAS, 2014) and explicit air toxics chemistry (CB05TUMP_AE6_AQ) was used for the model simulations. The meteorology input data (34 layers, ~130 hPa, Figure A1) were generated using the Mesoscale Meteorological (MM5 v3.7.2) model (Grell et al., 1994). We used 2005 National Emissions Inventory (NEI) (U.S EPA, 2007) to generate emissions for non-aviation sources, which were processed using Sparse Matrix Operator Kernel Emissions (SMOKE) model (Houyoux et al., 2000) to generate grid-based emissions that are speciated and temporally allocated. The initial and boundary conditions are nested from 12 × 12 km^2 CMAQ simulations for the Eastern U.S.

Table 2.1: Specifications and description of modeling scenarios in the study

Scenario name	Period	Grid Cell Resolution	Domain	CMAQ version	Background emissions	Aviation emissions
Base_36km	01/01/05 - 12/31/05	36 × 36 km^2	CONUS[a]	4.6	NEI[b]-2005	No
Sensairp_36km	01/01/05 - 12/31/05	36 × 36 km^2	CONUS	4.6	NEI-2005	EDMS[c] emissions (99 major airports)
Base_4km	01/01/05 - 12/31/05	4 × 4 km^2	Northeast US	5.0.1	NEI-2005	No
Sensairp_4km	01/01/05 - 12/31/05	4 × 4 km^2	Northeast US	5.0.1	NEI-2005	AEDT[d] emissions for PVD[e] airport
Sensairp_4km_4perc	07/01/05-08/31/05 & 11/01/05-12/31/05	4 × 4 km^2	Northeast US	5.0.1	NEI-2005	AEDT emissions for PVD airport with modified 4% thrust setting

a) CONUS: Continental United States, b) NEI: National Emissions Inventory, c) EDMS: Emissions Dispersion Modeling System, d) AEDT: Aviation Environmental Design tool e) PVD: T.F.Green airport, RI

In this study, the aviation emissions were based on FAA's Aviation Environmental Design Tool (AEDT) (Wilkerson et al., 2010) segment data. This tool predicts emissions and

aircraft fuel use for all global commercial flights. From this highly resolved emissions inventory, we selected flights arriving and departing from the PVD airport and processed them through AEDTProc (Baek et al., 2012) . AEDTProc is a processing tool that takes chorded segments of individual flight emissions and then creates CMAQ model-ready emissions inputs that were then merged with the other non-aircraft emissions inventories. Speciated HAPs emissions were estimated in AEDTProc using Total Organic Gases (TOG) speciation profile (FAA, 2009). This speciation profile (Table A1) for aircraft engines was established by FAA and U.S. EPA based on APEX (FAA, 2009) and EXCAVATE (Anderson et al., 2006) airport measurement campaigns.

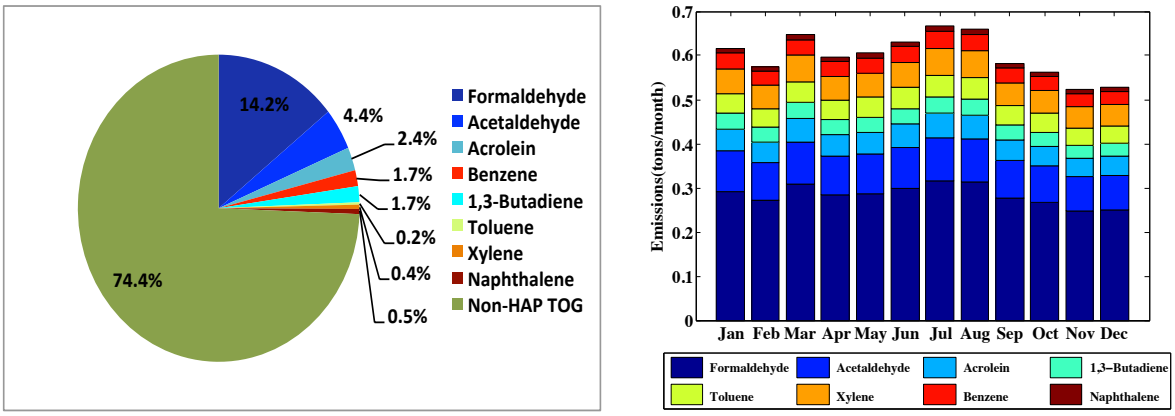

Figure 2.2: Pie chart representing the percentage contribution from HAPs to annual airport TOG emissions in the sensairp_4km case (left) and monthly airport emissions in the airport grid-cell (right).

For annual 2005, a total of 6.12 short tons of key HAPs were emitted by aircraft representing 10% of total anthropogenic sources HAPs in the PVD grid cell. The pie chart in Figure 2.2 (left) illustrates the composition of those emissions. NON-HAP TOG, defined as VOCs other than HAPs is the largest contributor to TOG, and is further speciated into lumped chemical species based upon the CB05 chemical mechanism. Formaldehyde, acetaldehyde, and

acrolein are key contributors (14.2%, 4.4%, 2.4%) to the annual aircraft HAPs emissions. Note that AEDT does not include emissions from ground supporting equipment (GSE), ground auxiliary vehicles (GAV) and stationary sources (Supp. Material Section2, Table A5). Figure 2.2 (right) shows the monthly total aircraft emissions of HAPs and shows the lack of any seasonal trend i.e., higher emissions during lower temperatures (during winter months, emission index is ~3.5 times higher at 0° C compared to 25° C) as mentioned in observation based studies (i.e., no (Herndon et al., 2012) temperature dependency in the emission inventory).

Finally we merged non-aviation emissions (background sources) with aviation emissions to generate emissions input for Sensairp_4km case. Two annual model simulation scenarios named, Base_4km and Sensairp_4km, are shown in Table 2.1. The difference in output between these two cases accounts for the incremental aviation emissions contribution to ambient air quality.

For this study we also completed an alternate emissions scenario (Sensairp_4km_4perc in Table 2.1) to assess sensitivity due to increased taxi/idle condition hydrocarbon emissions based on the findings from previous aircraft measurement studies (Herndon et al., 2006; Beyersdorf et al., 2012) . These observational studies indicated that the observed hydrocarbon emissions indices (g/kg) are a factor of ~1.5–2.2 times greater than the International Civil Aviation Organization (ICAO) specified certification benchmarks that are typically used to construct aircraft emissions inventories. Therefore, we considered the latest 2005 AEDT emissions, and modified the idle hydrocarbon emissions near PVD airport using the idling time spent by each flight and extrapolated 4% emission index (HC_EI_4perc) from the ICAO database for different engines (detailed methodology in supplementary section A1.1.2). These changes resulted in

doubling of aircraft LTO emissions at PVD when compared with sensairp_4km. However, compositional profile of emitted HAPs and the lack of seasonal pattern remained the same.

As shown in Table 2.1, we performed this sensitivity model simulation for 4 months (July–August (summer), November–December (winter)) to create the Sensairp_4km_4perc (background + 4% thrust airport emissions) case. Therefore, the difference between Sensairp_4km_4perc and Base_4km cases gives us the incremental aviation contributions with the improved idle emissions.

2.2.2 Observational Data

Availability of near-airport field-based measurements of HAPs at PVD provided us the opportunity for detailed model evaluations. These included measurements of HAPs completed by the Rhode Island Department of Environmental Management (RIDEM) in and around the PVD airport. In the RIDEM study campaign, sampling was conducted at five monitor sites near the airport for the period April 2005 to August 2006. Four of these sites (Fieldview, Firestation, Lydick, Smith) are located near the airport and one site (Draper) is located 2.3 miles from the main runway (RIDEM, 2008). The Fieldview site is ideally located near the main runway where 86% of airplane activity at PVD occurs (Dodson et al., 2009). All three sites Fieldview, Firestation and Lydick fall in the PVD airport 4×4 km^2 grid-cell in our modeling domain. Along with the five RIDEM sites near the airport, we used four additional sites from EPA's Air Quality System (AQS) to understand the relative difference in airport-attributable concentrations between urban, rural and airport sites. Figure 2.3 shows the spatial location of AQS sites (red symbols) and RIDEM sites (blue symbols). Table A3 gives the description of these sites.

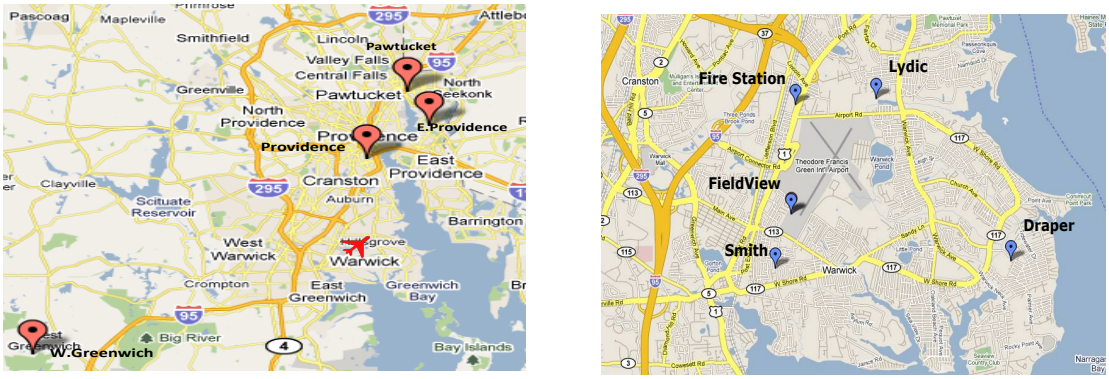

Figure 2.3: AQS monitoring sites (left, red pointers) with location of PVD airport (red aircraft icon) and RIDEM monitoring sites (right, blue pointers) around the airport (Courtesy: Google map).

We also compared model predictions against observations from the National Air Toxics Trends Stations (NATTS, (US EPA, 2009)) (Supp. Material Section A3.2). Figure A5 shows the U.S. map with red aircraft symbols indicating the 99 airports and blue pointers indicating the collocated NATTS sites near the airports for year 2005. Table A4 shows the location of NATTS sites and major airports in CMAQ model grid cells.

2.2.3 HAPs estimates from NATA

CMAQ predicted annual average concentrations were compared with annual estimates from the National Air Toxics Assessment (NATA) (US EPA, 2011). NATA is a state-of-the-science screening tool developed by U.S. EPA in collaboration with state and local agencies, to evaluate the health risks involved with air toxics both at regional and local level. NATA outputs are at census-block resolution for the entire nation. For these estimates, NATA used a combination of predictions from the AERMOD dispersion model for primary and CMAQ (using 12×12 km^2 resolution) for the secondary contribution of formaldehyde, acetaldehyde, and acrolein. The recent 2005 NATA annual modeling data were obtained from updated emissions inventory that considered airport emissions from 20,000 U.S. airports (US EPA, 2011).

2.3 Results

In this section, we organize our results into 3 major sub-sections – model evaluation against observations, comparison of model predictions from two different resolutions, and finally comparison against another published source. First we show the model evaluation for 4×4 km^2 applications against 4×4 km^2 observational data and discuss the trends in aircraft contributions in the airport grid-cell. We then compare 4×4 km^2 model performance with 36×36 km^2 and discuss differences observed between the two resolutions. Later we present the aircraft emission sensitivity results and the increase in aircraft-attributable concentrations due to the modified idle aircraft emissions. Finally we compare our CMAQ model results with those from EPA's NATA to understand the differences between these two model predictions.

2.3.1 Model Evaluation: 4×4 km^2 grid resolution

The sensairp_4km simulation's ability to predict concentrations accurately varies by pollutant and spatial location as shown by the overall Normalized Mean Error (NME) and Normalized Mean Bias (NMB) in Table 2.2. From Table 2.2 (top panel), the NME averaged for all sites is between 36–70% for all pollutants except for acrolein (NME: ~90%). Acrolein shows the largest NME of ~90% regardless of site location. This high underprediction of acrolein has been observed in prior studies. For example, (Luecken et al., 2006) pointed the uncertainties in emissions and highly challenging acrolein sampling (Seaman et al., 2009) as a source of observational difficulty. A recent study (Cahill, 2014) also measured acrolein background concentrations that were higher than the EPA's reference concentrations (for health risk), but due to sparse data they were unable to come to a definite conclusion on acrolein exceedances and their ambient levels.

Table 2.2 shows that NME was higher for the AQS sites when compared to RIDEM sites; 36% higher for xylene and 23% higher for toluene. Consistent with the NME results the model overpredicted (NMB: 24–41%) concentrations of xylene, toluene and benzene at all sites with the W. Greenwich and E. Providence AQS sites (Figure A3) showing the largest overpredictions. These errors for xylene and toluene are mainly driven by the W. Greenwich AQS site (Figure 2.3) at a rural location 33 km from the airport. This AQS site had a NME of 100-200% consistently throughout the year for xylene and toluene.

The RIDEM sites had a higher NME for formaldehyde (11%) and 1,3-butadiene (7%) when compared to the AQS sites. As shown in Table 2.2 (bottom panel) the formaldehyde NMB is -52% at RIDEM sites and -31% at AQS sites. The largest underprediction of formaldehyde was at the Fieldview RIDEM site with a NMB of -60%. Spatially (Figure A2), observations show ~1.5 times higher concentrations near Fieldview (3.93 $\mu g/m^3$) when compared to all other sites. The model-predicted period average of 1.44 $\mu g/m^3$ was far below the observed high concentrations at the Fieldview site.

To understand the contribution that the new highly resolved aircraft emissions had on HAP model performance we re-ran the simulation without aircraft emissions (base_4km). The NME and NMB values from base_4km are shown in Table 2.2 inside parenthesis. From Table 2.2 it is clear that aircraft emissions had an impact of less than 0.1% on model error at the AQS sites. The largest changes in model prediction from aircraft emissions occurred at the RIDEM sites where additional aircraft emissions improved the NME for formaldehyde (1%) and xylene (2.3%). It is clear from NMB that additional formaldehyde emissions reduced the underprediction by 1.1%. The increased aviation emissions had the largest impact on NMB and NME at the Fieldview, Lydick, and Firestation airport sites. At the RIDEM sites the additional

aircraft emissions did increase the NME in the case of 1,3-butadiene (4.6%), benzene (0.4%) and toluene (0.1%). The model was already overpredicting these species, so the addition of aircraft emissions caused the model to increase overprediction for these species.

Table 2.2: Annual NME (%, top) and NMB (%, bottom) using pollutant predictions from the sensairp_4km averaged for all sites and differentiating RIDEM and AQS sites. Also shown in parenthesis are the base_4km case (with no airport emissions) values.

Pollutant	All sites	RIDEM	AQS
	NME	NME	NME
Acrolein	91.6 (91.6)	92.4 (92.4)	92 (92)
Formaldehyde	49.1 (49.8)	52.4 (53.3)	41 (40.9)
Acetaldehyde	33.6 (33.6)	33.1 (33.1)	34.8 (34.8)
1,3-Butadiene	57.6 (57.5)	60.5 (57.9)	53.9 (53.8)
Xylene	69.1 (70.5)	55.3 (55.3)	89.6 (89.6)
Benzene	58 (57.5)	58.5 (58.1)	57.2 (57.1)
Toluene	71.7 (71.6)	61.7 (61.6)	84.2 (84.2)

Pollutant	All sites	RIDEM	AQS
	NMB	NMB	NMB
Acrolein	-91.6 (-91.6)	-92.4 (-92.4)	-91.7 (-91.7)
Formaldehyde	-45.6 (-46.4)	-51.5(-52.6)	-31.0(-31.0)
Acetaldehyde	-7.1 (-7.6)	1.1 (0.3)	-27.6(-27.6)
1,3-Butadiene	-2.3(-5.6)	9.0(3.1)	-16.4(-16.6)
Xylene	24.4(28.7)	17.6(17.4)	42.8(42.8)
Benzene	30.2(29.8)	31.9(31.2)	28.1(28)
Toluene	41.2(41.1)	28.5(28.4)	57.0(57.0)

From the model performance data it is clear that aviation emissions only impacted HAP concentrations at monitors that were within 1–2 km from the airport. Thus, our analysis focused on the contributions of HAPs from the newly added emissions in just the PVD airport grid-cell (which contains RIDEM monitors Fieldview, Lydick and Fire Station). In supplementary document, in Figures A4a-c and Table A8 we showed the spatial concentrations plots and the

contributions of the aircraft-attributable for January and July months, which are in the range of 0.5–28% in the airport grid-cell. Figure 2.4 shows the monthly averaged increases in concentrations of airport-related HAPs (sensairp_4km minus base_4km, bottom) and total concentrations from all sources (sensairp_4km, top) in the airport grid-cell. Though aviation emissions of HAPs were relatively constant throughout the year, the contributions of HAPs concentrations were higher during winter months than summer months due to their shorter lifetime in the atmosphere during summer than winter.

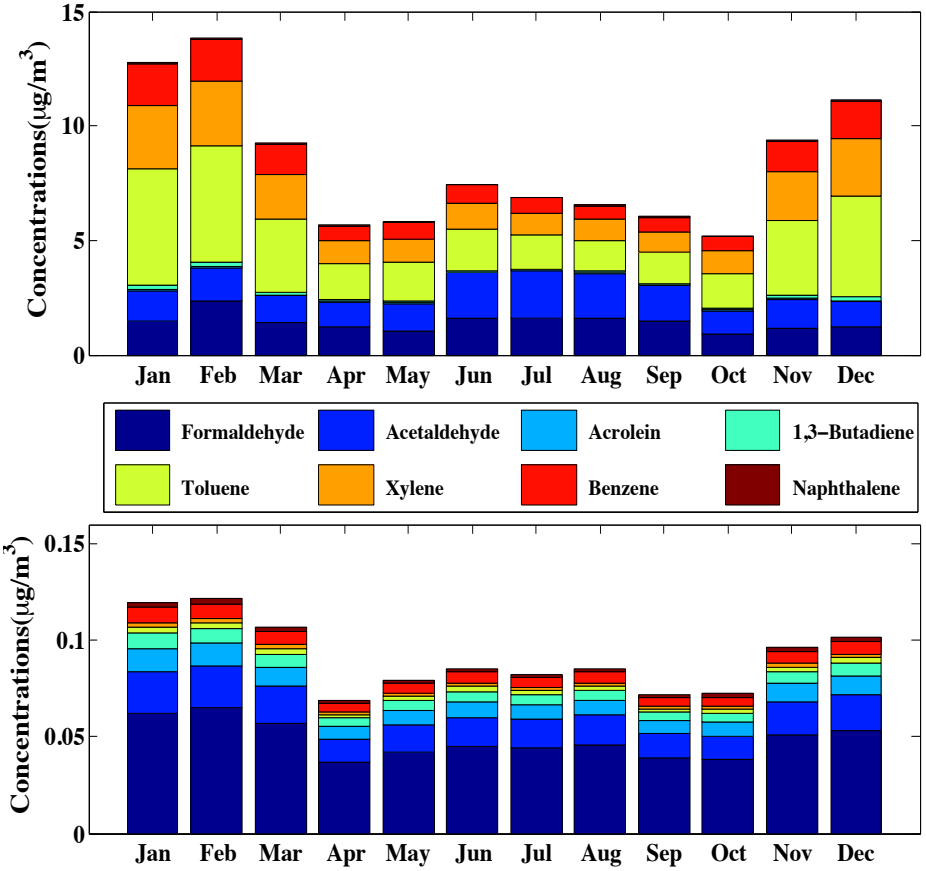

Figure 2.4: Monthly average all source (sensairp_4km) (top) and airport-attributable (sensairp_4km minus base_4km) (bottom) concentrations in the PVD airport 4×4km grid-cell.

Figure 2.5 shows the time series of observed and modeled (sensairp_4km) formaldehyde concentrations near RIDEM sites (not included Draper due to fewer hours of observation

available) for the RIDEM study campaign period. The model was able to capture the temporal variability near all sites, although it is clear that the concentrations are underpredicted. The underprediction is high mainly near Fieldview runway site where the highest formaldehyde concentrations were predicted. The model was also unable to predict the largest observed peaks during the summer months.

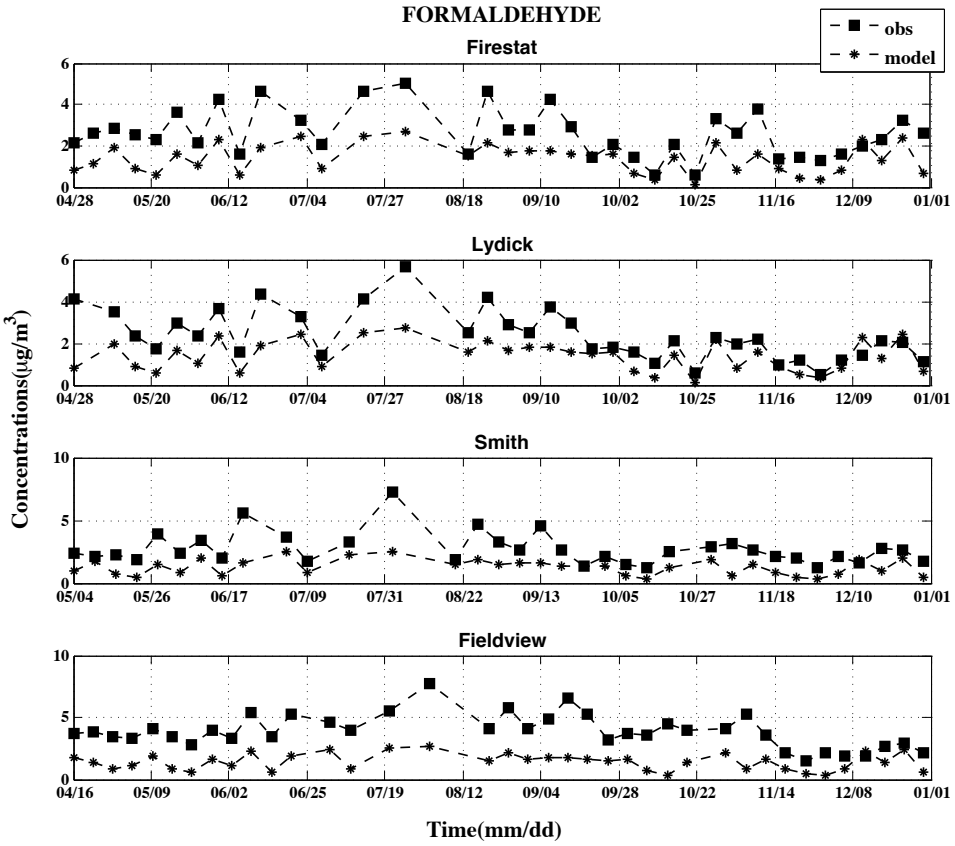

Figure 2.5: Time-series of modeled and observed formaldehyde daily average concentrations at RIDEM sites.

To understand the primary (directly emitted) and secondary (formed due to atmospheric chemistry) contribution to total formaldehyde in the airport grid-cell we looked at these concentrations separately. In this simulation of CMAQ, the formaldehyde emissions were reported explicitly as primary formaldehyde (FORM_PRIM) and tracked separately from total formaldehyde, which also includes secondarily produced formaldehyde via VOC oxidation.

Thus, from the total predicted formaldehyde (FORM) concentrations we subtracted primary (FORM_PRIM) to obtain the secondary concentration (FORM_SEC).

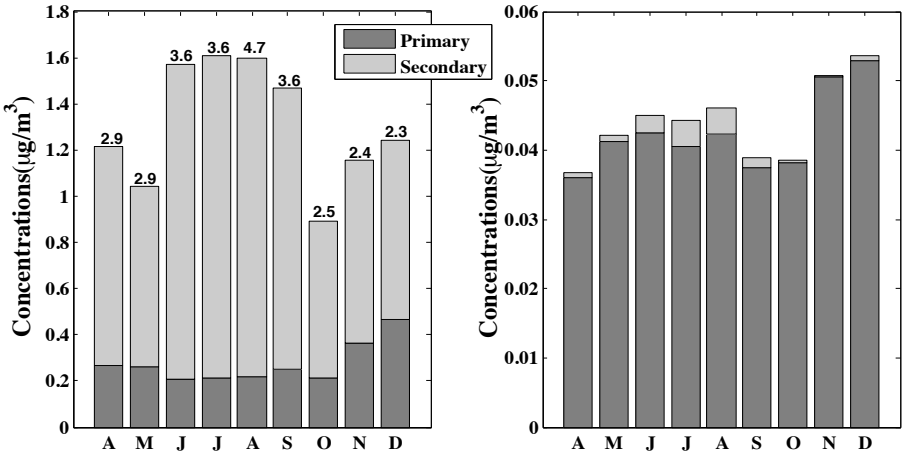

Figure 2.6: Secondary and Primary Formaldehyde monthly averaged concentrations from all sources (left) and airport-attributable (right) in the PVD airport grid-cell from April to December 2005. Also shown as labels on each bar plot in the left figure are monthly averaged observational data from three RIDEM sites (Fieldview, Lydick, Firestation) that fall in the PVD 4 × 4 km^2 grid cell.

In Figure 2.6, the monthly average concentrations of formaldehyde are reported at the PVD 4 × 4 km^2 grid cell along with the primary and secondary contribution. In the PVD airport grid-cell, nearly 50 – 85% of the FORM in the grid cell is secondary (Figure 2.6, left side). It is clear that any additional primary formaldehyde would have only a minimal impact on total formaldehyde concentrations. All the numbers shown as a label on each bar plot on the left are the averaged observed values in the PVD grid cell, and these are ~1.5 – 2 times higher than the model predictions. Further, the additional 50% of primary formaldehyde emissions from aircraft source in the airport grid-cell is insufficient to match observed concentrations near the airport. Also shown is the airport-attributable contribution (Figure 2.6, right side) in the PVD airport grid-cell; here 90% is from primary formaldehyde with only 8 – 9% secondary contributions limited to summer months. However, we also observed that the secondary components of

formaldehyde, acetaldehyde and acrolein contribute 3 – 20% to total PVD-attributable concentrations in the surrounding grid cells (16 – 20 km).

Formaldehyde is one of the most highly reactive HAP where 80 – 90% of the concentrations in the atmosphere occur due to secondary formation from VOCs such as methane, isoprene and other alkenes. Prior studies (Simon et al., 2010; Luecken et al., 2012) have reported uncertainties in both emissions and chemistry of VOC precursors, which can introduce bias in formaldehyde and acetaldehyde predictions.

2.3.2 Comparison of 4×4 km^2 with 36×36 km^2

In this section, we compared 36×36 km^2 and 4×4 km^2 model performance near PVD airport to quantify the differences between coarse and fine resolution model predictions. Table 2.3 shows the model performance of 36×36 km^2 (sensairp_36km) and 4×4 km^2 (sensairp_4km) model predictions near RIDEM and AQS sites. The overall U.S. wide HAPs (sensairp_36km) model evaluation with NATTS observational data (only sites collocated near an airport) is included in the supplementary material (Figure A5 and A6). It is also important to note that emission inventories were developed differently for sensairp_36km and the sensairp_4km simulations. Table A7 shows up to 30% differences in emissions of HAPs at the PVD grid cell for all pollutants except for toluene. For toluene, we observed a ~75% difference due to not including auxiliary and ground equipment sources emissions in the sensairp_4km simulation. Thus, toluene was not included in this analysis.

When compared with sensairp_36km, the sensairp_4km simulation shows a reduction in NME when averaged across all RIDEM and AQS sites: acrolein (2%), formaldehyde (6%), and acetaldehyde (1.5%). There was an increase in NME of 4.8% for 1,3-butadiene, 4.1% for xylene, and 15.8% for benzene. Due to the domain-wide change in grid resolution, the NME and NMB

for both RIDEM and AQS sites were impacted. For the AQS sites, the higher resolution reduced NME for all pollutants by up to 8% for formaldehyde and acetaldehyde. The exception was benzene where NME increased by 10% driven by higher overpredictions. The RIDEM sites also showed increases in NME for benzene, xylene, acetaldehyde, and 1,3-butadiene. For these pollutants the increased grid cell resolution caused increases in predictions as shown by higher NMB. For 1,3-butadiene, acetaldehyde, xylene this caused underpredictions to become overpredictions. For formaldehyde (5%) and acrolein (2%) alone, the NME was lower with a 4 × 4 km^2 resolution.

Table 2.3: Annual NME (%, top panel) and NMB (%, bottom panel) from all sources at (36 × 36 km^2) and (4 × 4 km^2) cases at all sites and differentiating between RIDEM and AQS sites

Pollutant	All sites		RIDEM		AQS	
	36-km	4-km	36-km	4-km	36-km	4-km
Acrolein	93.6	91.6	94.2	92.4	92.8	92
Formaldehyde	55.0	49.1	57.3	52.4	49.3	41.0
1,3-Butadiene	52.8	57.6	47.5	60.5	59.5	53.9
Acetaldehyde	34.8	33.6	31.6	33.1	42.9	34.8
Xylene	65.0	69.1	42.4	53.0	93.3	89.6
Benzene	42.2	58.0	38.1	58.5	47.2	57.2

Pollutant	All sites		RIDEM		AQS	
	36-km	4-km	36-km	4-km	36-km	4-km
Acrolein	-93.5	-91.6	-94.2	-92.4	-92.6	-91.7
Formaldehyde	-54.2	-45.6	-57.3	-51.5	-46.4	-31.0
1,3-Butadiene	-36.6	-2.3	-30.0	9.0	-44.8	-16.5
Acetaldehyde	-22.4	-7.1	-15.6	1.1	-39.3	-27.6
Xylene	1.4	24.4	-13.5	12.6	20.0	39.2
Benzene	5.2	30.2	6.8	31.9	3.3	28.1

The Fieldview site is closest to the airport and serves as an assessment of near-airport exposures. Figure 2.7 presents the NMB from different domain resolutions at Fieldview site. In the case of 1,3-butadiene and xylene, 4 × 4 km^2 showed slight overprediction whereas 36 × 36

km^2 showed an underprediction. Overall the model performance improved in right direction, but slightly overpredicted in 4 × 4 km^2. In the case of acetaldehyde and formaldehyde, corresponding improvements by 20% and 5% respectively were observed in the 4 × 4 km^2 model predictions when compared with 36 × 36 km^2.

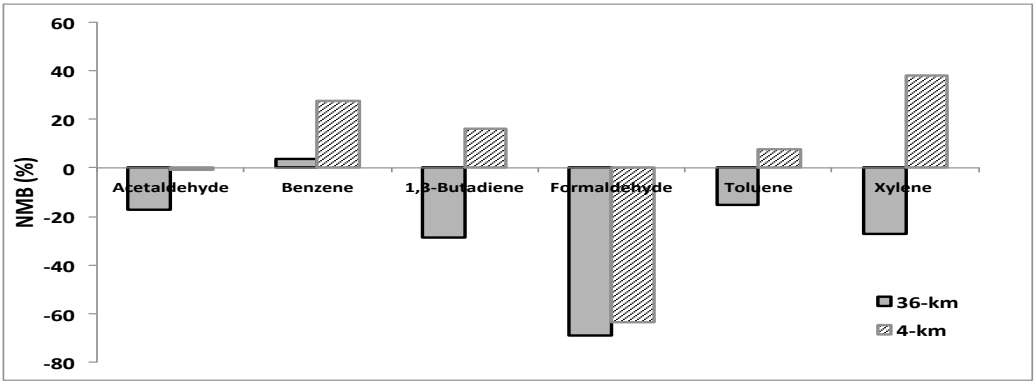

Figure 2.7: Comparison between sensairp_36km and sensairp_4km model scenarios normalized mean bias (%) at the Fieldview site.

2.3.3 Sensitivity of Aircraft emissions

The sensairp_4km simulation with aircraft emissions still underpredicts the HAPs concentrations near the airport. The characterization of aircraft emissions could be modified by considering lower thrust (4%) during idle conditions, which are usually not included in the emission inventory. As described in section 2.1.1 aircraft emissions were increased and model simulations were completed for four months (July–August and November–December) including summer and winter season. Model evaluation of this increased emission case (sensairp_4km_4perc) was compared with the standard 7% thrust emissions case (sensairp_4km). This change will impact formaldehyde the most since it is the dominant unburned hydrocarbon emitted during taxing and idling. Therefore, we showed only formaldehyde results here.

Table 2.4: Difference in NME [sensairp_4km (NME) minus sensairp_4km_4perc (NME)] at the RIDEM sites for four months.

	July	August	November	December
Firestation	1.30	1.65	2.93	2.75
Fieldview	0.91	0.85	1.91	2.84
Lydick	1.61	1.30	3.96	4.10
Smith	0.32	0.41	0.44	0.83

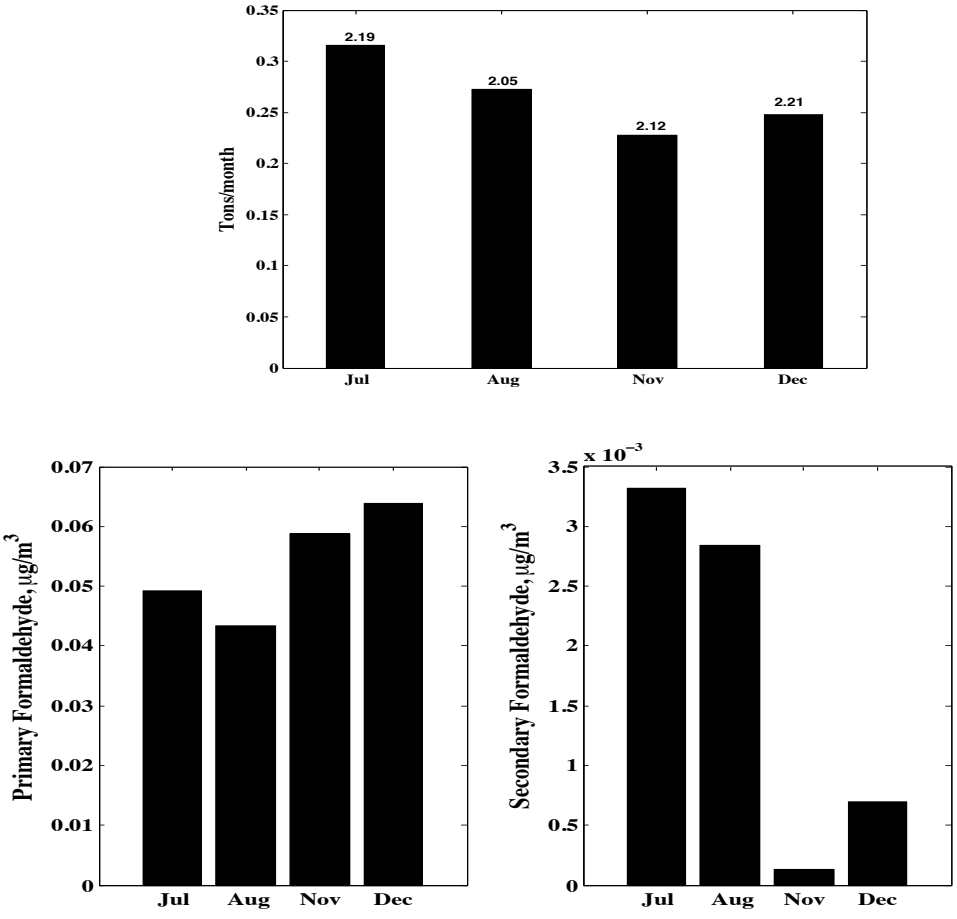

Figure 2.8: Top panel shows bar plot of formaldehyde aircraft emissions differences at the PVD airport grid-cell between sensairp_4km_4perc and sensairp_4km simulations with their fractional increase value shown as label on top of each bar. Bottom panel shows the primary (left) and secondary formaldehyde (right) aircraft attributable increases in the sensairp_4km_4perc simulation when compared with sensairp_4km.

In Figure 2.8 (top panel) we compared 4% (sensairp_4km_4perc) thrust emissions and 7% (sensairp_4km) thrust idle emissions near PVD airport. The 4% emissions are double that of the 7%, and show an increase of 0.25–0.3 tons/month for all four months considered. This increase is comparable to the findings from observational studies. With these updated emissions we show in Table 2.4 an improvement of 0.5 – 4% in NME at the RIDEM sites in the case of formaldehyde. At the AQS sites however (which are located further downwind from the airport), there was no change in model performance with updated emissions. The largest change in NMB (2 – 4%) is observed at the Firestation and Lydick sites followed by the Fieldview site (NMB: 0.8 – 1%). We also observed that the model improvement is higher (2%) during winter months than summer months in this sensitivity case suggesting the transport of primary formaldehyde (Figure 2.8, bottom) to downwind sites.

Figure 2.8 (bottom panel) also shows the increase of formaldehyde concentrations at the PVD airport grid-cell as a result of the additional emissions. The primary formaldehyde (left plot) increase (0.06 – 0.07 $\mu g/m^3$) was higher during winter months and the secondary formaldehyde (right plot) increase (0.0030 – 0.0035 $\mu g/m^3$) was higher during summer months. Overall the total formaldehyde (primary + secondary) airport concentrations increased by 2 – 2.5 times due to the increased emissions.

Though we doubled airport emissions of formaldehyde, we did not observe a significant increase in model performance. Even by increasing the aircraft emissions by a factor of 10, we only observed a 10 – 20% reduction in NME for formaldehyde predictions. As having such high aircraft emissions near a mid-sized airport like PVD is unrealistic, we suspect other uncertainties in the modeling system such as chemistry, meteorology, and other emission sources (not aircraft-related) require further investigation.

2.3.4 Comparison of 4×4 km^2 with NATA estimates

Currently, if a risk assessment of airport HAPs is conducted regulators could rely on the NATA assessment tool for their concentration estimates. The NATA estimates are only given as mean annual concentrations at a census tract level. Further, NATA does not report a mean annual concentration for the PVD airport census tract (Fieldview site in Figure A7) and we assume it could be likely due to no population living in the tract (FIPS code: 4400309800). Despite these shortcomings this would be the tool likely used by policy-makers to assess the health impacts from the PVD airport.

The observational data provided by the RIDEM and AQS sites were used to evaluate HAP concentrations predicted by both NATA and CMAQ (sensairp_4km) simulation. The CMAQ predictions and observational data were averaged over the period of April – December 2005. Based on these values we calculated NME and NMB shown in Table 2.5. We did not include acrolein due to sparse observational data. When looking at all sites, CMAQ shows an improvement of NME of 7.4% for 1,3-butadiene reducing bias by ~23%. The bulk of this improvement occurred at the RIDEM sites where NATA shows a NMB of -24.1% and CMAQ only a 6.7%. NATA is showing a better performance for all other pollutants with a maximum improvement of NME for all sites of up to 15% for toluene. In the case of formaldehyde, NATA model predicted higher concentrations reducing NMB for RIDEM sites by 9%. These increased concentrations of formaldehyde could be also partly due to the small double counting in NATA for non-point sources, where the secondary formation from dispersion model (simple secondary formation calculated) was not removed after including secondary formation from CMAQ (EPA, 2011). This could be compensating for part of the model underprediction. We also believe that

the census tract scale dispersion modeling predicted some of the primary concentrations much better than the 4 × 4 km^2 CMAQ, and thus reduced the NME.

Table 2.5: Comparison of CMAQ (sensairp_4km) and NATA model with NME (%, top panel) and NMB (%, bottom panel) values for all sites and differentiating RIDEM, AQS sites.

	All sites		RIDEM		AQS	
	NATA	**CMAQ**	**NATA**	**CMAQ**	**NATA**	**CMAQ**
Acetaldehyde	12.5	15.9	6.1	10.0	25.2	27.6
1,3- Butadiene	27.9	20.5	24.1	13.4	32.9	29.9
Xylene	24.6	26.4	19.1	21.1	31.9	33.4
Toluene	13.7	30.3	13.6	33.0	13.9	26.7
Benzene	17.4	31.3	14.5	32.2	21.3	30.0
Formaldehyde	33.8	42.7	39.4	48.5	22.6	31.0

	All sites		RIDEM		AQS	
	NATA	**CMAQ**	**NATA**	**CMAQ**	**NATA**	**CMAQ**
Acetaldehyde	-8.5	-10.7	-0.2	-2.3	-25.2	-27.6
1,3- Butadiene	-27.9	-4.4	-24.1	6.7	-32.9	-19.2
Xylene	-15.0	8.8	-10.9	21.1	-20.4	-7.6
Toluene	6.6	24.7	2.6	33.0	11.9	13.7
Benzene	12.6	25.6	9.0	32.2	17.4	16.8
Formaldehyde	-33.8	-42.7	-39.4	-48.5	-22.8	-31.0

Figure 2.9 shows box and whisker plots of observational data and hourly averaged CMAQ predictions at Smith and Providence sites. From Figure 2.9 we see that CMAQ predicted mean values, 25th, 75th quartiles (box lower and upper end) and interquartile range (1.5* IQR, whiskers) are within the ±10 –20% range of observational data, except for formaldehyde. Also shown in Figure 2.9 are the NATA predicted annual concentrations (star symbol) as overlay at Smith, Providence census tracts. In the case of formaldehyde, CMAQ predicted minimum and maximum concentrations of 0.28 – 2.56 μg/m^3 and 0.4 – 2.98 μg/m^3 near Smith and Providence, whereas NATA shows a mean concentration of 1.54 μg/m^3 and 1.76 μg/m^3. The NATA annual

mean concentrations are close to both CMAQ and observed mean values, but it is clear that NATA is reporting aggregate time-averaged information (missing many of the peak concentrations at shorter time-scales that are masked by presenting annual averages).

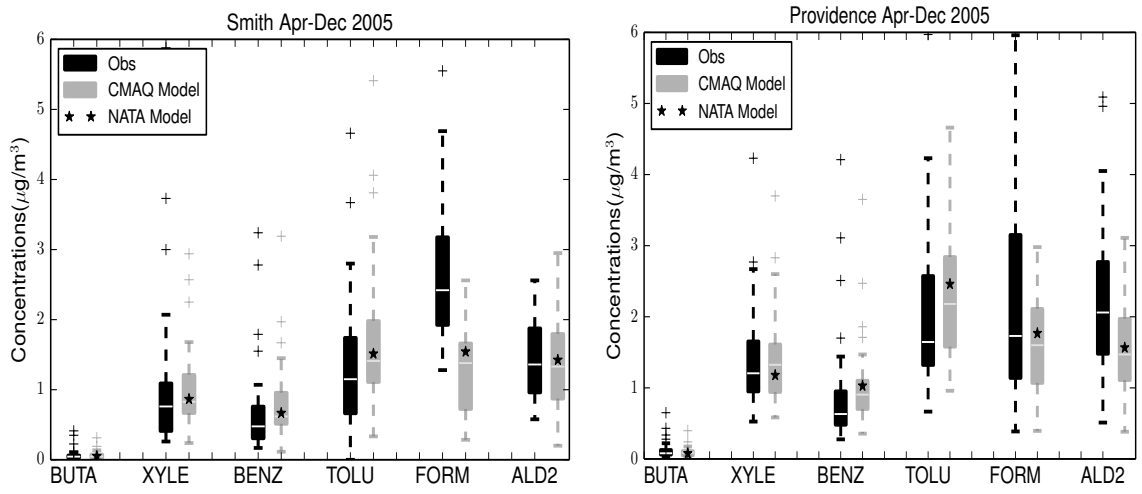

Figure 2.9: Box plots comparison of CMAQ data with observation data for April–December 2005 with an overlay of NATA census tract annual value (star symbol) near one RIDEM (Smith) and one AQS (Providence) site.

2.4 Future work and conclusions

In the future, additional efforts towards increased HAPs observations campaigns and evaluation of updated models ((CMAS, 2015), chemistry updates) are necessary. Combining both temporally and spatially highly resolved model predictions and available observational data could be a better direction to obtain HAPs concentrations near localized source for health assessment purposes in near future. Advanced techniques such as Bayesian Maximum Entropy (Nazelle et al., 2010) need to be tested for this kind of application. Prior studies (Friedfeld et al., 2002) already integrated regression models with time series data to predict the primary and secondary HAPs. Further investigation of the secondary formation chemistry for key air toxics in the atmosphere and its implementation in the models is crucial.

In this study, we completed a CMAQ model-based characterization of HAPs near a mid-sized U.S. airport (T.F. Green airport, Providence, Rhode Island). The simulations included a 4 × 4 km^2 grid resolution with a higher fidelity aircraft emissions inventory and evaluated with highly spatially resolved observational data collected near the T.F. Green airport. The 4 × 4 km^2 model had a NME for acrolein of 90% and for all HAPs species within the range of 36–70%. The addition of aircraft emissions improved predictions mainly near the airport monitors. Our model results indicated airport contributions to HAPs concentrations in the airport grid-cell vary from 2 – 4% in the case of formaldehyde to 19 – 28% in the case of acrolein. The inclusion of highly resolved (both spatially and temporally) aircraft emissions only made incremental improvements to model performance. The use of a 4 × 4 km^2 versus a 36 × 36 km^2 grid cell resolution improved model performance by 20% stressing the importance of a finer resolution grid. A doubling of aircraft formaldehyde emissions (including 4% thrust) only decreased NME by 1 – 4% and increasing emissions 10-fold showed only 10 – 20% reduction. As increasing primary emissions showed only a nominal improvement in model performance and the underprediction still exists, we attribute this to model underpredicting secondary formaldehyde.

Current HAPs estimates from NATA had similar poor performance near the airport. Comparison of CMAQ (4 × 4 km^2) and NATA estimates showed that their mean concentrations were similar to each other. By reporting annual averages, NATA is ignoring some of the peak concentrations, as we observed a standard deviation in the range of 0.6 – 1.8 from the mean value in our CMAQ predictions.

Overall the current modeling systems have poor model performance in regards to predicting HAPs at the PVD airport. The addition of a finer highly temporally resolved aircraft emissions estimate showed only incremental improvements in performance. The poor

performance suggests other uncertainties in the modeling system such as meteorology, HAP chemistry, or other emission sources require increased scrutiny. Better characterizations of aircraft emission inventory such as incorporating low thrust emissions during idle and temperature dependency could improve model predictions and health assessments near larger airports.

2.5 Acknowledgements

This work was funded by the Federal Aviation Administration through grants under the Partnership for AiR Transportation Noise & Emissions Reduction (PARTNER) (http://partner.mit.edu). PARTNER is a FAA/NASA/Transport Canada/US DOD/EPA-sponsored Center of Excellence. The emissions inventories used for this work were provided by U.S. Department of Transportation's Volpe Center. Any opinions, finding, and conclusions or recommendations expressed in this material are those of the author(s) and do not necessarily reflect the views of the sponsors. We also thank Mohan Gupta and Chris Sequeira of FAA for helpful discussions in the design of this study. We gratefully acknowledge Barbara Morin of RIDEM for providing the PVD observations used in this study. We would also like to acknowledge Bok Haeng Baek of UNC Institute for the Environment for developing the AEDTProc tool and Matthew C. Woody of UNC Institute for the Environment for providing 4% thrust emissions MATLAB code.

Supporting Information

Further details regarding HAPs speciation profile, parameterizations considered in CMAQ modeling, low thrust aircraft emissions sensitivity method, emission analysis, spatial plots showing concentrations, 4×4 km^2 model evaluation, 36×36 km^2 U.S wide NATTs model evaluation and NATA comparison can be found Appendix A supporting information.

CHAPTER 3: MODELED FULL-FLIGHT AIRCRAFT EMISSIONS IMPACTS ON AIR QUALITY AND THEIR SENSITIVITY TO GRID RESOLUTION

3.1 Introduction

In the atmospheric and air quality community, we have a better understanding of the chemical and physical processes occurring in the troposphere and stratosphere. Only limited knowledge is available, however, concerning the chemistry and transport of pollutants at the boundary of the upper troposphere and lower stratosphere (UTLS) (Barbara J. Finlayson-Pitts and James N. Pitts Jr, 2000). The physical and chemical properties of the UTLS and mid-troposphere are different than the surface and pollutants found there have the potential for a global intercontinental impact on surface air quality. For example, oxides of nitrogen (NO_x) have a lifetime of 1-2 weeks in the UTLS, compared with just a few hours when present in the troposphere (Jaegle, 2007). Thus, UTLS pollutants are subject to intercontinental transport (ICT) (Stohl, 2002) due to the strong winds and synoptic flow (Holloway et al., 2003). Recently, increased focus has been devoted to study intercontinental transport (Reidmiller et al., 2009; Leibensperger et al., 2011), its impact on human mortality (West et al., 2009; Anenberg et al., 2009) and interaction of UTLS with the troposphere (Jaffe et al., 1999; Jacob et al., 1999; C. Lin et al., 2000; J. Lin et al., 2014). Yet, model predictions disagree (Henderson et al., 2011; Zyryanov et al., 2012) with observations in the upper troposphere region. Studies (Allen et al., 2012) have highlighted the lack of emission sources in the UTLS region leading to uncertainties in model predictions. One important and less studied emissions are those generated by aviation. This rapidly growing transportation sector is a critical anthropogenic emission source in the upper troposphere. Globally 92.5% of aviation fuel is burned in the northern hemisphere and

74.6% of it is burned at cruise altitudes (Wilkerson et al., 2010; Olsen et al., 2013) near the UTLS region. These full-flight emissions are also categorized into Landing and Takeoff emissions (LTO, emissions occurring < 1km) and cruise altitude aviation emissions (CAAE, emissions occurring > 1km).

Though aviation contributes ~3% of total anthropogenic NO_x emission sources (Wauben et al., 1997), majority is directly released in UTLS and their surface impacts can be higher due to intercontinental transport (Leibensperger et al., 2011). Few studies have attempted to quantify the contribution of this pollution source on atmospheric processes in the UTLS and surface air quality. An earlier study (Beck et al., 1992) used a two-dimensional longitude and height model to assess the impact from civil aircraft emissions, and found that aircraft emissions can increase NOx concentrations by 40% (20 pptV) and O_3 by 16% (8 – 10 ppbV) near cruise altitudes (9 – 12 km). Later studies (Wauben et al., 1997; Kentarchos et al., 2002; Gauss et al., 2006) saw slightly higher perturbations by using 3-D chemistry transport model. Gauss et al., (2006) predicted that near the tropopause aircraft emissions increased zonal (30–60N) mean odd reactive nitrogen (NO_y = NO_x+PAN+HNO_3+other nitrogen related pollutants) by 156 – 322 pptV and O_3 mixing ratios by 3.1 – 7.7 ppbV during different seasons in the Northern Hemisphere. Kohler et al., (2007) investigated the sensitivity to aircraft NO_x emissions as a function of location, altitude and emission perturbation magnitude. The authors emphasized that the aviation NO_x emissions at altitudes 11 – 15 km plays a crucial role in changing O_3 concentrations and predicted a 6 ppbV maximum increase in zonal annual mean O_3. These early studies predominantly focused on ozone and NO_x perturbations due to aviation emissions in the upper troposphere. These studies, however, relied on global models with coarser resolution (such as 5.6° × 5.6°) and used older emission inventories such as AERO2k and Abatement of Nuisance

Caused by Air Traffic/European Commission (ANCAT/EC) (Gardner et al., 1997). These inventories can differ in spatial and temporal resolution when compared with the most recent emission inventories developed by the Aviation Environmental Design Tool (AEDT) (Wilkerson et al., 2010). The AEDT has greater utilization of actual radar tracking and highly resolved emissions distribution (Olsen et al., 2013). Therefore assessing aviation perturbations with most recent emission inventories and updated models is important to improve scientific understanding of aviation environmental impacts with increasing growth in aviation sector.

In recent years, efforts to study the surface air quality impacts due to the full-flight aircraft emissions that include both CAAE and LTO aircraft emissions have increased due to their potential impact on human health. This major concern arose as Barrett et al., (2010) predicted globally ~8000 premature mortality attributable to cruise altitude emissions, which motivated researchers to understand the chemical and physical processes responsible for surface impacts associated with cruise emissions. A tracer-based study with no chemistry and only transport and wet deposition processes (Whitt et al., 2011) using the GATOR-GCMOM model (Jacobson et al., 2011) was conducted to study the transport of cruise emissions. This study found that the time-scale for vertical mixing is longer than the lifetime of the tracer and emphasized that the surface air quality is unlikely to be affected from cruise emissions solely due to transport. Later, Lee et al., (2013) approached this question differently and relied on predictions from the full chemistry-transport CAM-Chem model (Lamarque et al., 2012) and found aviation-induced perturbations of O_3 and NO_y are less than 1 ppb. In addition, they mentioned that these perturbations can have negligible effect on the surface air quality when compared with other anthropogenic source impacts and also showed that ground-level aviation impacts from cruise-level emissions are higher than LTO emissions. These results are further

supported by Jacobson et al., (2011), where an one-way nesting chemistry-transport model was used with a sub-grid processes and found that aircraft emissions increased O_3, PAN, and temperature near the surface by ~0.4%, ~0.1%, ~0.01K and in the upper troposphere by ~ 2.5%, ~5% and ~0.03K.

These prior studies analyzing aviation-attributable predicted concentrations utilizes global model operating on relatively coarse horizontal resolutions of 4° × 5° (Barrett et al., 2010), 4° × 5° (Jacobson et al., 2011), and 2° × 2.5° (Lee et al., 2013). Recent studies (Ma et al., 2014; Ma et al., 2015) found that finer horizontal resolution in global models can improve physical and chemical interactions (such as aerosol-cloud interactions) in model predictions and reduced model bias by a factor of 5 in black carbon concentrations and aerosol predictions. The authors also stated that finer resolution model predictions agree better with observations. Additionally, these global models (Yan et al., 2016) can underrepresent some of the non-linearities in O_3 changes, emissions contrasts between urban and rural locations, and vertical transport due to coarser resolution. To address these differences in scale researchers have recently (Yim et al., 2015) quantified aviation impacts using a combination of global, regional, and dispersion models. Their results indicated that near–airport population exposure to aviation-attributable $PM_{2.5}$ is higher (factor of ~ 3.2) than global average exposure at near 23% of all major airports. The authors also indicated that by including different nested regional model in a global model, the aviation-attributable ground level O_3 increased by 12% and $PM_{2.5}$ decreased by 29%. Nevertheless there are many challenges in the implementation of this complex compilation of different modeling systems. For example, there are differences in chemical mechanisms and transport schemes among the different models that would influence aviation contributions resulting in an inconsistency when trying to make a regional versus a global comparison.

The assessment of aircraft emissions on air quality could be improved with the full-flight profile in emission inventories and a computationally efficient application of a finer spatial resolution modeling. In this study we investigate the impact of full-flight emissions on surface air quality at hemispheric and regional levels. Here the Community Multi-scale Air Quality (CMAQ) model with a domain covering the entire northern hemisphere (Mathur et al., 2012) at a horizontal grid cell resolution of 108 × 108 km^2 is used to study the aviation impact. This hemispheric model is ~2 – 4 times finer than the typical horizontal resolution (4° × 5°, 2° × 2.5°) used in prior global model studies. Additionally, having a finer vertical resolution is particularly crucial while investigating the impact of emission source like aviation occurring in upper troposphere/tropopause region to better represent the sudden inversions and transport. So in this study, we further refined the model vertical structure to have finer resolution (~ 44 layers) than the model vertical resolutions (~ 17 and ~ 34 layers) typically used in regional applications. We examine the aviation-attributable perturbations for both hemispheric scale and as well as for three major sub-regions (North America (NA), Europe (EU) and East Asia (EA)) that have relatively higher aviation emissions globally. We also studied the aviation-attributable perturbations using mass flux vertical profiles and cross-sectional isentropic analysis to understand the vertical transport of aviation emissions. In addition to hemispheric modeling, we also performed regional scale modeling utilizing a 36 × 36 km^2 Continental U.S scale to compare the differences in aviation-attributable impacts for different model resolutions. Overall, this framework may reduce uncertainties in model predictions and provide an improved understanding of physical and chemical changes occurring in the upper atmosphere due to aviation and its impacts on surface air quality.

3.2 Methodology

3.2.1 Air Quality Modeling

We used the CMAQv5.0.2 model (Byun and Schere 2006) with updated new CB05 condensed toluene gas phase mechanism (Whitten et al., 2010; Sarwar et al., 2011) and AERO6 aerosol module to carry out both regional and hemispheric-scale modeling and to assess air quality impacts of aircraft emissions. We used Weather Research and Forecasting model (WRFv3.6.1) (Skamarock et al., 2008) to downscale NASA's Modern-Era Retrospective Reanalysis (MERRA) (Rienecker et al., 2011) inputs to produce meteorological input data to CMAQ. MERRA is a global reanalysis data that assimilates observations and satellite products and has a horizontal grid resolution of 0.5° × 0.67° with 72 vertical levels extending to 0.01hPa. We initialized WRF at 0000 UTC January 1, 2004 and run continuously through 0000 UTC January 1, 2006 using MERRA data. The first 12 months of the simulation (January 1 through December 31, 2004) were used as a spin-up period for the model. The domain configurations, model vertical structure and physical options used in WRF are included in Supplementary Information (Table B1-B3). We ran WRF over two standalone domains: 1) 108 × 108 km^2 (here after denoted as 108-km) Northern Hemispheric (HEMI) with a Polar Stereographic projection, and 2) 36 × 36 km^2 (here after denoted as 36-km) Contiguous United States (CONUS) with a Lambert Conformal projection, as shown in Figure 3.1. CMAQ northern hemispheric application (HEMI) is a newer platform with 108-km horizontal resolution that has been used in recent studies (Sarwar et al., 2014; Xing et al., 2015) and this is the first study to use that application for studying impacts of aircraft emissions. For the CONUS domain, we used a traditional North American domain at 36-km horizontal resolution. We also used consistent meteorology for both

the hemispheric and regional scales, and drove the regional scale application using downscaled boundary conditions from the hemispheric model.

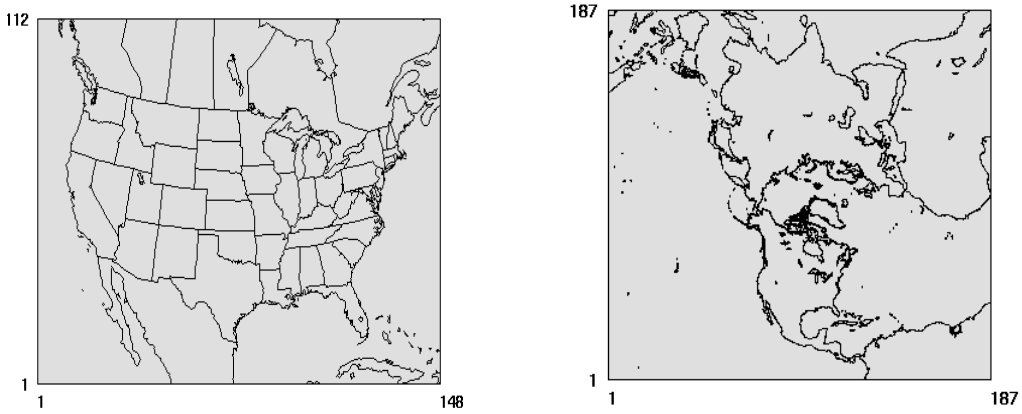

Figure 3.1: Modeling domains (CONUS – left) and (HEMI – right).

Table 3.1: Modeling configuration and data sources for HEMI and CONUS domains.

Category	**HEMI 108km**	**CONUS 36km**
Model version	CMAQv5.0.2	
Non-aviation emissions	EDGAR*-v4.2	NEI*-2005
Horizontal resolution	108 × 108 km^2	36 × 36 km^2
Vertical resolution	44 layers (top ~ 50hPa)	
Meteorology	WRFv3.6 with MERRA* reanalysis data	
Aviation emissions	AEDT* (full-flight)	
Boundary conditions	Clean air profile based conditions	Downscaled from Hemispheric CMAQ
Lightning NOx emissions	Based on empirical calculation	Based on NLDN* observations

***NEI – National Emissions Inventory; EDGAR – Emissions Database for Global Atmospheric Research; MERRA - AEDT – Aviation Environmental Design Tool; NLDN – National Lightning Detection Network**

For regional domains, incorporating dynamically and chemically downscaled boundary conditions from global models is important given the increased role of hemispheric transport on regional studies (C. Lin et al., 2000; J. Lin et al., 2014). Prior studies (Lam and Fu, 2009; Henderson et al., 2014) showed higher ozone mixing ratios in the upper regional model layers when downscaled from global models and discussed the vertical incompatibility between regional and global models. Here in this study we use the HEMI model with identical physical and chemical model processes to generate boundary conditions for the CONUS domain. By doing this, we are able to maintain consistency in the chemical mechanisms and dynamics for the boundary conditions in the regional domain.

The CMAQ model configurations and data used for two domains are in Table 3.1. We used the National Emissions Inventory (NEIv4.3) for the year 2005 (US EPA, 2007) and SMOKE model (Houyoux et al., 2000) to generate gridded emissions for all anthropogenic sources except aviation for the CONUS domain (Table B6). For the HEMI domain, we used the Emissions Database for Global Atmospheric Research (EDGARv4.2) (European Commission, 2016) for all emission sources except aviation and generated model-ready emissions (Table B5) that are gridded, speciated and temporalized as described in Xing et al. (2015). In both domains we used aircraft emissions generated from the Federal Aviation Administration's (FAA) Aviation Environmental Design Tool (AEDT) (Wilkerson et al., 2010). AEDT is an environment policy tool that predicts emissions for all global commercial flights throughout the flight time. These chorded emissions consisting of fuel burn and key gaseous (CO, NO_X, SO_2, VOC) and particulate (PSO4, POC, PEC) for each and every individual flight (high temporal and spatially resolved). Note that AEDT has three primary $PM_{2.5}$ species directly emitted by aircraft, i.e., primary sulfate (PSO4), primary organic carbon (POC) and primary elemental carbon (PEC)

with emission estimates based on the First Order Approximation (FOA) Version 3 (Wayson et al., 2009). We gridded these emissions using the AEDTProc (Baek et al., 2012) tool that allocates emissions both vertically and horizontally to the model grid. Lightning NOx (LNOx) emissions were calculated in the CONUS modeling domain based on the recent update available in CMAQ (Ott et al., 2010; Allen et al., 2012), that uses National Lightning Detection Network (NLDN) flash counts and the number of NO moles produced per unit flash. In the HEMI domain, due to the lack of flash count observational data outside the U.S., we used the convective precipitation based empirical approach. In this empirical approach, rather than constraining with observational data, constant values are used for number of flashes (148) and moles of emissions (500 N) per flash (Pickering et al., 1993; Allen et al., 2010, 2012). Note that using some of these constant values throughout the northern hemisphere (NH) can introduce some uncertainties in lightning emissions as these values can vary regionally.

Using these inputs, we carried out two annual simulations for both domains as shown in Table 3.2: a) NoAirc: scenario with all sources of emissions except aviation b) Airc: scenario with all sources of emissions including aircraft emissions. Therefore, the difference between Airc ($Conc_{Airc}$) and NoAirc ($Conc_{NoAirc}$) gives us the incremental concentrations that are attributable to the full-flight aircraft emissions denoted as aviation-attributable contributions (AAC) in this study.

$$AAC = Conc_{Airc} - Conc_{NoAirc} \qquad (3.1)$$

We also calculated the incremental contribution of aviation impacts when compared with all other sources impacts defined as Aviation Contribution Percentage (ACP) as following

$$\mathrm{ACP} = \left(\frac{\mathrm{Conc_{Airc}} - \mathrm{Conc_{NoAirc}}}{\mathrm{Conc_{Airc}}}\right) * 100 \qquad (3.2)$$

Table 3.2: Description of modeling scenarios

Model Scenario	Domain	Description	Period
NoAirc36	CONUS	All source emissions (NEI) except aircraft	2005 annual year with one month spinup
Airc36	CONUS	All source emissions (NEI) including aircraft (AEDT)	2005 annual year with one month spinup
NoAirc108	HEMI	All source emissions (EDGAR) except aircraft	2005 with three month spinup
Airc108	HEMI	All source emissions (EDGAR) including aircraft (AEDT)	2005 with three month spinup
NoAirc108_NEI, Airc108_NEI	HEMI	Replaced EDGAR emissions with NEI for North America.	January, July with one month spinup

3.2.2 Observation data

To evaluate our model predictions we used surface observations from Air Quality System network (AQS; http://www.epa.gov/aqs) for the U.S. in both the CONUS and HEMI domains. We also evaluated our model predictions in the upper troposphere using in-situ aircraft observational data from the Intercontinental Chemical Transport Model (INTEX-NA) (Singh et al., 2006) and Measurement of OZone and water vapor by AIrbus in-service aircraft (MOZAIC; http://www.iagos.fr/web/rubrique3.html; (Thouret et al., 2005)) campaigns. The INTEX-NA campaign observations are confined only to the U.S., but MOZAIC observational data includes some major airports in other regions (Europe, Asia) of the HEMI domain. Note that Xing et al., (2015) evaluated the CMAQ-HEMI application in U.S., Europe and East Asia using surface monitoring data from those regions and found that the model was able to represent the

observational trends. Here we included the MOZAIC vertical evaluation in the supplementary material (Figure B8 and Figure B9).

3.2.3 Mass Flux

Mass Flux can be defined as the rate of the mass transferred across the model domain gridcell per unit time per unit area. To calculate mass flux of AAC we followed the technique as discussed in Klich and Fuelberg, 2014. We considered vertical velocity (V_c, m/sec) from meteorology (WRF) data and aviation-attributable concentrations for O_3 and $PM_{2.5}$ from model output. We converted model predicted mixing ratios (MR, ppbV) to mass concentrations (M_c, kg/m^3) and multiplied it by vertical velocity to obtain mass based flux ($kg/m^2.sec$) across each model layer as shown in equation 3.3 and 3.4. We named this metric as aviation-attributable mass flux (AMF). The positive vertical velocity indicates the updrafts occurring in the atmosphere and the negative vertical velocity indicates the downdrafts occurring in the atmosphere. Therefore the negative AMF indicates the downward transport of AAC mass and positive AMF indicates the upward transport of AAC mass.

$$M_c = MR * 10^{-9} * \left(\frac{MW_i}{MW_{air}}\right) * DENS \qquad (3.3)$$

Where MR = model predicted mixing ratio; MW_i = molecular weight of pollutant; MW_{air} = molecular weight of air; DENS = density of air

$$\text{Mass Flux} = M_c * V_c \qquad (3.4)$$

Where V_c = vertical velocity from meteorology data

3.2.4 Isentropic Analysis

The CMAQ model vertically resolved concentrations and meteorology data are considered to conduct isentropic analysis for both hemispheric and regional domains. Note that

we did not run the model using potential temperature θ as vertical coordinate system but post-processed modeled aviation-attributable concentrations along the isentropic levels. We calculated potential temperature from meteorology data as follows for all model vertical layers.

$$\text{Theta } (T_h) = T * \frac{P_s}{P_h}^{0.286} \qquad (3.5)$$

Where T = Temperature at model vertical layers

P_s = Surface pressure

P_h = Pressure at different model vertical layers

We interpolated the model concentrations from vertical layers to calculated theta vertical levels (range 380 – 280K) to illustrate the effect of isentropes on the vertical transport of cruise altitude emissions to the surface and their seasonal variability.

3.3 Results And Discussions

3.3.1 Aviation emissions impact at hemispheric scale

3.3.1a Surface Analysis

The impacts of aviation emissions on surface air quality were assessed in the HEMI (108-km) domain. The model predicted aircraft-attributable contributions (AAC) is calculated as the difference between the simulations 'with aviation' (Airc) and 'without aviation' (NoAirc) as shown in equation 3.1. In other words, AAC are the aviation-attributable perturbations of pollutants due to aviation emissions. Model predicted hourly outputs were used to calculate various temporal (annual, monthly and daily averages) and spatial (land grid cells domain average) metrics in this analysis. Table 3.3 shows the domain wide annual average of the MDA8 O_3 and $PM_{2.5}$ AAC. As shown in Table 3.3 the model predicted AAC of 0.46 ppbV and 0.013

$\mu g/m^3$ for O_3 and $PM_{2.5}$, with maximum concentrations reaching 1.92 ppbV and 0.14 $\mu g/m^3$ throughout the entire hemispheric domain. These results are consistent with the global scale aviation surface impacts as discussed in recent studies (Lee et al., 2013; Yim et al., 2015) where annual perturbations of ~ 0.5 – 0.6 ppbV for O_3 and 0.006 $\mu g/m^3$ for $PM_{2.5}$ were reported. Also shown in Table 3.3 is the relative contribution of aviation when compared with impacts from all other sources as shown in equation 3.2. Overall CMAQ predicted values show that aviation impacts contribute 1.3% and 0.2% for O_3 and $PM_{2.5}$ at surface in hemispheric domain with slightly varying impacts in key sub-regions in NH. EU shows the highest impacts of 1.9% and 0.5% for O_3 (0.69 ppbV) and $PM_{2.5}$ (0.031 $\mu g/m^3$), which is ~ 1.4x and ~2.2x higher than the overall hemispheric average aviation impacts (O_3: 0.46 ppbV, $PM_{2.5}$: 0.013 $\mu g/m^3$). NA and EA show similar impacts as EU in the case of O_3, but the $PM_{2.5}$ impacts are lower when compared with EU.

Figure 3.2 shows the annual average AAC spatial plot for O_3 and $PM_{2.5}$ at the surface. In the HEMI domain, maximum annual O_3 impacts occurred near Tibet plateau throughout the year (monthly spatial plots included in supplementary material Figure B1). This is consistent with other studies (Barrett et al., 2010), who reported this impact was due to the relatively higher convective flux in the high altitude region. Other than this hot spot, maximum annual impacts of ~ 0.8 ppbV are seen in the mid-latitudes 30^oN to 50^oN band (sub-tropical zone), with modest impacts near other high convective and warm weather regions such as the Western U.S. and North Africa. In the case of $PM_{2.5}$, higher annual impacts occurred near major urban corridors such as the Eastern U.S., Western EU, and Eastern Asia (China) where aviation emissions and $PM_{2.5}$ precursor emissions are relatively higher (Supplementary material Figure B2).

Table 3.3: Domain wide annual average of predicted O_3 and $PM_{2.5}$ aviation-attributable contributions (AAC) for overall HEMI domain and the sub-regions of NA, EU and EA. The relative percentage of aircraft emission contribution when compared with all sources is shown in parenthesis. Also shown are the maximum annual AAC in the domain for both pollutants.

Domain	O_3 (ppbV)		$PM_{2.5}$ ($\mu g/m^3$)	
	Mean	Maximum	Mean	Maximum
HEMI	0.46 (1.3%)	1.92	0.013 (0.2%)	0.14
HEMI-NA	0.65 (1.7%)	1.03	0.021 (0.4%)	0.09
HEMI-EU	0.69 (1.9%)	0.94	0.031 (0.5%)	0.15
HEMI-EA	0.57 (1.5%)	1.05	0.021 (0.2%)	0.10

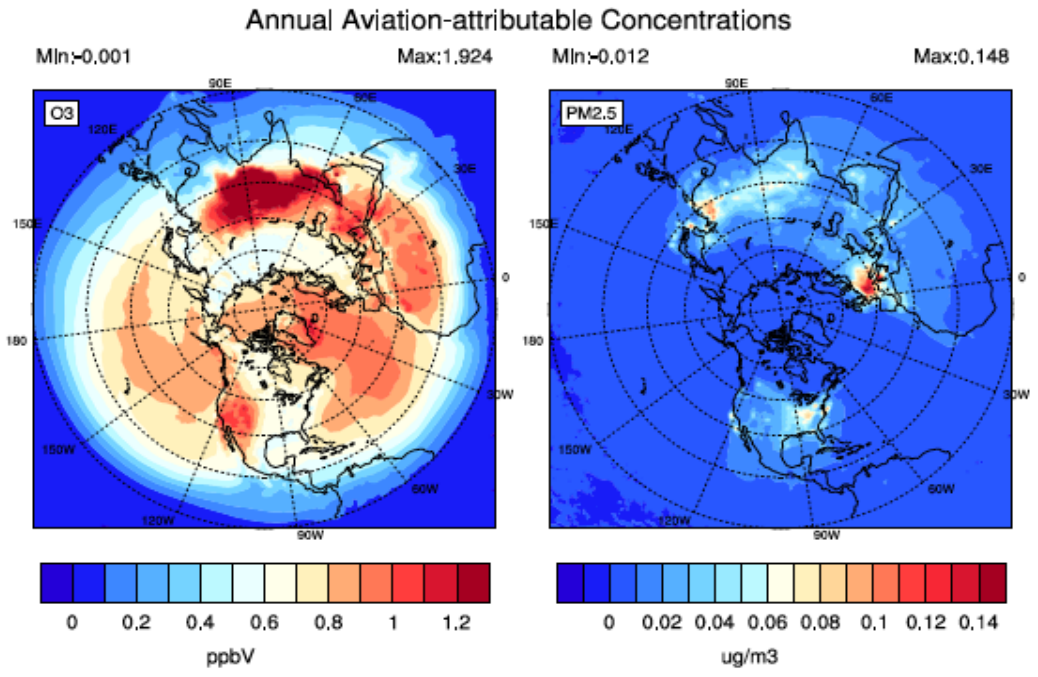

Figure 3.2: Aviation-attributable contributions of annual averaged O_3 (left) and $PM_{2.5}$ (right) for the hemispheric domain (HEMI) at the surface.

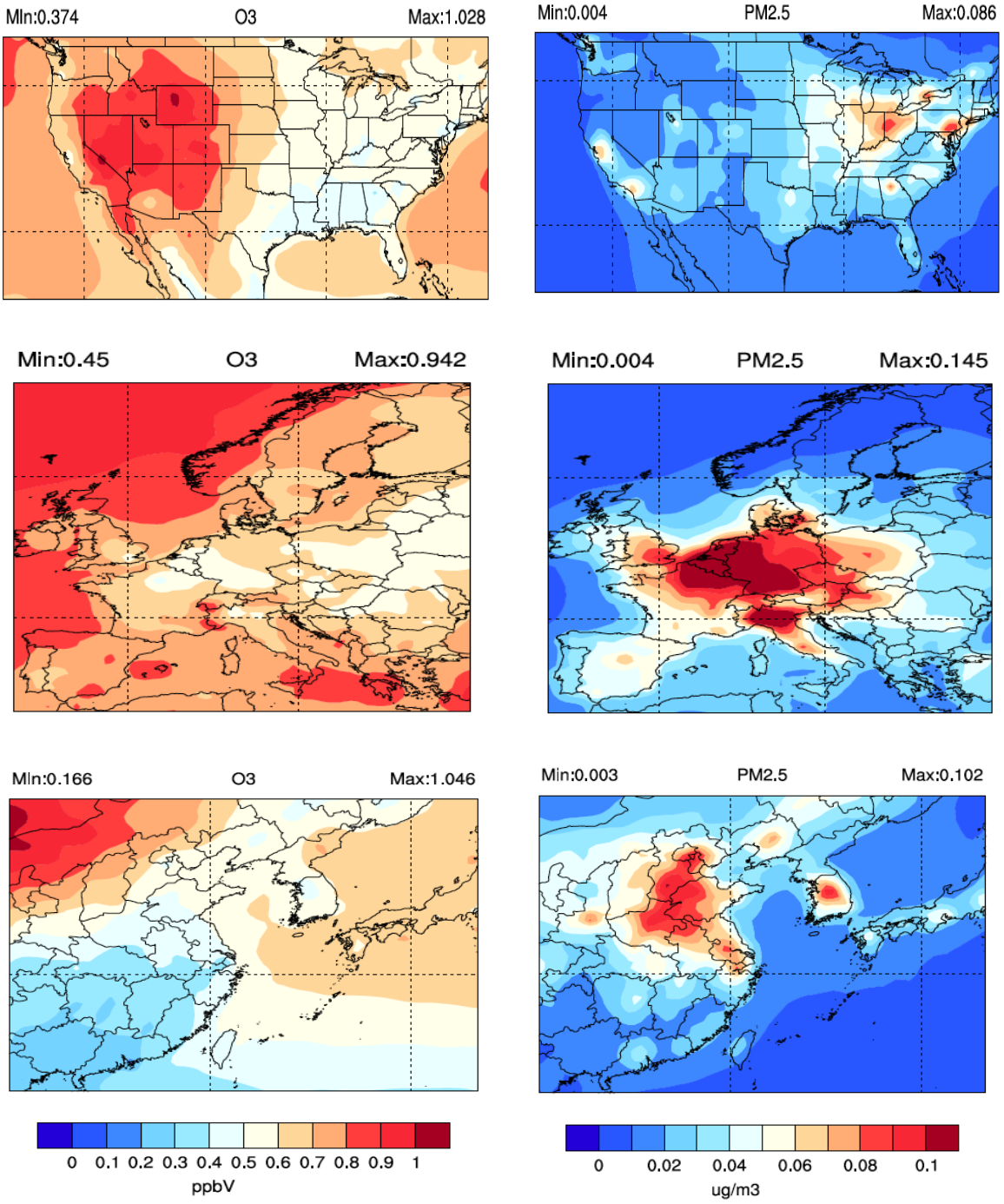

Figure 3.3: Aviation-attributable contributions of annual averaged O_3 (left) and $PM_{2.5}$ (right) at the surface for three sub-regions NA (top), EU (middle), and EA (bottom).

We next focused on model predicted AAC for O_3 and $PM_{2.5}$ in three sub-regions with the highest aviation emissions. Figure 3.3 shows the spatial extent of annual average AAC of O_3 and $PM_{2.5}$ in NA, EU, and EA. The maximum AAC for O_3 is comparable between the three sub-regions (NA: 1.03 ppbV, EU: 0. 95 ppbV, EA: 1.05 ppbV) with EA showing slightly higher impacts. In the NA sub-region (Figure 3.3, top left), ~ 2x higher impacts of O_3 occurs near western U.S. compared to eastern part of the country. In the EU sub-region (Figure 3.3, middle), higher impacts of ~ 0.8 ppbV of O_3 occur near Madrid, Munich and Frankfurt. In EA sub-region (Figure 3.3, bottom), higher O_3 impacts are observed near the west side of EA (higher latitudes). Overall looking at the spatial distributions, we can notice that the circulation and synoptic flow drives the aviation-attributable O_3 perturbations.

The maximum $PM_{2.5}$ AAC of 0.145 $\mu g/m^3$ occurs in the EU sub-region, which is ~ 1.42 and ~1.68 times higher when compared to the EA and NA regions. For $PM_{2.5}$, annual average peaks of ~ 0.08 $\mu g/m^3$ are observed near urban and major airports regions such as LAX, ATL, JFK airports and the Ohio valley region (Figure 3.3, top right). The increase of aviation-attributable $PM_{2.5}$ in Ohio valley is due to the presence of higher NOx emissions and free ammonia from non-aviation emissions in the model. This combination lead to the increase in aviation-attributable ammonium nitrate aerosol that increased the aviation-attributable $PM_{2.5}$, similar results are seen in Woody et al., (2011). In EU, higher $PM_{2.5}$ impacts of ~ 0.1 – 0.08 $\mu g/m^3$ are predicted near Frankfurt, Munich and London regions followed by Madrid and Rome regions (~ 0.06 $\mu g/m^3$). In EA region, highest impacts of ~ 0.1 $\mu g/m^3$ are observed near densely populated Beijing region followed by Shanghai and Seoul region.

Figure 3.4 (left) shows the domain-wide average of daily maximum 8-hour average O_3 and daily averaged $PM_{2.5}$ AAC for HEMI domain throughout the entire year. As shown in Figure

3.4 (left), the winter months ~ 1.5x higher O_3 contributions than summer months and falls in the range of ~0.2 – 0.5 ppbV. In the case of daily averaged $PM_{2.5}$, impacts in winter months are twice as seen in summer months. These seasonal $PM_{2.5}$ differences are mainly influenced by modeled inorganic aerosols (sulfate, nitrate, and ammonium) as shown in Figure 3.4 (right). Figure 3.4 (right) shows the monthly average of individual speciated $PM_{2.5}$ predicted by the CMAQ model (sum of sulfate, nitrate, ammonium, elemental carbon, primary organic aerosol, secondary organic aerosol and other crustal species). The speciated $PM_{2.5}$ shows that sulfate aerosol (ASO_4) has larger contributions to total $PM_{2.5}$ during summer and fall months (Apr – Nov) than during winter months (Dec – Mar). During winter, nitrate aerosol (ANO_3) is more prominent due to the presence of more HNO_3 (lesser reduction of HNO_3 through photolysis in winter season) to react with NH_3 to form nitrate aerosol and nitrate tends to stay in particle phase at low temperatures. We also examined the temporal trend in the AAC for each sub-region and speciated aerosols (Figure B3). In all three regions, the winter season impacts are slightly higher than summer impacts for both pollutants similar to the trend observed in Figure 3.4.

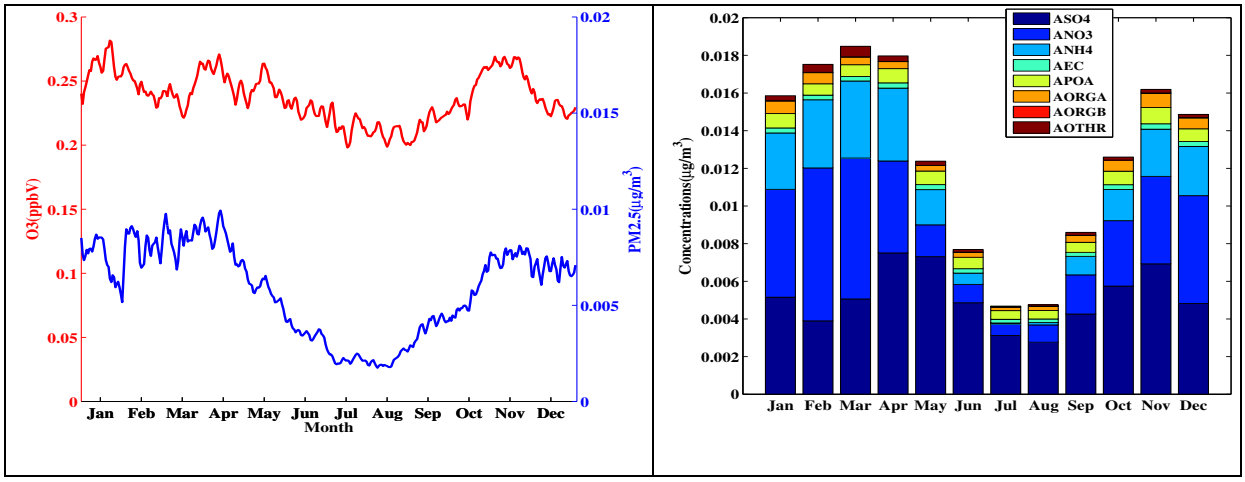

***Speciated aerosols: ASO4= sulfate, ANO3= nitrate, ANH4= ammonium, AEC = elemental carbon, APOA = primary organic, AORGA = anthropogenic, AORGB = biogenic, AOTHR = other aerosols.**

Figure 3.4: Aviation-attributable contributions domain wide average of 8-hour daily maximum O_3 (red) and daily averaged $PM_{2.5}$ (blue) in the HEMI domain (left). Domain wide average of monthly averaged speciated aerosol $PM_{2.5}$ AAC in the HEMI domain at the surface (right).

3.1.1b Vertical Analysis

We studied the vertical profiles of O_3 and $PM_{2.5}$ impacts due to full-flight aviation emissions at different altitudes. Throughout this vertical analysis hourly O_3 and $PM_{2.5}$ concentrations at all model layers are used. The annual vertical impacts were averaged across three atmospheric regions: Boundary Layer (BL) of < 2 km, mid-troposphere (MT) of 2 – 8 km, and upper troposphere (UT) of > 8 km. Figure 3.5 (left) shows the annual average percentage contribution of AAC in BL, MT, and UT for O_3. In the HEMI domain, the UT and MT impacts are shown as ~ 2 – 2.3 %, which is double the BL impacts. The sub-regions shows ~ 1.2 – 2 times higher impacts than the overall HEMI impacts near all three vertical bins. In the case of O_3, EU shows higher impacts of ~4 – 4.5% in MT and UT followed by EA and NA, which expectedly confirm that aviation the impacts are consistently higher in the upper altitudes than in BL and surface across all sub-regions. Figure 3.5 (right) shows the percentage contribution of AAC in boundary layer (BL), mid-troposphere (MT) and upper troposphere (UT) for $PM_{2.5}$. Overall across the HEMI domain, the UT impacts are estimated to be ~ 2.7%, which is ~ 2 times higher than MT impacts and 10 times higher than BL impacts. For $PM_{2.5}$ there are more decreases in predicted impacts near the BL when compared with UT. The decreases in BL are larger for $PM_{2.5}$ than O_3.

To better quantify the vertical transport of the higher cruise altitude emissions, we calculated (using equations 3.3 and 3.4) mass fluxes and performed isentropic analysis. Figure 3.6 represents aviation-attributable mass flux (AMF) vertical profile of O_3 and $PM_{2.5}$ in HEMI domain; the general trend (during all seasons) shows negative AMF (downward flux) near the UT region, with change in direction towards positive AMF in the MT region and changes to negative AMF near surface. In the MT, the change in the direction is mainly due to the

downward flux occurring in the upper altitudes and upward flux occurring in lower altitudes, therefore the overall mass flux is influenced by both the upper altitude transport and surface mixing. In summer, as mixing is high near the surface the upward flux is predominant, hence near the surface and in lower troposphere positive mass flux is indicated in the vertical mass flux profiles. The shape of O_3 profile looks smooth and consistent in all seasons, with higher negative AMF during winter (Dec – Feb) and early spring (March). Near the surface (we also closely looked at zoomed only lower 2000 meters AMF plots that are not presented), winter months show negative AMF than summer months due to lower photochemistry rates, higher downward transport and most common deep stratospheric intrusion events during winter and spring months. A recent CMAQ hemispheric study (Xing et al., 2016) saw similar higher impacts during winter month due to downward transport from upper altitudes. This similar trend of maximum stratospheric tropospheric ozone downward flux in winter and spring has been reported in other global model study (Yang et al., 2016).

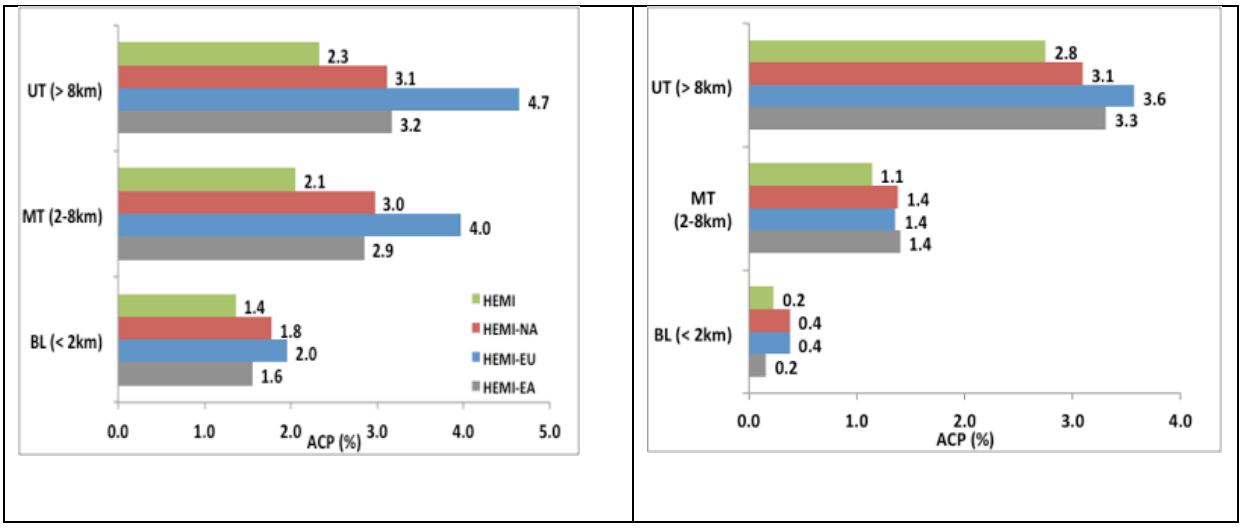

Figure 3.5: The aviation contribution percentage (ACP,%) to total annual average O_3 (left) and $PM_{2.5}$ (right) when compared with all other emission sources in the entire HEMI domain and for all three sub-regions of NA, EU and EA. The vertical data is stratified into near boundary layer (BL), mid-troposphere (MT) and upper troposphere (UT).

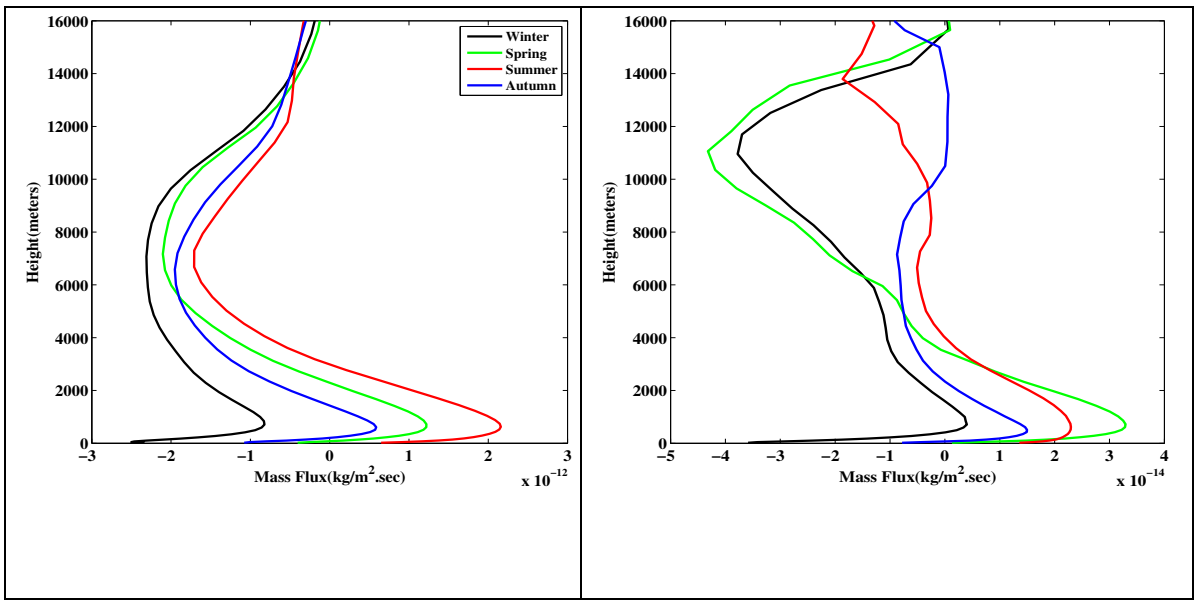

Figure 3.6: Vertical profile of O_3 (left) and $PM_{2.5}$ (right) aviation-attributable mass flux (AMF) in the entire HEMI domain. Data is averaged over each season in 2005 defined as: Winter = December – February, Spring = March – May, Summer = June – August, and Autumn = September – November.

In the case of $PM_{2.5}$, the vertical profiles look different between all seasons highlighting the influence of seasonal factors such as humidity, temperature, and deposition velocities on mass flux. For $PM_{2.5}$, only winter and spring months predicted a negative AMF (downdraft) near UT region, but not during summer and autumn months. Near the surface a similar downward flux (negative AMF) as seen in O_3 was predicted in winter months. This indicates that the transport of cruise altitude emissions emitted in the upper troposphere is highly influenced by the seasonal circulation pattern. Model predictions indicate downward transport only during winter months in the overall northern hemisphere when downdrafts/westerlies are high and boundary layer/surface mixing is less. As these transport phenomena and seasonal circulation changes with different region at hemispheric scales, we further analyzed mass flux profiles in individual sub-regions.

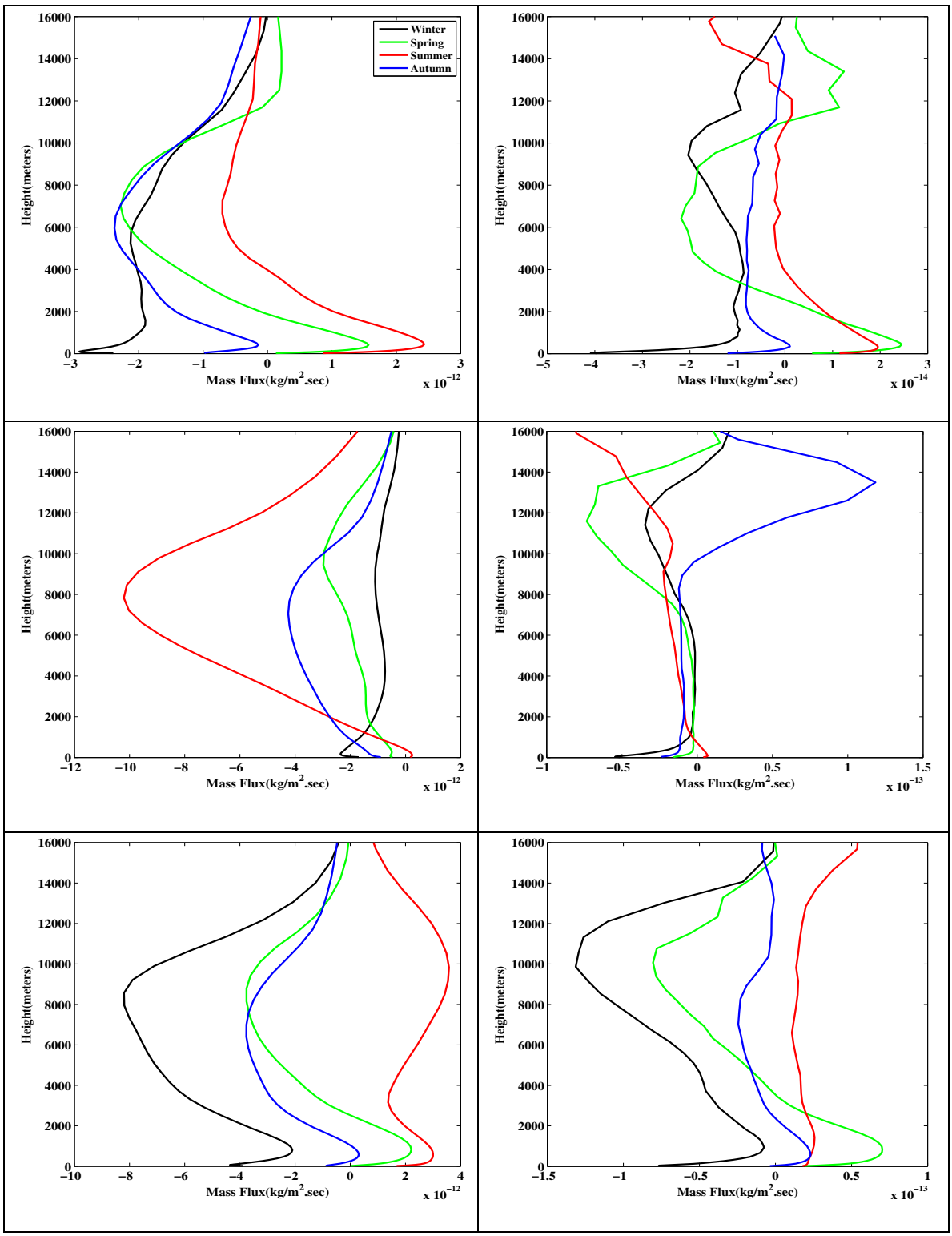

Figure 3.7: Vertical profile of O_3 (left) and $PM_{2.5}$ (right) aviation-attributable mass flux (AMF) from NA (top), EU (middle) and EA (bottom) sub-regions from HEMI domain. The data is seasonally averaged similar to description mentioned in Figure 3.6.

Figure 3.7 shows AMF vertical profiles for both pollutants separated by regions clearly show regional differences among the three sub-regions. In the case of O_3, near the UT region, a higher downward flux was predicted during the spring and autumn in NA, summer in EU and winter in EA. Though the profiles show different profiles in the UT and MT, the near surface profiles in the winter months consistently predicted a negative AMF for all three regions. A higher negative AMF for O_3 is shown in EA during winter, indicating that the downward transport is higher due to a higher convection during winter monsoons in EA. The vertical velocity flux based concentrations discussed here is based on the kinematic transport but it did not clearly explain the reason behind the higher downward flux during winters. Since cruise altitude emissions occur mainly near tropopause, region where isentropic mixing/transport is important and highly influenced by potential temperature. Therefore, we also studied the isentropic based AAC for all seasons to understand the transport process.

Figures 3.8 and 3.9 show the seasonal latitude-potential temperature cross sectional plots to illustrate the transport of aviation-attributable concentrations of O_3 and $PM_{2.5}$ along isentropic levels. Aviation-attributable concentrations are vertically interpolated along designated isentropic surfaces from 280 K to 380 K, by calculating potential temperature values for all model layers using equation 3.5. Figure 3.8 shows that across all seasons, a higher O_3 AAC occurs near 340 – 380 K isentropic surface (~ 9 – 16 km average altitude range). The mid-troposphere (~320 – 300 K) isentropic surfaces get closer to the lower isentropes near higher latitudes (60 – 90 N) for all seasons. During winter season (left top), higher isentropes intersect with the lower isentropes close to surface near mid-latitudes (~ 40 – 60 N). Compared to other seasons, the O_3 AAC are higher during winter starting from below ~320 K, which suggests that the meridional transport of O_3 AAC occur particularly when the higher isentropes get closer to

the lower isentropes. Similar results are reported in a recent study (Runde et al., 2016) that discussed the stratosphere-troposphere transport occurrence along 280 – 350 K isentropes in extratropics during winter season. During summer season, the higher isentropic surfaces intersect with the near surface isentropes further north towards the pole. Additionally in summer, higher isentropic surfaces show upward trend, which suggests the transport of O_3 AAC into lower stratosphere than towards free troposphere.

In the case of $PM_{2.5}$ AAC, as shown in Figure 3.9, the seasonal trends vary significantly and thus emphasizing the influence of precipitation patterns, wet deposition, chemical transformations and cloud properties on PM intercontinental and vertical transport (Dentener et al., 2010). In Figure 3.9, during the winter and spring seasons the model predicted higher concentrations in upper isentropic levels around 360 – 340 K near higher latitudes. Compared to spring season, the winter season exhibits slightly higher AAC of $PM_{2.5}$ at lower isentrope levels between 320 – 280K and transport of $PM_{2.5}$ AAC to the surface, similar to the trend observed in O_3. The summer season shows relatively lower AAC both near the higher and lower isentropes. Another interesting feature of higher concentrations around 380K isentrope near mid-latitudes (25 – 50N) was observed in summer, which indicates the upward transport of AAC during that season. The autumn season shows relatively higher $PM_{2.5}$ AAC in MT region (340 – 300 K) than other seasons due to the higher nitrate aerosol and nitric acid (HNO_3) concentrations. During the summer there is increase in NOx concentrations in MT region that increased the HNO_3 and nitrate aerosol concentrations during autumn seasons, which eventually increased $PM_{2.5}$. The downward fluxes observed in vertical mass flux profiles and isentropic trends explain the transport of cruise altitude emissions during winter season and hence higher impacts are observed at the surface in winter when compared to other seasons at hemispheric scale. The main

objective of isentropic analysis is to study the quasi-horizontal and vertical transport of aviation-attributable perturbations. There are several other transport processes occurring in the atmosphere but however, illustrating those processes based on isentropic analysis is not very appropriate and beyond the scope of this paper.

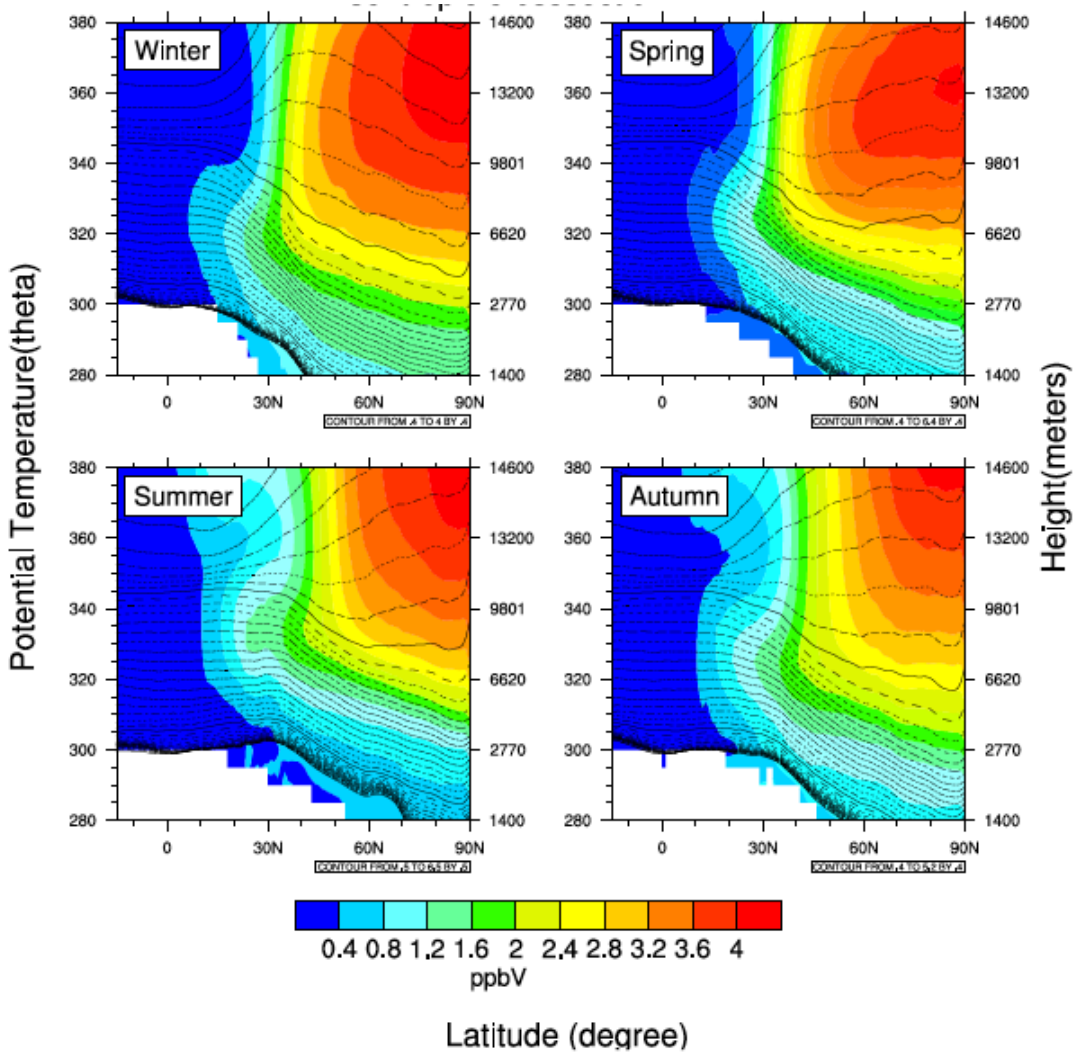

Figure 3.8: Latitude cross-sectional plot of seasonal average O_3 aviation-attributable concentrations interpolated along isentropic levels for all four seasons in HEMI domain. The left axis represents the isentropic levels, right axis represents the average height for those isentropic model vertical levels and bottom axis shows the latitudes in HEMI domain. The black dashed overlay lines are the potential temperature (theta) in our modeling domain.

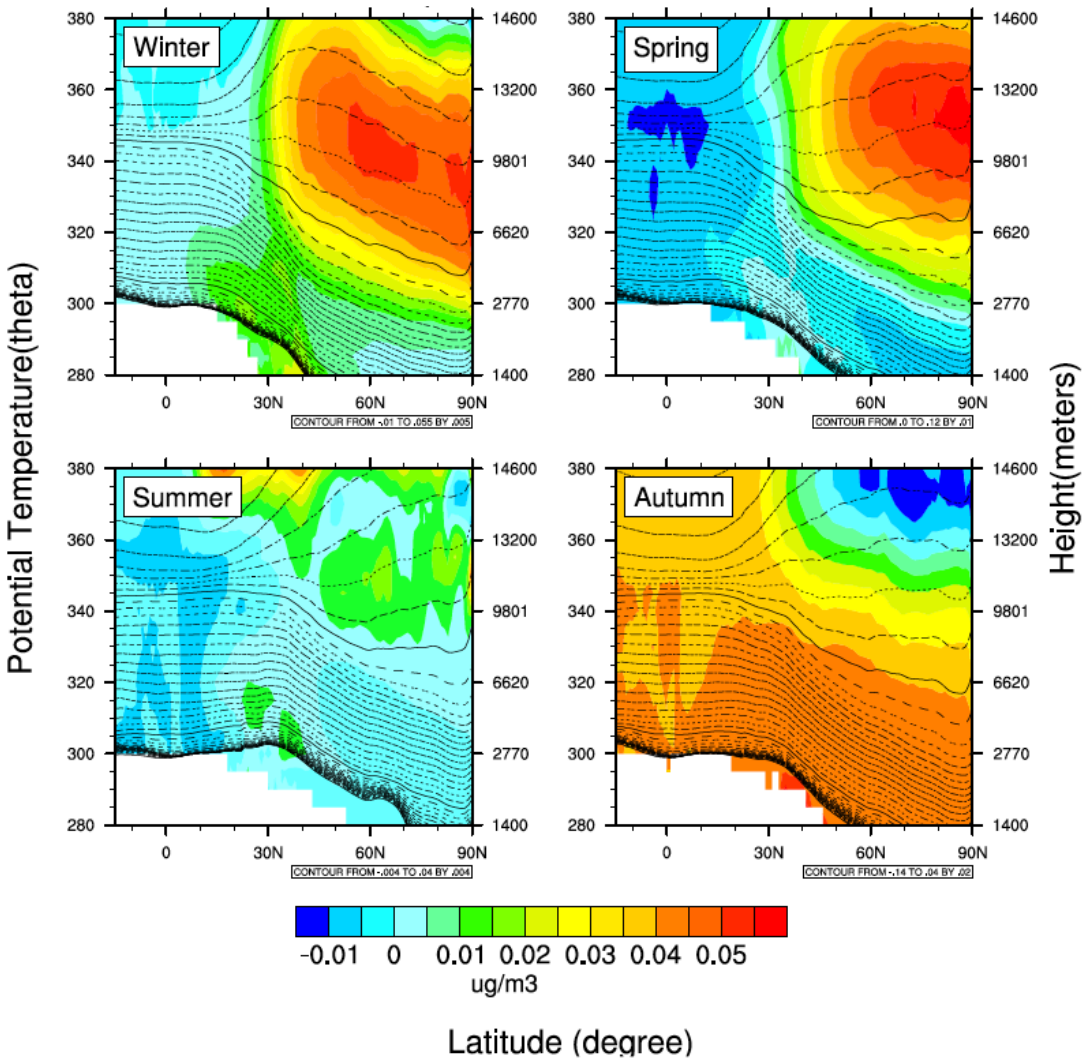

Figure 3.9: Latitude cross-sectional plot of seasonal average $PM_{2.5}$ aviation-attributable concentrations interpolated along isentropic levels for all four seasons in HEMI domain. The left axis represents the isentropic levels, right axis represents the average height for those isentropic model vertical levels and bottom axis shows the latitudes in HEMI domain. The black dashed overlay lines are the potential temperature (theta) values in our modeling domain.

3.3.2 Grid Resolution Sensitivity

3.3.2a Model Evaluation

We evaluated the regional scale 36-km (fine) CONUS and 108-km (coarse) NA model predictions with observations both near surface and vertically. 'Airc36' (all sources + aviation case, CONUS) and 'Airc108' (all sources + aviation case, HEMI-NA) scenarios hourly model

predictions are compared with AQS data near surface for O_3 and $PM_{2.5}$. Note that along with grid resolution, the all sources emission inventory is also different between these two scenarios, so any differences seen here are due to these two factors. For O_3, the annual NMB and NME appear similar between both model scenarios, however a few localized differences occur spatially (Figure B4 and B5). For example, the coarser resolution (Airc108) increased NMB from -10% to -25% in northeast U.S for O_3 when compared with fine resolution (Airc36). These underpredictions in coarse resolution near northeast US are due to the inability of coarse resolution to represent some of the urban scale emissions and processes. Temporal model performance (Figure B6 for monthly performance reference) was calculated by averaging seasonal NMB (%) of: Winter (December, January, February), Spring (March, April, May), Summer (June, July, August) and Autumn (September, October, November).

Table 3.4: Seasonal Normalized Mean Bias (%) of hourly O_3 and $PM_{2.5}$ concentrations predicted by Airc36 and Airc108 model scenarios in comparison with hourly AQS observations. All Airc108 predictions were limited to the NA region. Also shown are the NME (%) differences (Airc108 –Airc36) between scenarios.

Seasons	O_3 (%)			$PM_{2.5}$ (%)		
	Airc36	**Airc108**	**Difference**	**Airc36**	**Airc108**	**Difference**
Winter	38.3	65.0	26.6	2.3	-24.9	22.6
Spring	8.9	17.8	8.9	0.8	-14.7	13.9
Summer	23.5	11.0	-12.4	-29.4	-58.5	29.1
Autumn	34.2	41.7	7.5	-12.4	-44.0	31.6

Winter = December – February, Spring = March – May, Summer = June – August, and Autumn = September – November

Table 3.4 shows that coarse resolution (NMB: ~18 – 65%) showed higher overpredictions for O_3 compared to fine resolution (NMB: ~8 – 39%) during winter, spring and

autumn seasons. In summer, however fine resolution showed ~12% higher overprediction than coarse resolution for O_3. In case of $PM_{2.5}$, the model predicted an improvement in model performance for $PM_{2.5}$ at the finer horizontal resolution throughout all seasons (Table 3.4). Overall annual average of NMB differences shows that coarse resolution showed ~ 25% higher underpredictions in $PM_{2.5}$ and ~7% higher overpredictions in O_3 compared to fine resolution.

Model predictions from three modeling scenarios Airc108 (all sources + aviation), Airc36 (all sources + aviation), NoAirc36 (all sources + no aviation) for North America region are evaluated vertically with observations from the INTEX campaign as shown in Figure 3.10. We also included model evaluation from MOZAIC campaign near major airports in Supplementary information (Figure B8 and B9). Figure 3.10 shows vertical profiles of the model predicted concentrations of O_3 and NO_2 paired with INTEX observations during the period July – August 2005. The paired data are binned based on the altitudes and each point in the vertical profile represents the average of all the paired data that falls in that particular altitude bin. The number of pairs considered for calculating the average value in each bin differs (Figure 3.10, right). Previous studies (Allen et al., 2012; Fang et al., 2010) showed that including lightning NOx emissions reduced model error for O_3 and NO_x and pointed out possibility of another missing emission source. In our study, the addition of lightning NOx emissions and including aircraft full-flight emissions improved the model performance by decreasing the NME 5 – 11 % (Table B8) for NO_2 (difference between Airc36 and NoAirc36) particularly in the upper troposphere (7 – 10 km). Figure 3.10 clearly shows that fine resolution with aviation emissions (Airc36, red line) is close to the observations than compared to other model scenarios. Averaging all altitudes, NME values show an overall decrease of ~ 0.2%, ~ 4%, ~ 2% (Table 3.5) for O_3, NO_2 and NO

respectively in the vertical column of model predictions due to incorporating aircraft emissions aloft.

Table 3.5: Normalized Mean Bias (%) metric of O_3, NO_2 and NO from three model scenarios NoAirc36, Airc36, Airc108 in comparison with INTEX-NA observations. Here we are showing the maximum, minimum and average values of all altitudes (0 – 12km). Also shown are the Normalized Mean Error (%) differences between Airc36 with NoAirc36, Airc108 model scenarios.

Scenarios	O_3			NO_2			NO		
	Max	Min	Average	Max	Min	Average	Max	Min	Average
NoAirc36 (NMB, %)	19.8	-52.9	-8.41	46.5	-85.7	-38.1	-41.8	-84.1	-68.5
Airc36	20.1	-52.7	-7.75	50.9	-84.7	-34.3	-40.3	-83.3	-66.6
Airc108	-2.4	-55.1	-19.4	73.5	-96.6	-53.1	-34.5	-90.8	-76.5
Airc36-NoAirc36 (NME, %)	1.6	-1.3	**-0.18**	5.17	-11.7	**-3.5**	-0.1	-5.5	**-1.9**
Airc36-Airc108 (NME, %)	17.6	-21	**-8.22**	38.9	-56.9	**-16.7**	26.0	-32.6	**-9.9**

Overall the model performance using the finer resolution (Airc36) resulted in NME decrease of ~8%, ~16% and ~9% for O_3, NO_2, and NO when compared with coarse resolution (Airc108) averaged over all altitudes. Model underprediction still exists in the case of NO, NO_2, O_3 in 36-km and this underprediction could be explained by the over prediction of the model for sink species such as PAN, HNO_3 (Figure B7). One explanation for this trend was discussed in

prior studies (Henderson et al., 2011). There the authors mentioned that photochemical models age NOx too rapidly and chemical mechanisms convert it (partition ~25% total nitrogen) to HNO_3 in the UTLS region. We again reiterate the prior study findings that updating reaction rates as suggested in Henderson et al., (2011) in the chemical mechanism is important particularly to improve model performance near UTLS.

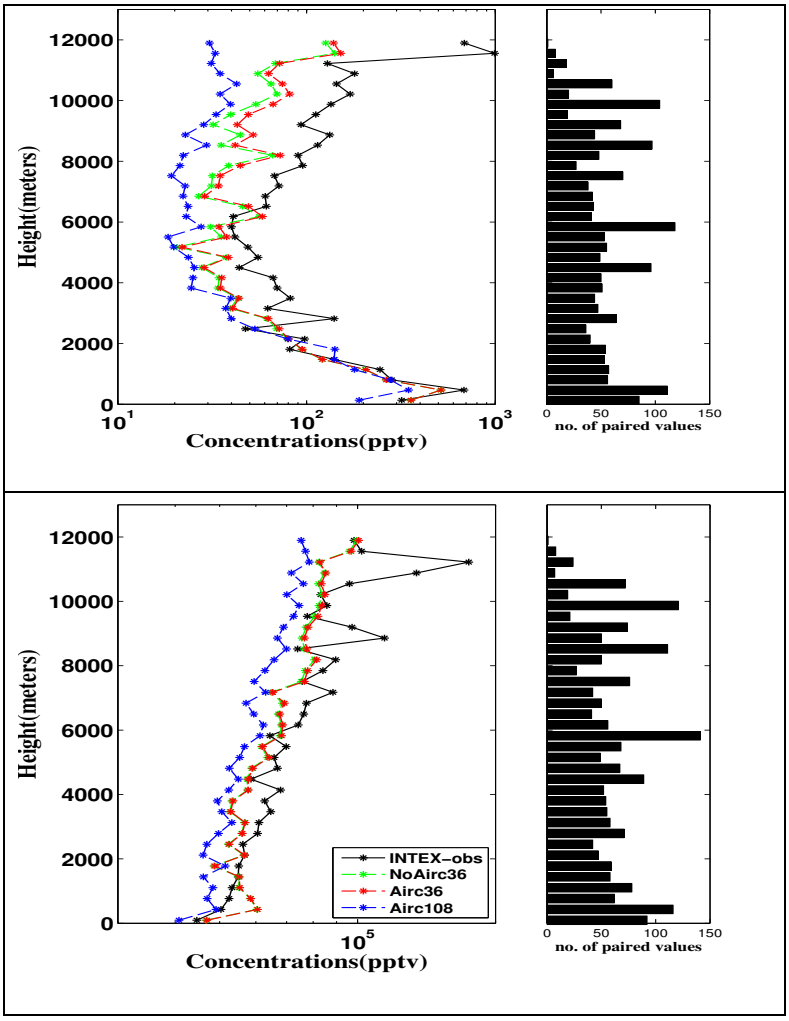

Figure 3.10: Comparison of modeled predictions of NO_2 (top) and O_3 (bottom) from scenarios NoAirc36 (green), Airc36 (red), and Airc108 (blue) paired with INTEX-NA observations (black) and binned vertically. Each point represents the mean concentration value in a particular altitude bin of paired modeled and observations. The bar plot (right) shows the number of paired values in each bin.

3.3.2b Aviation impacts comparison

Figure 3.11 shows the spatial plot of annual average O_3 and $PM_{2.5}$ AAC at the surface in the 36-km CONUS domain. In the CONUS domain, the annual domain averages AAC are 0.03 ppbV and 0.002 μg/m^3 for O_3 and $PM_{2.5,}$ with maximum concentrations reaching 0.23 ppbV and 0.06 μg/m^3 respectively. Spatially, aviation impacts lower O_3 concentrations near major airports (in the grid cell containing the airport), primarily during winter months (Figure B10). Excess aviation NOx emissions reacted with O_3, causing titration effect and a decrease in AAC for O_3. Increases of ~0.1 – 0.2 ppb were seen mainly near areas of high convection (western U.S.) and downwind of major airport areas: Atlanta (ATL), Houston (HOU), Dallas (DFW) and Phoenix (PHX). As shown in Figure 3.11 (right), $PM_{2.5}$ had higher impacts of ~ 0.04 – 0.06 μg/m^3 predicted near these major airport (Figure B11) and urban areas: J.F. Kennedy (JFK), O'Hare (ORD), Atlanta (ATL), Los Angeles (LAX)), Eastern US, Texas and California.

When we compare annual AAC of 36-km NA (CONUS, Figure 3.11) with 108-km NA (HEMI-NA, Figure 3.3 (top)) the overall spatial trend looks similar, however HEMI-NA shows relatively higher O_3 AAC in western U.S. The 36-km resolution showed negative AAC near major airports and higher AAC downwind of these regions, differentiating the VOC and NOx limited regions chemistry with excess aviation NOx, whereas 108-km resolution did not capture this trend. Due to these resolution differences the temporal trends of aviation impacts appeared to be different between 36-km and 108-km NA regions. In 36-km, summer months showed higher impacts than winter months (Figure B10, B11 and B12) whereas in 108-km we saw higher impacts in winter months.

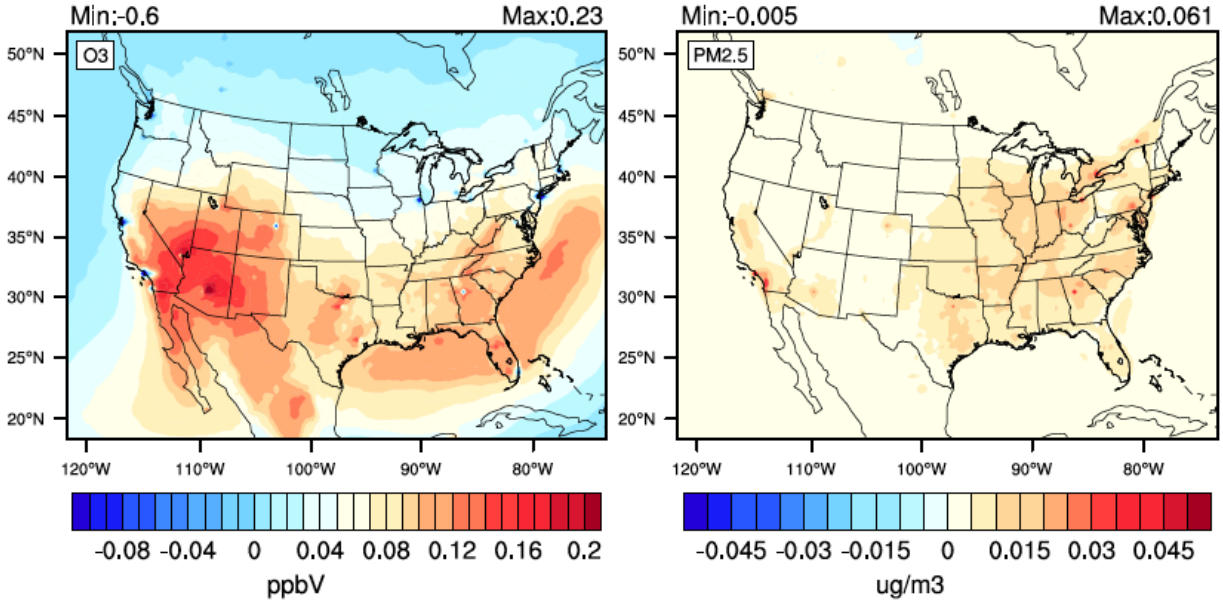

Figure 3.11: Annual average aviation-attributable contributions of O_3 (left) and $PM_{2.5}$ (right) for CONUS (36 km) domain.

In 36-km, model predicted annual domain wide ACP as ~0.1% for both O_3 and $PM_{2.5}$, whereas in 108-km it was predicted to be 1.7% and 0.4%. The maximum annual AAC of O_3 in 108-km NA is predicted to be ~ 1 ppbV, which is ~5x higher than the 36-km maximum AAC of O_3 (~ 0.2 ppbV). For $PM_{2.5}$, the maximum annual AAC predicted in 108-km AAC is ~ 0.02 $\mu g/m^3$ higher than 36-km. Even vertically, the ACP in 36-km near boundary layer, mid-troposphere, upper troposphere appear to be ~0.16%, 0.4%, 0.4% and ~0.1%, 0.26%, 0.48% for O_3 and $PM_{2.5}$. In HEMI-NA, these impacts are ~ 1.7%, 2.4%, 3.1% and 0.4%, 1.4%, 3% for O_3 and $PM_{2.5}$, which is relatively higher when compared with 36-km domain.

Table 3.6: Domain-wide monthly average aviation-attributable contributions (AAC) of O_3 and $PM_{2.5}$ from model scenarios a) Airc108-NoAirc108 (HEMI-NA) b) Airc108_NEI-NoAirc108_NEI (HEMI-NEI-NA) and c) Airc36-NoAirc36 (CONUS). Also shown are the ratio comparisons of these scenarios for January and July months.

	Months	HEMI-NA	HEMI-NEI-NA	CONUS	HEMI-NEI-NA/HEMI-NA	HEMI-NEI-NA/CONUS
O_3	Jan	0.69	0.70	0.01	1.0	63
	Jul	0.53	0.64	0.06	1.2	10
$PM_{2.5}$	Jan	0.027	0.027	0.002	1.0	16
	Jul	0.008	0.013	0.003	1.6	4

3.3.2c Emission Inventory Sensitivity

In all of the annual simulations discussed above, National Emissions Inventory (NEI) emissions were used for the CONUS domain and EDGAR emissions for the HEMI domain (as shown in Table 3.1). Therefore, in our NA region coarse and fine scale resolutions comparison, while similar aircraft emission inventory was used, the non-aviation emission inventory is different. To address the inconsistencies and to make a consistent comparison, we ran two sensitivity simulations 'Airc108_NEI' and 'NoAirc108_NEI' by replacing the HEMI domain EDGAR with NEI emissions (consistent with CONUS domain) for NA region. These simulations were conducted for the months of January and July as sensitivity.

The ‘Airc108’ and ‘Airc108_NEI’ model scenarios predictions were compared with AQS surface observations of O_3 and $PM_{2.5}$ for NA region. The 108-km with NEI emissions scenario (Airc108_NEI) improved model performance by reducing domain average NME by ~10% for both $PM_{2.5}$ and O_3 near urban areas. The overall NMB spatial trend in HEMI-NEI-NA looks similar to the CONUS domain with better model performance near urban regions due to better characterization of emissions with bottom-up approach. This change in model performance did impact the predicted AAC. Table 3.6 shows the domain wide monthly AAC of O_3 and $PM_{2.5}$ from three modeling scenarios: a) HEMI-NA b) HEMI-NEI-NA c) CONUS. Table 3.6 also shows the fractional increase in AAC occurred due to NEI emissions and fine grid cell resolution. Due to NEI emissions the domain wide average AAC increased ~ 1.2 and 1.6 times for O_3 and $PM_{2.5}$ particularly during the summer month (July) in HEMI-NA region (spatial plot showing this trend are included in supplementary Figure B13, B14). The largest differences in AAC occurred due to change in grid cell resolution. As shown in Table 3.6 the HEMI-NA-NEI scenario predicted ~ 63 (January) and ~ 10 (July) times higher AAC for O_3 and ~ 16 (January) and ~ 4 (July) times higher AAC for $PM_{2.5}$ when compared to CONUS domain. These differences occurred mainly near urban areas (Figure B15 and B16) where the fine resolution captured some of the decreases in concentrations due to aviation emissions where as the coarse resolution did not show this trend. Overall even the domain – wide daily average and maximum AAC were consistently higher in HEMI-NEI-NA case when compared to the CONUS case for both O_3 and $PM_{2.5}$ (Figure B17 and B18). Note that we are seeing these higher significant differences only in the case of aviation-attributable perturbations, however the differences are not high in base scenarios (Airc108, Airc108_NEI, Airc36) as shown in Figure B19. We believe the higher AAC in coarser resolution could be due to the relatively higher diffusion in upper

model layers and high concentrations near airports with coarse horizontal grid. The coarse resolution can transport upper altitudes perturbations quickly (more diffusive with coarse grid) to lower altitudes than the fine resolution. Also in HEMI application due to the overall northern hemisphere extent, we saw higher concentrations of aviation-attributable ozone in ocean (particularly in winter) due to deposition process that contributed to the overall increase in domain-wide AAC. In coarse resolution, also higher concentrations are observed near major airports due to larger spatial extent, ~ 9 times bigger than the fine resolution. We attribute these as to the cause of increased AAC in coarse resolution (HEMI, 108-km) when compared to fine (CONUS, 36-km).

3.4 Conclusions

The key focus of this paper is to assess and quantify full-flight emissions impacts on air quality at hemispheric and regional modeling scales and to study the influence of horizontal grid resolution on aviation impacts. It was clear from our analyses that the grid resolution had the largest influence on model performance and AAC predictions when compared to just including full-flight emissions. Going from predictions relying on a coarse (108-km) resolution to those relying on a finer (36-km) resolution for North America region improved the domain wide average of NME by ~7% for O_3 and ~25% for $PM_{2.5.}$ Vertically, the finer resolution model improved model performance by up to ~11% for NO_2 in the UTLS region. Averaged across all altitudes, the finer resolution model decreased NME by ~8%, ~16% and ~9% for O_3, NO_2, and NO respectively. Our results also highlight that by incorporating full-flight aircraft emissions at a fine resolution, the model performance was improved by up to ~ 5–11% for NO_2 in UTLS region. For North America region, AAC predictions using a 36-km resolution captured both titration effects during winters and higher photochemistry during summer months. Predictions

using the 108-km domain was incapable of capturing the local-scale photochemistry effects, and thus did not decrease O_3 AAC during winter when compared with summer. On the other hand, hemispheric model captures the intercontinental long-range transport that can transport pollutants from higher altitudes to lower altitudes during periods of strong westerly winds, which increases the O_3 AAC during winters.

At the hemispheric scale on an annual domain-average basis, aviation contributes only 1.3% and 0.2% for O_3 (0.69 ppbV) and $PM_{2.5}$ (0.03 $\mu g/m^3$) at the surface. We also examined three sub-regions (EU, NA and EA) that have significant aviation activity to emphasize the differences in impacts occurring at continental scales. This sub-regional analysis provides additional insights support potential emissions reductions strategies, as the impacts can vary significantly by region. Among these three sub-regions, EU had the highest impacts, where aviation contributed ~1.9% and 0.5% for O_3 and $PM_{2.5}$ at the surface followed by NA and EA. The maximum O_3 impacts were predicted near mid-latitudes 30^oN to 50^oN band and maximum $PM_{2.5}$ aviation impacts were predicted near large airports throughout the hemisphere. The aviation contribution percentages (ACP) are ~ 2 times higher in UT (2.3%) when compared with surface (1.3%) for O_3, whereas for $PM_{2.5}$ the ACP is ~ 10 times higher in UT (2.7%) than surface (0.2%). Our analyses showed that the model predicted AAC downward mass flux and vertical transport along the isentropes occurred particularly during winter months at hemispheric scales, indicating the influence of seasonal circulation patterns on vertical transport of cruise emissions in the model. Overall, the spatial distribution shows that the O_3 aviation impacts were driven by the atmospheric circulation and convective transport while $PM_{2.5}$ aviation impacts were influenced by localized precursor emissions near urban regions.

The chemical processing and physical transport of aircraft emissions is heavily influenced by grid resolution. The use of a model that was 9 times more finely resolved horizontally made significant changes in the magnitude and location of AAC. The fine resolution (36-km) application at regional-scale captured the non-linearities in chemistry that are not captured by the coarser resolution; however the use of a hemispheric scale (108-km) captures the intercontinental transport. Future studies should consider these changes in model implementations for studying aviation emissions. Therefore, running a nested fine scale near major aviation source regions (NA, EU and EA) in a global/northern hemispheric model might capture both the fine-scale and global scale intercontinental, transport and chemistry processes in a more efficient manner. One of the limitations of this study is the absence of stratospheric chemistry in CMAQv5.0.2, which explains the model underpredictions near the UTLS region in our model evaluation. The presence of stratospheric chemistry in the UTLS region can also affect the NO_x and HO_x radical budgets that in turn influence the model predictions for O_3 and $PM_{2.5}$. Eastham et al., (2014) demonstrated the importance of stratospheric chemistry in upper altitudes (16 – 20 km) and showed how the unified stratospheric tropospheric chemistry reduced the overall global ozone column discrepancy from 9.9% to 3.6%. Therefore not including detailed stratospheric chemistry in the model can influence the radical budget and oxidative capacity of troposphere, which can introduce uncertainties in the upper few model layers. Here in our study we do not have stratospheric chemistry for accurate representation of lower stratosphere, however we do have the tropospheric chemistry occurring in the model upper layers, so it can still account for the fundamental ozone, NOx photolysis reactions in the UTLS region. Future studies should consider these changes in modeling implementations to further improve our understanding of aviation-attributable air quality impacts.

CHAPTER 4: TRACER STUDY TO ESTIMATE THE TRANSPORT OF CRUISE ALTITUDE AVIATION EMISSIONS IN NORTHERN HEMISPHERE

4.1 Introduction

Aviation is one of fastest growing modes of transportation with a unique 4D emissions profile and the only anthropogenic source that emits pollutants directly into higher altitudes. Aviation emissions that occur between 9 – 12km are considered as cruise altitude emissions (CAAE). The CAAE contributes ~ 60 – 75 % (Wilkerson et al., 2010; Olsen et al., 2013) of the total aviation emissions (in terms of NOx, fuel burn) and dominate by ~ 75% (Yim et al., 2015) of model predicted total aviation premature mortalities. These emissions are directly released into upper troposphere and lower stratosphere (UTLS) region where the atmospheric conditions differ from that of surface. Some conditions such as larger residence times, lower background pollutant concentrations, lower temperature and larger radiative efficiency (Schumann 1997) make aviation an important emission source in UTLS region. It is also crucial to attribute the role of UTLS physical processes in characterizing the emitted pollutants fate and transport (Toohey et al., 2010). Additionally, chemical budgets are also highly influenced by atmospheric transport processes in the UTLS region. Prior studies (Liang et al., 2009; Cooper et al., 2011; Lin et al., 2014) highlighted that pollutant levels increase in highly convective areas and downwind sites due to transport mechanisms and circulation patterns. Therefore, better understanding of the influence of transport processes on the overall impacts of an emission source is very essential. Few aviation related studies (Tarrason et al., 2002; Lee et al., 2013) also predicted that the air quality impacts from CAAE emissions at surface are relatively higher than due to landing and takeoff (LTO, emissions below 3000ft) emissions. These studies raised the question about the

involvement and role of transport (physical) processes on the impact of CAAE emissions to near the surface.

Many modeling studies (Unal et al., 2005; Arunachalam et al., 2011; Woody et al., 2011; Vennam et al., 2015) investigated the aviation-attributable perturbations due to aircraft emissions (LTO and CAAE) at local, regional to global scales and their role in causing human health effects (Stettler et al., 2011; Levy et al., 2012; Koo et al., 2013; Yim et al., 2015). The traditional way to assess the impacts of any individual emission source in atmosphere is to calculate differences between 'with emission source (perturbed)' and 'without emission source (unperturbed)' modeling scenarios. However, with this approach, we cannot tease out the effect of physical and chemical processes individually on the overall emissions source impacts in chemistry-transport model. To attribute the effect of transport process solely, an inert tracer modeling approach was implemented previously in few early chemistry-transport studies (Alapaty and Mathur 1998; Allen et al. 1996). In these studies, all the atmospheric processes except for transport processes are turned off. This approach is computationally efficient and gives us the opportunity to characterize the transport pathways of emitted source. Various lagrangian trajectory models (Schoeberl and Morris 2000; Stohl et al. 2002) as well as chemistry transport and circulation models (Koch et al., 1996; Li and Chang, 1996) were previously used to conduct these tracer-based simulations. This inert tracer modeling approach was also used in testing the mass conservation (Hu et al., 2006) and vertical mixing characterization (Gerbig et al., 2008) in atmospheric models. Some of the recent studies (Wang et al., 2014; Jiao and Flanner 2016) implemented tracer-tagging technique in global chemistry transport model to quantify source-receptor relationships and transport pathways of black carbon (BC) aerosol. Hence, here

in this study we implemented the same approach to study the transport of CAAE and to understand the source-receptor relationships.

Till date, very limited studies have looked at the transport of aviation emissions in the UTLS region. An earlier study (Wauben et al., 1997) pointed out that passive transport studies could reproduce the general pattern of aviation NOx perturbations. Van Velthoven et al., (1997) looked at the transport of aviation NOx passive tracer in ensemble of models ranging from two-dimensional to three-dimensional chemistry transport and global models. This study indicated that horizontal transport is more efficient in winter season and vertical transport is efficient during summer season. They also illustrated that the vertical exchange processes show minor contribution to NOx concentrations at varying altitudes and all the models well captured these trends. Lastly, the authors clearly specified few limitations that some of the models used in this study lacked parameterization of convective transport, which is crucial for vertical transport and need to be considered in future studies. Efforts (Forster et al., 2003) have also been made to study the residence times of aircraft emissions by using Lagrangian dispersion model. This study indicated that the North Atlantic Flight Corridor (NAFC) emissions are transported in the northeasterly direction towards polar region with maximum occurring over Europe and North Africa. This study specifically studied only the NAFC stratospheric (above tropopause) aircraft emissions and considered Measurement of Ozone and Water Vapor by Airbus In-Service Aircraft (MOZAIC) campaign flight tracks which does not cover the complete aircraft inventory in that region. This approach worked for the question that the authors tried to address but will not provide generalized overall hemispheric scale CAAE transport. Moreover, even this study did not consider deep convection and turned it off to reduce the computational time. However, recently Hauglustaine et al., (2012) concluded that by using a deep convection in the model, they

observed ~10 - 30% change in surface ozone associated with aircraft emissions. This illustrates the role and importance of deep convection transport scheme in the models while studying higher altitude emissions. From past few years, global as well as regional models transport schemes were adequately tested and the uncertainty in the formulations were reduced. Therefore, it is beneficial to address this issue with recent modeling platforms and updated transport calculation schemes.

A recent study (Whitt et al., 2011) conducted passive tracer simulations by placing CAAE at ~ 11km in the GATOR (Jacobson et al., 2011) global model with $4^{o} \times 5^{o}$ horizontal resolution. Their findings concluded that the extra-tropical cruise altitude emissions do not directly affect surface air quality through dynamical vertical mixing processes alone. This study strengthened the hypothesis that the chemical and wet removal processes lifetimes are much shorter than the vertical mixing processes, hence CAAE do not transport to surface directly through dynamical processes. However, uncertainties still exists with assessing the aviation (CAAE + LTO) attributable perturbations and their health impacts (Morita et al., 2014:406 deaths; Jacobson et al., 2011: 620 deaths; Yim et al., 2015: 16000 deaths) near the surface. Given these widely varying findings, on the first hand the transport of CAAE to the surface needs to be further investigated with fine model resolution (both horizontal and vertical) (Klich and Fuelberg 2014) to improve the understanding of the air quality impacts and mortality attributed to aviation sector.

In this study, we characterized the role of dynamic processes in transporting the CAAE to the surface and seasonal distribution associated with those processes by conducting passive tracer simulations. Compared to previous studies our study is a new experimental setup with different methodology, in terms of continuous tracer emissions, no decay rate (seasonal runs) and

a relatively fine model grid resolution. These conditions make this an idealized as well as worst-case scenario tracer test to quantify the amount of CAAE transported to the surface with maximum emission input and zero loss. Clear evidence was already shown in prior studies (Land et al., 2002; Rauscher et al., 2010; Klich et al., 2014; Gan et al., 2016) regarding better representation of model processes at fine vertical and horizontal resolution. Therefore, studying the aviation CAAE tracer at fine resolution will advance our understanding of the processes influencing the CAAE emissions near UTLS region. Vennam et al., (2016, In preparation) also addressed the better prediction of aviation impacts at hemispheric resolution when compared to other global models and suggested the need to understand the role of transport at this resolution.

Given the increasing aviation emissions trends in developing regions (Wasiuk et al., 2016) at rapid rate, it is important to understand the intercontinental transport involved among developed and developing regions to address any potential future mitigation strategies in aviation sector. To quantify the intercontinental transport, we also tagged the emissions in three key high aviation activity regions such as North America (NA), Europe (EU) and East Asia (EA) and conducted tagged tracer simulations. To our knowledge, for the first time tagging tracer simulations for aviation emissions were conducted in this study to illustrate the intercontinental transport role. From these modeled tracer simulations we quantified the fraction of the source emissions near receptor regions.

4.2 Methodology

4.2.1 Tracer Model

The state of the art Community Multi-Scale Air Quality (CMAQv4.7.1) chemistry-transport model (Byun and Schere 2006) was used for hemispheric (108 × 108 km^2, HEMI) scale application, the spatial extent of the domain and typical monthly NOx emission distributions for

key sub regions (NA, EU, EA) are shown in Figure 4.1. We carried out tracer transport simulations by completely turning off chemical process in the model and focusing mainly on the transport processes. To do this we made a new tracer mechanism in the source code (.EXT files) and considered only the NOx species as the species list in all processes. For transport schemes, we used Yamartino (YAMO) (Byun and Schere 2006) scheme for advection process and Asymmetric convective mechanism (ACM2) (Pleim 2007a) scheme for diffusion process. The ACM2 vertical mechanism has been evaluated (Pleim 2007b; Tang et al., 2011) and used in various modeling applications. As mentioned in Pleim et al., (2007a), ACM2 is convective model combined with eddy diffusion scheme that can better represent even sub-grid scale components of turbulent transport.

4.2.2 Model Inputs and Specifications

We used NASA's Modern-Era Retrospective Reanalysis (MERRA) (Rienecker et al., 2011) meteorology downscaled data as inputs to Weather Research and Forecasting model (WRF) (Skamarock et al., 2008) model to generate meteorology data. We used a fine scale vertical resolution for our modeling and improved the vertical structure to 44 model layers instead of the traditional 34 (or even 17) layers CMAQ regional scale modeling. We generated gridded aviation emissions from FAA's Aviation Environmental Design Tool (AEDT) (Roof et al., 2007; Wilkerson et al., 2010) raw data by using a processing tool that spatially and temporally allocates the data. In this study, as our focus is mainly on cruise altitude aviation emissions we zeroed out all emissions other than the aircraft emissions in model layers (ranging from 33 – 38) that falls in the cruise altitude range of 9 – 12 km. We considered NOx as a passive tracer, which is chemically inert and undergoes only transport processes in our tracer modeling. Instead of considering random emission mass we considered actual cruise altitude

NOx emissions, to capture the spatial and temporal variation of aviation emissions. As NOx is one of the highly emitted pollutant at cruise altitudes from aircraft, therefore we considered NOx as our proxy for the cruise altitude emissions.

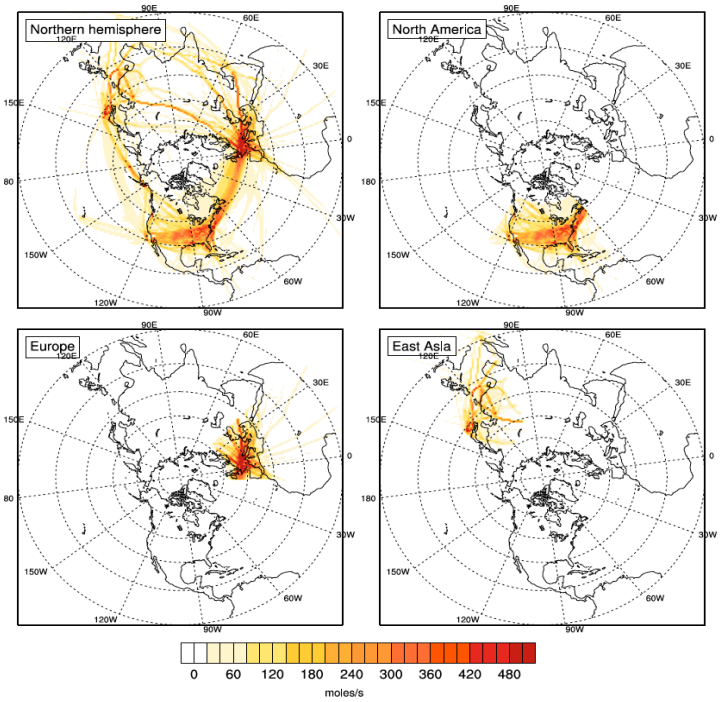

Figure 4.1: Hemispheric modeling domain with cruise altitude emissions distributions for complete northern hemisphere (top, left). Also shown are the tagged cruise aviation emission scenarios for North America (top, right), Europe (bottom, left) and East Asia (bottom, right).

Using these emissions, we ran tracer simulations continuously for three months modeling period by constantly adding emissions at cruise altitudes. In other words, we restarted the model run freshly for every three months, for example each season was categorized into consecutive three months (winter: DJF (December – February), spring MAM (March – May), summer: JJA (June – August), autumn: SON (September – November)). The reasons for considering this approach are: 1) to provide sufficient time period (typical time 3 months: ~ 90 days) for the tropospheric mixing to occur at hemispheric scale 2) to isolate the issue of accumulation in the model as we did not consider any decay rate in our tracer runs 3) this approach even enables us

to look at the tracer transport processes on seasonal basis as we are doing a fresh initialization for each season. The vertical transport of pollutants from PBL takes 1-2 days to reach the surface, from mid-troposphere it takes ~ 1 week and from tropopause it takes ~ 1 month. The horizontal transport in subtropics takes ~ 2 weeks and the transport from subtropics to tropics or towards poles takes ~ 1- 2 months (Jacobs, 2004). Stohl et al., 2002 clearly indicated that intercontinental transport occurs on timescales of 30 days and 90 days (Liang et al., 2009) to transport from lower stratosphere to lower troposphere. Liang et al., 2009 clearly demonstrated that it takes one month to cross the tropopause, one month to transport from upper troposphere to middle troposphere, and another month to get transported to lower troposphere. Therefore, taking into consideration these timescales from literature we considered 90 days as our simulation period for tracer modeling to capture intercontinental, cross tropopause, and upper troposphere to lower troposphere transport processes.

Another set of tracer simulations were carried out in hemispheric domain by tagging the three major aviation emissions contributors North America (NA: 20N – 60N, 130W – 60W), Europe (EU: 20N – 60N, 10W – 60E), East Asia (EA: 20N – 60N, 100E –150E). We considered emissions that fall in the spatial bounds of these three sub-regions and in cruise altitudes and tagged them with the specific region name (for example: NO_NA, NO_EU, NO_EA) to perform our source-receptor tracer simulations. We conducted these simulations for three months modeling period for each season by constantly adding emissions for each three sub-regions.

4.2.3 Analysis metrics

We carried out quantitative analysis using the metrics discussed here to study the CAAE tracer transport. We calculated mass fraction (MF) in each model layer (in other words different altitudes in the atmosphere) as shown in equation 4.1 which defines the amount of mass present

in each layer for each month with respect to the total mass available in the model domain (Column Burden). For the total mass available in the domain we calculated the total column burden (molecules/cm^2) by integrating the concentrations (ppbV) available in all model layers. For individual layer mass we converted the mixing ratio into mass (molecules/cm^2) by multiplying by the density of air and layer height differences. This metric indicates the amount of tracer transported from cruise altitude to different altitudes.

$$\text{Mass Fraction}\left(\text{MF}_{\text{layer}}\right) = \frac{\text{Mass}_{\text{layer}}}{\text{Column Burden}} \times 100 \qquad (4.1)$$

In order to study the source-receptor relationships we implemented one other metric as mentioned in Wang et al., 2014. We calculated fractional tracer contribution of the source region emissions at receptor region. Here we considered the tracer column burden as our property to analyze the source-receptor relationship. The contribution metric is calculated by taking the ratio of column burden of the source (i) in the receptor region (j) with respect to the total column burden in receptor region from different sources (N = 3 sources (NA, EU and EA)).

$$\text{Contribution}_{\text{i,j}} = \frac{\text{Column Burden}_{\text{i,j}}}{\sum_{\text{i=1}}^{\text{N}} \text{Column Burden}_{\text{i,j}}} \times 100 \qquad (4.2)$$

4.3 Results

4.3.1 Tracer surface distribution

The tracer simulations are run over a three-month period corresponding to seasons with a fresh initialization for beginning of each season. In other words, we let the tracer model run continuously for 90 days. Throughout our calculations, other than where we specifically

mentioned each month, we considered the last month as our representative month for that season. Therefore throughout the results whenever we say season it means the last month in that 90 days run.

In this section, to study the surface tracer distribution we calculated surface mass fraction percentage using Equation 4.1. When averaged across the domain, as shown in Table 4.1, the winter season (0.23%) is ~ 1.6x higher when compared to summer months (0.14%). The winter is followed by autumn (0.21%) and spring (0.18%), both showing ~1.5x and ~1.2x higher than summer average MF.

Table 4.1: Domain wide averaged surface mass fraction percentage for each season

Season	**Surface Mass Fraction %**
Winter	0.23
Spring	0.18
Summer	0.14
Autumn	0.21

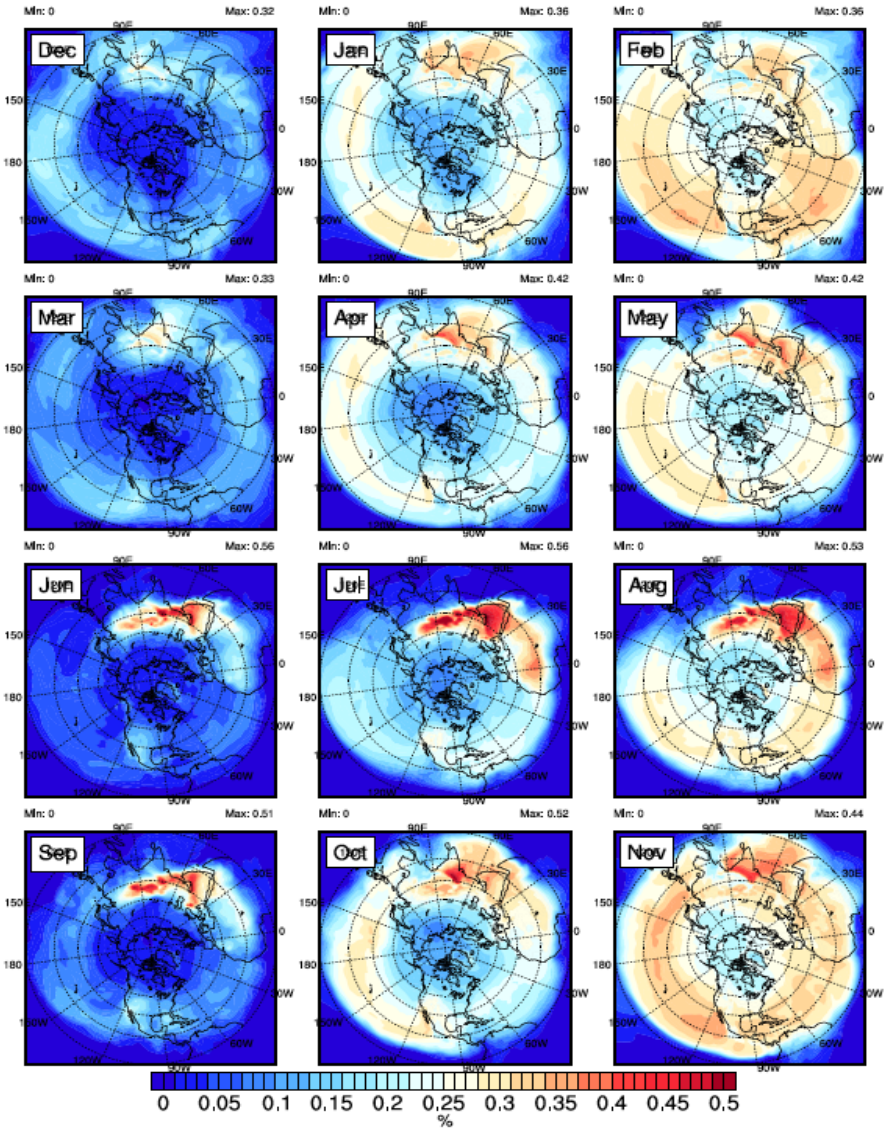

Figure 4.2: Tracer surface mass fraction percentage with respect to the total mass available in the each month. Each row is a single simulation where tracers were reset to zero at the first month of each row and represents each season.

Figure 4.2 shows spatial distribution of the surface mass fraction percentage for all months. Throughout all the seasons (each row in Figure 4.2), the maximum tracer MF near the surface with respect to the total mass available in the model domain is < 0.6%. The maximum tracer surface MF of ~ 0.5% occurred at over the Tibetan Plateau and Middle East region in summer months, whereas in winter season the maximum MF is slightly lower ~0.3%. In summer

months, the higher tracer concentrations near Middle East and Eastern Mediterranean regions could be due to the tropopause folds (Akritidis et al., 2016) and tracer getting trapped in the subtropical high that descends near Middle East (Stohl et al., 2002) due to downwelling. This transport pathway is consistently seen during summer months that indicated sink process near this region. Though the maximum tracer surface MF is higher in summer the overall average tracer mass near the surface is high during winter (as shown in Table 4.1). During summer season the tracer transport occurred mainly at high convection regions, which produced maximum tracer concentrations near these regions. During winter season, as it is more dominated by horizontal transport due to high westerlies near higher altitudes, and globally relatively more tracer mass was transported to the surface.

4.3.2 Tracer vertical distribution

We calculated the mass fraction throughout the model vertical altitudes to understand the transport in the free and upper troposphere regions. Throughout the vertical analysis to discuss the results we keep referring to regions that fall in these altitude bins: 13 – 20 km (UTLS), 9 – 12 km (cruise altitude region, CA), 3 – 8 km (mid-troposphere, MT), 0.05 – 3 km (lower troposphere, LT) and surface. Figure 4.3 shows the vertical profiles of three months binned by each season for all model altitudes. Recall the first month tracers are set to zero. During the first month in each season, 45 (summer) – 50 (winter)% of tracer still remains at cruise altitude region and after 30 days it decreased to 28 – 40%. This change in contribution shows the average transport time of ~1 month near tropopause and cruise altitude region, similar results are also shown in Liang et al., (2009). During winter and autumn seasons, after 3 months, 10 – 11% of the tracers transported to UTLS, 23 – 29% of tracer remained in CA, 37% transported to MT and 18 – 23% transported to LT. During spring and summer season, after 3 months, 14 – 17% of

tracer transported to UTLS, 32 – 36% of tracer remained in CA, 33 – 36% appeared in MT and 11 – 15% occur in the LT region. These seasonal differences indicate that during winter, transport of CAAE tracer to mid-troposphere is higher than compared to summer. In summer, the transport of tracer to UTLS region is slightly higher than compared to winter and other seasons due to more upward flux. This vertical analysis illustrates that significant portion of tracer is transported to MT and UTLS region with only 0.2 – 0.5% tracer mass reaching the surface even after 90 days of simulation.

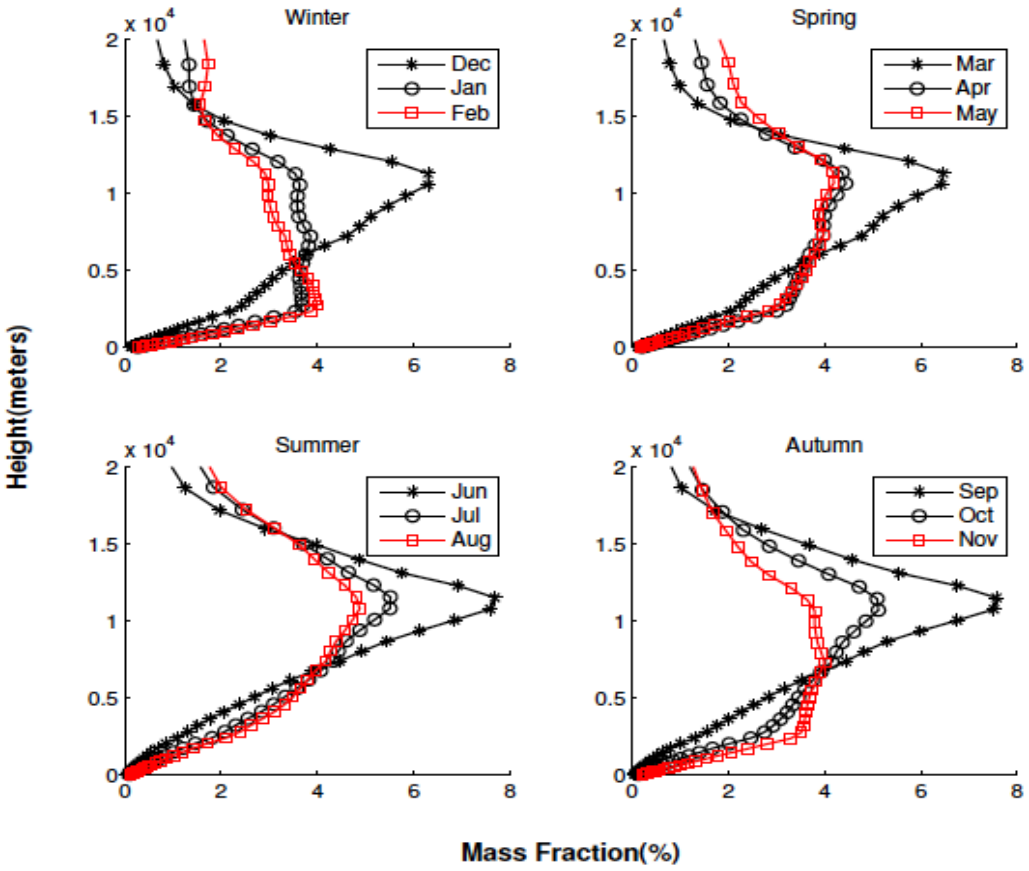

Figure 4.3: The amount of tracer (%) in each model vertical altitude (points on the line) with respect to the total mass available in the model domain for each month in a season.

Figure 4.4 shows the zonal vertical distribution of tracer mixing ratio last month in each season simulation. The tracer data were binned into three latitude bands: tropics (0 – 30 N), sub-

tropics (30 – 60 N) and artic (60 – 90 N) regions. Further the data were binned by altitudes. Consistently in all seasons, the sub-tropics and arctic regions have higher tracer concentrations in CA region and UTLS, since most of the cruise altitude emissions occur in these regions. In the tropics, tracer concentrations are lower in CA than compared to sub-tropics and arctic region due to relatively lower aviation activity. However, as we reach lower altitudes and come close to the surface the tracer concentrations showed an increasing trend in the tropics, indicating that some of the sub-tropics CAAE tracer is transported to tropics. We observed that tracers in upper altitudes are mainly driven by horizontal transport that is followed by vertical transport along isentropes near large downward flux convection regions.

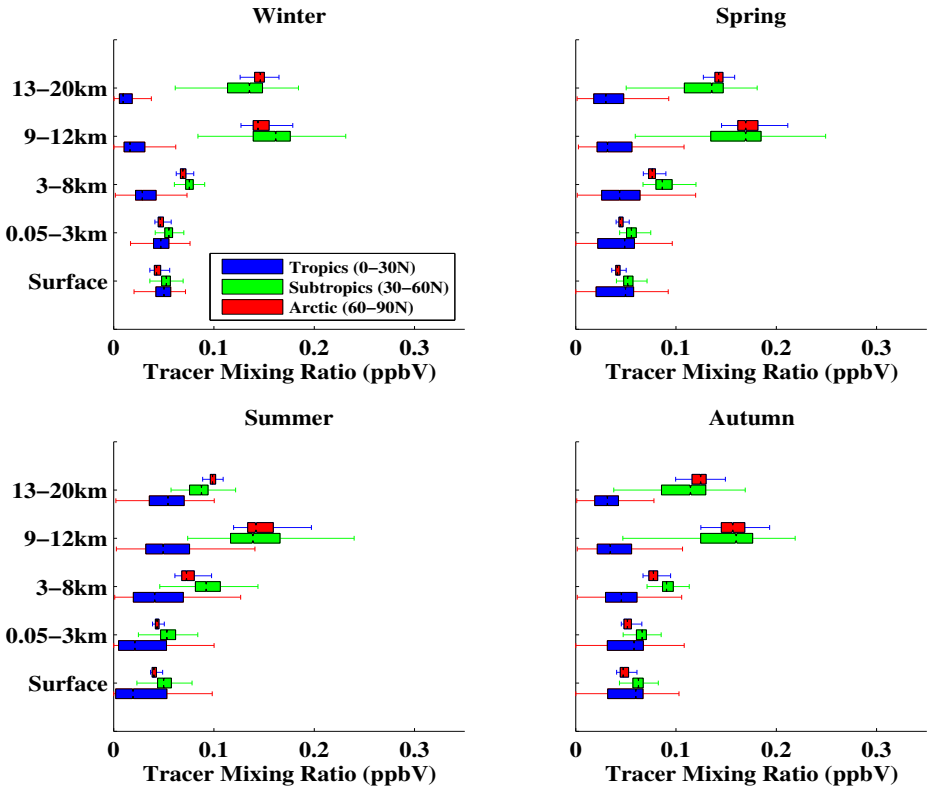

Figure 4.4: Tracer mixing ratios for the last month in each 90 day simulation. Each box plot represents the tracer mixing ratios for all horizontally grid cells containing latitude bins of 0 – 30N (blue), 30 – 60N (green), and 60 – 90N(red). The tracer mixing ratios are further binned vertically by altitudes.

4.3.3 Source-receptor distributions

In this section we discussed the results from simulations where tracers were tagged from three sub-regions: North America (NA), Europe (EU), and East Asia (EA) and run for 90 days.

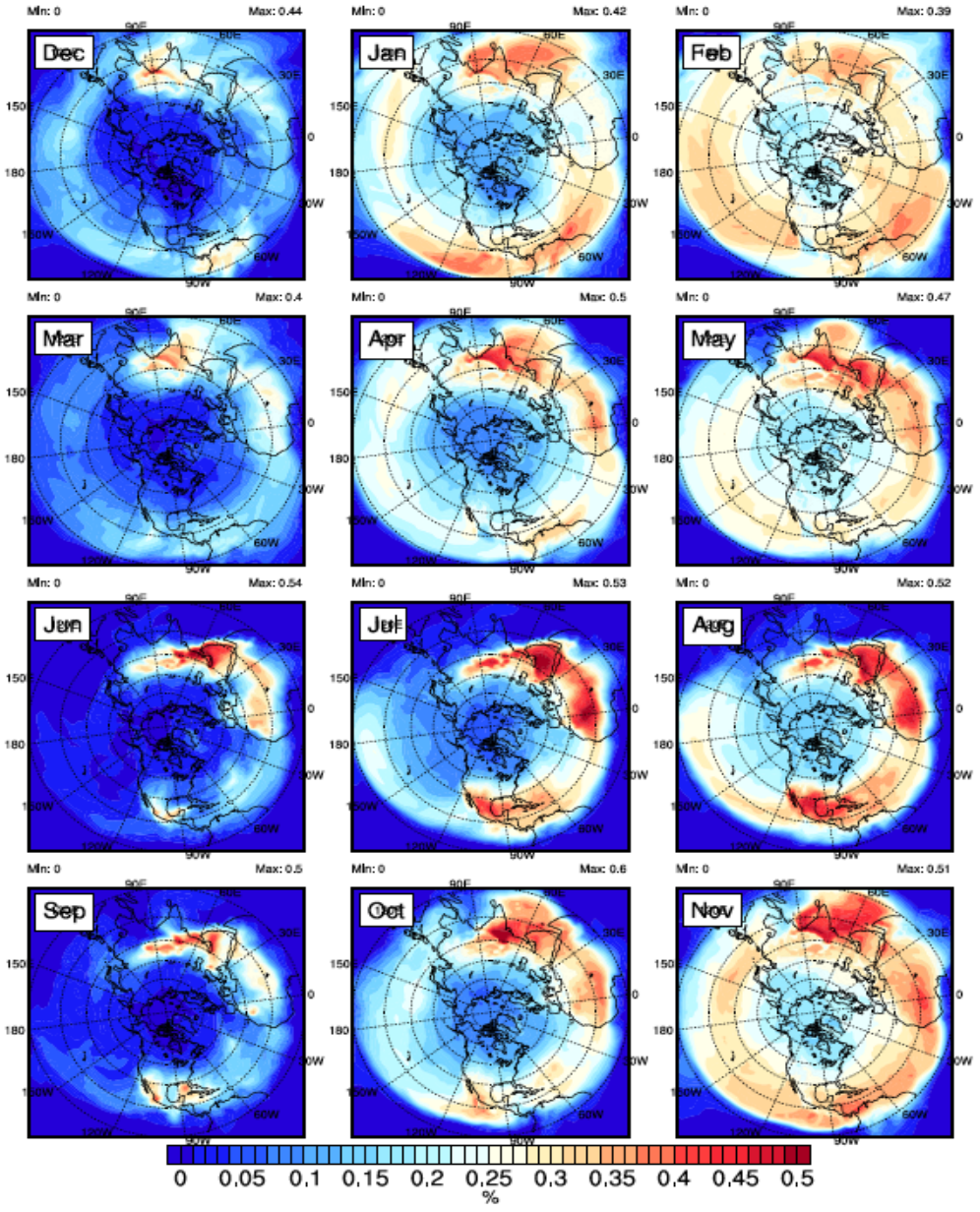

Figure 4.5: North America tracer surface mass fraction percentage with respect to the total mass available in the model domain for each month. Each row is a single simulation where tracers were reset to zero at the first month of each row and then ran for 3 months in each season.

Figure 4.5 shows the spatial distribution of tracers released from NA for all 3 months in each season. The figure shows that the more tracer MF predominantly occurs mainly in the downwind continents. During winter, spring, and autumn seasons higher tracer MF percentage in the range of 0.4 – 0.5 % mass fraction occurred mainly near India, Indian Ocean and further towards tropics. During summer higher tracer MF percentage (0.4 – 0.5%) mainly occurred near Mexico, North Africa and Middle East. Only in summer, due to high convection NA tracer was transported to western and southern NA than compared to other seasons. Though most of the NA cruise altitude tracer emissions occurs in the 30 – 45 N, we observed that tracer was transported to the surface towards 0 – 20 N latitude band.

Figure 4.6 shows the spatial distribution of tracers released from EU for all 3 months in each season. Similar to the NA tracers, the EU tracers shows higher MF percentage near South East Asia, Tibet Plateau and Middle East. The EU tracer surface maximum MF percentage (0.8%) is ~2x higher than the NA tracer particularly in summer near Tibet Plateau and Middle East. During summer and autumn seasons, a maximum of ~1.2% appeared in these regions in the first month itself. One interesting trend to be noticed is EU tracer (0.3 – 0.4%) was transported to western NA particularly in winter and autumn seasons through trans-pacific synoptic transport due to strong westerly transport in cruise altitude region.

Figure 4.7 shows the spatial distribution of tracers released from EA for all 3 months in each season. Unlike NA and EU where the surface maximum MF is observed during summer, here in EA the maximum MF percentage of 0.4% occurred in the Pacific region during spring season. This strong westward transport in spring from EA was already observed in previous studies (Lin et al., 2012) and we are seeing the similar pattern with EA CAAE tracer.

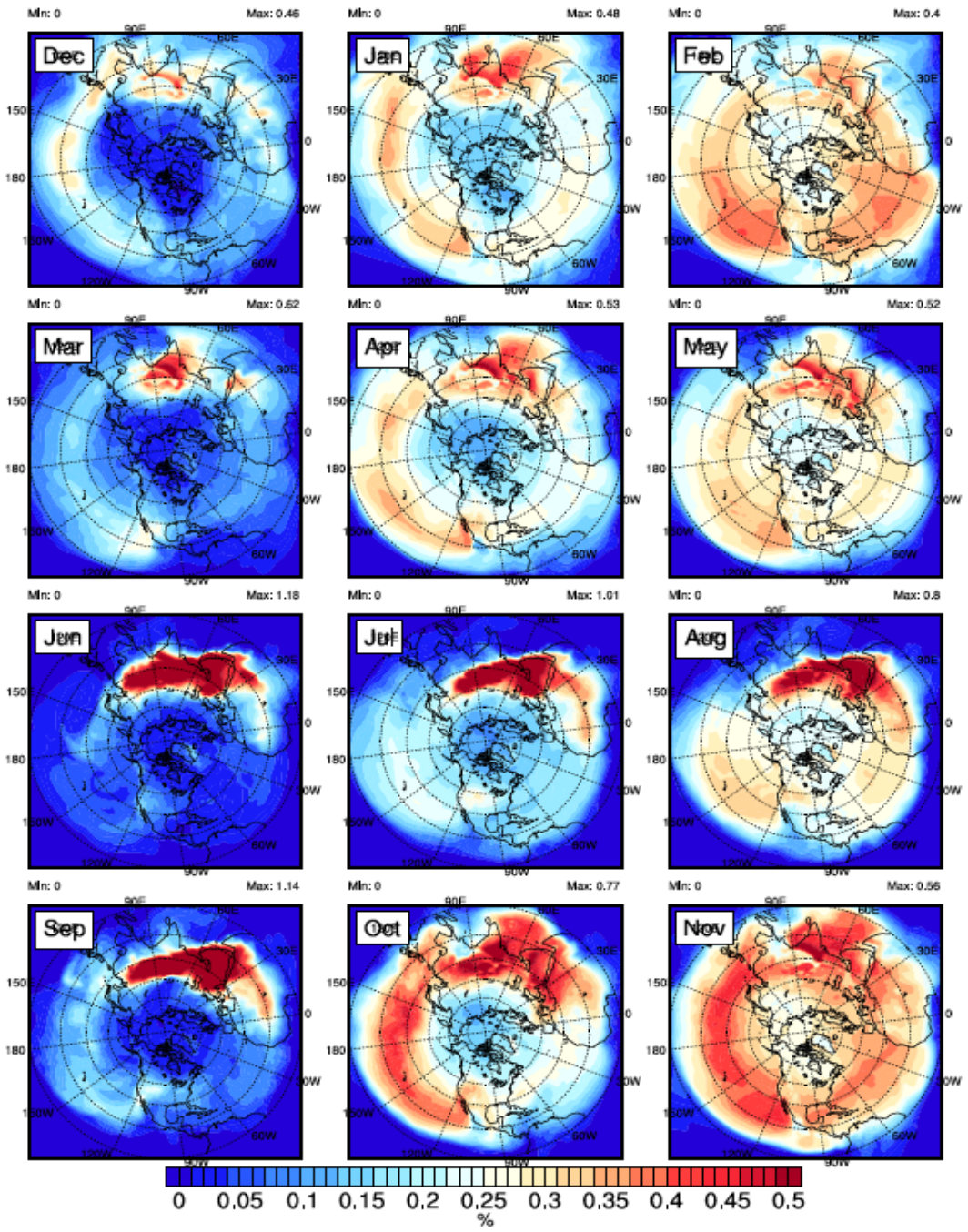

Figure 4.6: Europe tracer surface mass fraction percentage with respect to with respect to the total mass available in the model domain for each month. Each row is a single simulation where tracers were reset to zero at the first month of each row and then ran for 3 months in each season.

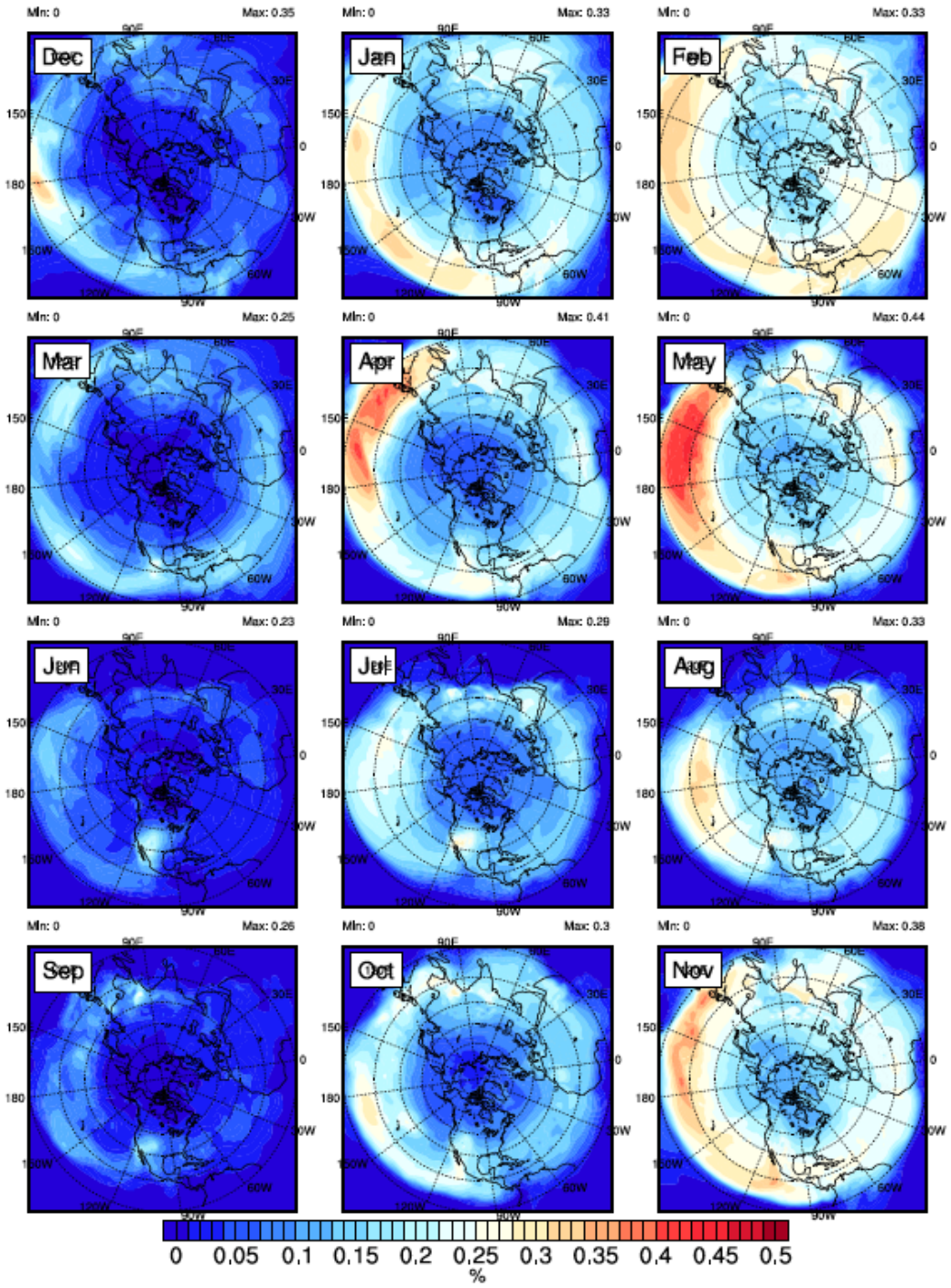

Figure 4.7: East Asia tracer surface mass fraction percentage with respect to the total mass available in the model domain for each month. Each row is a single simulation where tracers were reset to zero at the first month of each row and then ran for 3 months in each season.

Table 4.2: Tracer source-receptor contribution metric (Equation 4.2) for four seasons of North America (NA), Europe (EU) and East Asia (EA) sources.

	NA Receptor		
Source	**NA**	**EU**	**EA**
Winter	51	28	21
Spring	50	30	19
Summer	69	21	11
Autumn	46	34	19
	EU Receptor		
Source	**NA**	**EU**	**EA**
Winter	45	40	15
Spring	48	36	15
Summer	45	46	9
Autumn	43	41	16
	EA Receptor		
Source	**NA**	**EU**	**EA**
Winter	45	31	24
Spring	45	33	22
Summer	29	40	31
Autumn	40	37	23

Table 4.2 shows the contribution of the three source regions near the receptor regions calculated using Equation 4.2. In NA receptor region, 46 – 50% of NA contribution is due to NA tracer emissions and the remaining 28 – 34% and 19 - 21% is due to EU and EA tracer emissions in all seasons except in summer. In summer, 69% is due to NA emissions with the remaining 21% and 11% contributions incurred from EU and EA tracer emissions. This high contribution in summer is mainly due to the transport of NA emissions to the surface near high convection regions like western NA. In EU receptor region, 43 – 48 % contribution is due to NA source followed by 36 - 41% and 15% contributions from EU and EA sources for all seasons except summer. During summer, both NA and EU tracer shows equal contribution of 45% and EA

shows 9% in EU receptor region. This highlights that in EU, the influence from NA is prominent in all seasons due to strong westerly transport. In EA receptor region, 40 – 45% contribution occurred from NA and 33 – 37% contribution came from EU source followed by EA source with 22 – 24% in all seasons except summer. In summer, the NA source contribution decreased to 29% whereas EU and EA contribution increased to 40% and 31%.

Throughout all three receptor regions, their own source contribution increased in summer season indicating the influence of vertical transport due to relatively high convection when compared to all other seasons. During winter and spring seasons, the downwind source region contributions are higher indicating the influence of horizontal transport. These results are comparable to findings mentioned in Van Velthoven et al., 1997, however here we illustrated the intercontinental transport in detail by calculating contribution for individual key source regions considered in this study.

4.4 Conclusions

In this study we implemented a tracer approach to understand the role of physical processes in transporting cruise altitude aviation emissions in the atmosphere using a high resolution modeling platform. Overall model predictions indicated < 0.6% of CAAE in the total column was transported to the surface in northern hemisphere for all seasons. This is similar to the results reported by Whitt et al., (2011) concerning the distribution of CAAE. Winter season shows higher proportion of tracer mass near the surface than summer season, summer season showed maximum tracer near high convection regions. These predictions showed that most of the tracer still exists in the mid-troposphere and upper troposphere during all seasons. CAAE tracers tended to concentrate in sub-tropics and arctic region at cruise altitudes. As we approach

the surface, however, tracer concentrations began to increase in the tropic regions. This is the result of the model transporting CAAE tracers from the sub-tropics towards the tropics.

From our source/receptor analysis we found that both NA and EU are primarily impacted by their own emissions. Overall we see that NA source emissions can significantly affect EU and EA regions in all seasons, and both NA as well as EU source emissions can affect EA region. Our intercontinental tracer study showed evidence that NA and EU cruise emissions can show impacts near high terrain regions like Tibet Plateau and places with relatively lower aviation emissions regions such as UAE, North Africa, India and South East Asia. This partly explains some of the aviation-attributable high mortality estimated by Barrett et al., (2010) in Asia. Here we studied the role of dynamic processes, to further improve our understanding, it is also beneficial to study the chemical processes role in UTLS region as future work. Lastly, considering recent version of CMAQ model to take advantage of the recent model updates for any of this future work is highly suggested.

CHAPTER 5: CONCLUSIONS

The overall objective of this dissertation is to quantify the aviation-attributable perturbations at multiple scales and improve the assessment of aviation air quality impacts using a chemistry transport model. To achieve this objective, we conducted CMAQ modeling simulations from fine scale (4×4 km^2) focusing near an airport to hemispheric scale (108×108 km^2) focusing on the overall northern hemisphere. In this research we tested our central hypothesis through use of a finer spatially resolved model to characterize aviation impacts on air quality and quantified an improvement in model performance when compared with observations. Overall we showed the importance of fine scale resolutions for modeling applications at local (near an airport), regional (continental U.S.) and hemispheric scales. Firstly, we quantified the aviation-attributable hazardous air pollutants (HAPs, air toxics) near an airport and showed improvement in model performance with fine scale (4×4 km^2) when compared with coarse resolution (36×36 km^2), using observations from a field study at the airport. Secondly, we studied the full-flight aircraft emissions impacts on O_3 and $PM_{2.5}$ near the surface and showed the influence of grid resolution on aviation impacts between 36×36 km^2 and 108×108 km^2 scales. Lastly, we focused mainly on the cruise altitude aviation emissions (CAAE) and looked at the role of dynamic processes in transporting CAAE to the surface. We addressed these three key research areas related to aviation emissions that required further investigation to advance the scientific understanding of aviation-attributable air quality assessments.

In our first study, we carried out fine scale modeling and studied the spatio-temporal variability of aviation-attributable HAPs near a medium-sized airport (PVD: Providence T.F. Green, Rhode Island). We used FAA-EPA developed new aircraft specific speciation profile to generate HAPs emissions near the airport, which is one of the significant update we made in this HAPs modeling. Results demonstrated that modeled aircraft-attributable contributions near a medium-sized airport such as PVD are in the range of 2 – 4% and 19 – 28% for key HAPs such as formaldehyde and acrolein. The maximum impacts are seen only within 4 – 16km from the airport grid cell. Comparison of fine (4×4 km^2) and coarse (36×36 km^2) resolutions showed a 5 – 20% reduction in error with fine scale when evaluated with HAPs observations from a measurement campaign held near PVD airport. Our comparison of fine scale CMAQ model predictions with data from the U.S EPA's National Air Toxics Assessment (NATA) showed similar mean concentrations. This provides further evidence that the fine scale CMAQ model predictions in the vicinity of airport can be utilized to calculate health risk assessment from aviation-related HAPs. Nevertheless we showed that underprediction of HAPs exists with different modeling platforms and we think this is mainly due to the underprediction of secondary contribution in chemistry transport models such as CMAQ.

Current estimates of HAPs are a challenge for modeling systems and refinements to simulate aircraft emissions have made only incremental improvements. Two key areas that need to be addressed in near future are improvement of HAPs secondary formation in CMAQ and additional monitoring campaigns near airports to measure aviation-related HAPs. Regarding the uncertainties in secondary contribution of HAPs (such as formaldehyde, acetaldehyde and acrolein), studies (Luecken et al., 2011) stressed that it is mainly due to improper representation of primary precursor emissions (isoprene and VOCs) and their chemistry. To perform extensive

model evaluation more measurements are also necessary near various busy airports to completely understand the model performance and the HAPs impacts in the vicinity of the airport. Measuring HAPs is also a key challenge at ambient conditions as they are highly reactive (Cahill et al., 2015), limitations still exists with reliability and consistency of these measurements. Lastly, in the 4×4 km^2 scale modeling conducted for this study, most of the airport emissions occurred in a single grid cell. However the HAPs emissions are high during idling stage and decreases during takeoff stage. Therefore, it may be further beneficial to conduct modeling at an even finer scale (2×2 km^2 or 1×1 km^2) for better modeling of aircraft HAPs emissions in the immediate vicinity of the airport.

In the second study, we shifted our focus to full-flight aviation emissions (landing and takeoff, and cruise altitude emissions) and quantified the perturbations of O_3 and $PM_{2.5}$ at hemispheric scale. Based on domain-wide averages in hemispheric domain, full-flight emissions contributed ~1.3% and 0.2% of O_3 and $PM_{2.5}$ respectively at the surface, which increased to ~2.5% and ~3% in upper altitudes. Overall, the spatial distribution shows that O_3 aviation impacts were driven by atmospheric circulation and convective transport while $PM_{2.5}$ aviation impacts were influenced by localized precursor emissions and Ammonia (NH_3) emissions. Our comparison of coarse (108×108 km^2) and fine (36×36 km^2) scale aviation-attributable perturbations in North America (NA) showed decrease in aviation impacts with fine scale at the surface, as fine scale captured some of the non-linearities in the chemistry such as titration of excess NO_x near airport and urban areas. The model error reduced by ~7% for O_3 and ~25% for $PM_{2.5}$ with fine resolution when compared to coarse resolution in NA domain against surface observations. In UTLS, the model error decreased by ~5 – 11% for NO_2 with full-flight emissions and fine scale resolution when compared to model predictions without full-flight

emissions and coarse resolution. We computed seasonal aviation-attributable mass flux vertical profiles and aviation perturbations along the isentropic surfaces to quantify the transport of cruise altitude emissions at hemispheric scale. With this analysis we showed that the winter perturbations are higher due to the downward flux. Yet, as the model undergoes chemistry and transport simultaneously we were not able to individually attribute the role of the transport on CAAE. Therefore, it is important to clearly understand the role of various atmospheric processes to attribute the transport processes influence on CAAE, which was studied in Chapter 4.

There are few limitations associated with second study (Chapter 3) modeling framework such as lack of stratospheric chemistry in CMAQv5.0.2 (latest version available at the time of research) that affects the ozone and hydroxyl chemistry in upper altitudes, and thus introduces some level of uncertainty in the UTLS model predictions. Another key limitation in hemispheric scale CMAQ is the use of lightning NOx empirical emission calculation update that has been fully tested for U.S applications, but not at hemispheric scale. These limitations can change some of our model predictions in the upper altitudes but will change our surface air quality predictions to a relatively lesser degree. As more efforts are underway to improve hemispheric CMAQ applications (such as potential vorticity, SMOKE emissions processing), these limitations need to be considered in future model development. Lastly, it is also crucial to extensively evaluate models at higher altitudes and very limited efforts are undertaken in this aspect mainly due to sparse availability of observational data. Nevertheless, the air quality community noticed the need for more observation data in UTLS and free troposphere region, and started various aircraft observation campaigns to address model uncertainties in higher altitudes.

For the third study, we needed to understand how the CAAE is transported in a finer spatial resolution model and the role of intercontinental transport. The second study has also

suggested the importance of understanding the transport processes role to address how CAAE can impact surface air quality. Therefore, we conducted passive tracer (chemically inert) seasonal simulations to study the influence of transport processes on CAAE. The results from this modeling effort should be considered as the ideal case scenario and should be viewed as more diagnostic approach. We found that most of the tracers released at cruise altitudes remains in the upper altitudes and only < 0.6% with respect to the total column burden reaches the surface. In the upper altitudes, for the first 30 days ~ 50% of tracer remain at cruise altitudes and after 90 days ~ 23% stays at cruise altitudes transporting the remaining tracer to mid-troposphere. Zonal vertical distribution clearly showed that higher tracer levels occur in sub-tropics and arctic region at cruise altitudes, and relatively lower tracer levels occur in tropics at these altitudes due to lesser aviation activity in that region.

Additionally, our tagged tracer simulations highlighted the source-receptor relationships between the key sub-regions (North America (NA), Europe (EU) and East Asia (EA)). It also provided evidence that NA as well as EU emissions can impact the relatively lower aviation regions such as North Africa, Middle East, India and South East Asia. This can lead to relatively higher mortality in densely populated tropics region as mentioned in Barrett et al., (2010) despite lower aviation precursor emissions. However, the significantly lower aviation-attributable perturbations even with fine scale modeling in the second study and lesser CAAE tracer near the surface in third study make mortality estimates in Barrett et al., (2010) questionable. Overall our results explained the intercontinental role of aircraft emissions in where they are emitted, where the impacts are seen and more importantly provide inputs for future policy development in decreasing aviation impacts on air quality and health.

One key limitation associated with the third study (Chapter 4) is our tracer modeling we used old model version (CMAQv4.7). The recent updates in new CMAQ versions (v5.0, v5.1) such as turbulent mixing during stable conditions, modifications in vertical advection scheme (ACM2) (Pleim et al., 2007) to reduce numerical diffusion in upper model layers can influence the tracer trends observed in our study as we used old CMAQ version (v4.7). The stability functions in ACM2 for heat and momentum and Monin-Obukhov Length calculations are also modified in recent CMAQ version (v5.1) to make it consistent with the WRF model formulation. The change in stability function calculation based on heat and momentum during stable conditions is intended to allow more mixing during stable atmospheric conditions such as early evening. Overall these modifications can change vertically transported tracer concentrations and their contribution in the planetary boundary layer (PBL).

The various multi-scale modeling conducted in this dissertation have shown that finer spatial scales will provide improved estimates for air quality impacts from aviation. Therefore, conducting a nested model application considering all these different scales will advance our knowledge further and should be considered as a valuable future work. For future global policy development, we suggest this kind of nested modeling application that captures both local as well as hemispheric level aviation impacts variability and can provide accurate air quality as well as health based assessments. There are some more future work ideas based on the work performed in this dissertation. Firstly, in the first study we conducted HAPs modeling for one single airport, however there is no study till date that looked at the aviation-attributable HAPs at regional level with fine scale modeling, therefore this should be considered as one of the potential future work. Secondly, the hemispheric modeling platform developed in the second

study is a chemistry transport model whereas few studies (Xing et al., 2015) already used this kind of application to conduct coupled chemistry meteorology modeling. Therefore, for future work conducting a coupled hemispheric modeling for 10 – 20 years period will advance our knowledge regarding aviation-related long-term climate and air quality impacts. Lastly, future studies should implement tracer approach in recent CMAQ version (v5.1 or 5.2) to take advantage of transport updates incorporated in the model.

APPENDIX A: SUPPLEMENTAL MATERIAL: EVALUATION OF MODEL PREDICTED HAZARDOUS AIR POLLUTANTS (HAPS) NEAR A MID-SIZED U.S. AIRPORT

A.1 METHODOLOGY

A.1.1 Air Quality Model:

A.1.1.1 36 × 36 km^2 CMAQ Model Simulations:

Woody et al., 2011 carried out 36 × 36 km^2 model simulations for the continental U.S. using CMAQv4.6 with aircraft emissions based upon the Emissions Dispersion Modeling System (EDMS) from 99 major US airports processed through EDMS2Inv (Baek et al., 2007) along with other background emissions (NEI inventory emissions, EPA, 2007b). In that study the authors did not discuss HAPs, as the main aim of their study was to access aviation contributions to fine particulate matter ($PM_{2.5}$) under current and future emissions scenarios. The model however was indeed configured for treatment of air toxics or HAPs, and we used that data to perform a U.S. wide assessment of aviation-related HAPs.

Table A1: Total Organic Gas (TOG) speciation profile of HAPs for aircraft engines developed by EPA/FAA (EPA, 2009)

HAP Species*	Mass Fraction
Formaldehyde	0.1231
Acetaldehyde	0.0427
Benzene	0.0168
Toluene	0.0064
Acrolein	0.0245
1,3-Butadiene	0.0169
Xylene	0.0045
Naphthalene	0.0054

*Note: The HAP species considered in this study are a small subset of all species in the TOG. The remaining species are further speciated in the model based on the Carbon Bond 2005 chemical mechanism speciation profile.

Table A2: Transport and chemical processes parameterizations used in CMAQ v5.0.2 for the 4 × 4 km^2 simulations.

Processes	Model Scheme
Horizontal advection	hyamo
Vertical advection	vyamo
Horizontal diffusion	multiscale
Vertical diffusion	acm2_mp
Deposition	m3dry_mp
Photolysis	jtable
Chemistry solver	ebi_cb05tump
Aerosol	aero6_mp
Cloud module	cloud_acm_ae6

A.1.1.2 Aircraft emission sensitivity for PVD 4 × 4 km^2 case:

According to ICAO, the different stages in flight path based on the power settings are defined as idle (7%), approach (30%), climbout (85%) and takeoff (100%). From linear extrapolation of fuel flow corresponding to four ICAO thrust settings (100%, 85%, 30%, 7%) we obtained fuel flow for 4% thrust setting (FF_4perc) for each engine present in ICAO database. Considering fuel flow (FF) and hydrocarbon emission index (HC_EI) of four ICAO thrust settings for each engine, we calculated slope ($S_{HC\_EI\_FF}$) and intercept ($I_{HC\_EI\_FF}$) values of the linear logarithmic fit. The slope ($S_{HC\_EI\_FF}$) and intercept ($I_{HC\_EI\_FF}$) are then used to calculate the 4% HC EI (HC_EI_4perc) of a 4% fuel flow (FF_4perc) (HC_EI_4perc = ($S_{HC\_EI\_FF}$)*FF_4perc + ($I_{HC\_EI\_FF}$)). The chorded AEDT emission inventory consists of mode-specific emissions for individual flights starting from ground roll and taxing (emissions mode 0 and 10), takeoff (emission modes 1–3), cruising (emissions modes 4–6) to approach and landing (emission modes 7–9). The new HC_EI_4perc was applied to both '0' and '10' emission mode's fuel burn when the AEDT-reported segment time is higher than the respective unimpeded average taxi time (Unimpeded taxi out time = 9.6 min, Unimpeded taxi in time = 3.8 min) near PVD. The idling fuel burn is multiplied by 4% hydrocarbon index (HC_EI_4perc) to obtain 4% hydrocarbon idle emissions. We then used the AEDTProc tool to generate CMAQ-ready emissions of gridded and speciated new aircraft HAPs.

A.1.2 Observational Data:

Table A3: Monitoring sites and their description near PVD airport

Field Study Name	Site Name	FIPS CODE	Site Description
RIDEM[a]	Fieldview	440030015	Runway site, close to major runway
	Firestation	440030011	0.9km from airport terminal building
	Lydick	440030012	Opposite to Fieldview (downwind)
	Smith	440030014	Site located in residential area
	Draper	440030013	Away from airport and located near bay area
AQS[b]	Providence	440070022	Urban
	Pawtucket	440070026	Residential (near interstate highway)
	East Providence	440071010	Suburban
	W. Greenwich	440030002	Rural

a) RIDEM – Rhode Island Department of Environmental Management b) AQS – Air Quality System

Table A4: NATTS observation sites and airport grid-cells in 36 × 36 km^2 domain.

NATTS ID	State	Location	Gridcell (col,row)	airport	Gridcell (col,row)
06-085-0005	California	San Jose	14,57	OAK	14,58
11-001-0043	District Of Columbia	Washington	122,58	IAD	121,58
12-057-3002	Florida	Tampa	115,23	TPA	114,23
12-103-0026	Florida	Pinellas county	114,22	TPA	114,23
13-089-0002	Georgia	Atlanta	107,39	ATL	107,39
17-031-4201	Illinois	Chicago	95,64	ORD	95,64
25-025-0042	Massachusetts	Boston	133,72	BOS	133,72
26-163-0033	Michigan	Detroit	106,66	DTW	105,66
29-510-0085	Missouri	St. Louis	91,53	STL	90,53
36-005-0083	New York	Bronx	128,66	JFK	128,65
36-005-0110	New York	Bronx	128,66	JFK	128,65
36-055-1007	New York	Rochester	118,71	ROC	118,71
44-007-0022	Rhode Island	Providence	132,70	PVD	132,70
48-201-1039	Texas	Houston	80,25	HOU	79,25
48-203-0002	Texas	Karnack	82,34	HOU	82,34
49-011-0004	Utah	Bountiful	40,62	SLC	40,62
53-033-0080	Washington	Seattle	22,87	SEA	22,87
55-027-0007	Wisconsin	Mayville	93,68	MSN	92,68
55-079-0010	Wisconsin	Milwaukee	95,67	MKE	95,67

A.2. EMISSIONS ANALYSIS

In this section we included analysis of HAPs emissions from airports, and their percentage contribution in the airport grid-cells when compared with the total emissions (airport + background) for both 36 × 36 km^2 and 4 × 4 km^2 domains.

Table A5 represents the annual emission totals in tons/year. In the 36 × 36 km^2 domain we calculated the emission totals by summing up all the HAP emissions in 99 airport grid-cells. Overall, formaldehyde showed higher airport emissions among all the HAPs followed by benzene, acetaldehyde and acrolein. If we look at the airport contribution to the total emissions from all 99 airport grid-cells, however, acrolein shows a higher value (22%) than formaldehyde

(9.2%) (Note that this contribution can vary with airport). In the 4 × 4 km^2 domain, since it is a finer resolution (than 36 × 36 km^2), the airport contribution to the total emissions in that PVD grid-cell is obviously higher and in the range of 50–70% for key pollutants (formaldehyde, acetaldehyde and acrolein). In Table A7 we compared just the emissions in the PVD grid-cell from 36 × 36 km^2 and 4 × 4 km^2 domains.

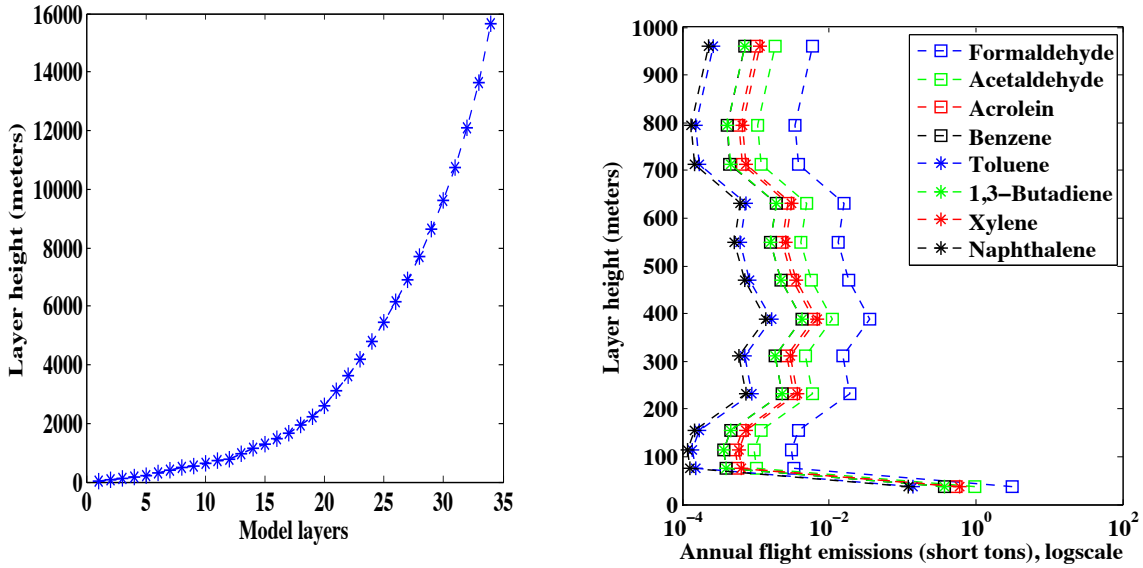

Figure A1: Vertical profile of model layers height (left) and aircraft annual emissions (right) for all HAPs. Note that aircraft emissions during LTO are only represented within the lowest 1000 meters.

In 4 × 4 km^2 emissions we considered only the aircraft emissions but not the emissions from ground supporting equipment (GSE), ground auxiliary vehicles (GAV). As mentioned in previous observation-based studies we should note that majority of airport emissions of HAPs come from aircraft (> 80–90%) during idling and taxing stage for key species (formaldehyde, 1,3-butadiene, acrolein). This explains the reason for relatively lower emissions of remaining HAPs such as benzene, toluene and xylene where GSE and GAV contribute relatively high. But as AEDT inventory used in PVD does not include those emissions sources, we are missing certain proportion of emissions.

Table A5: HAPs airport emission totals for 99 airport grid-cells in the sensairp_36 km case and PVD airport grid-cell in sensairp_4km case. Contributions of these emissions to the total emissions (airport + background) are also shown.

HAPS (tons/year)	**99 airport emissions** (99 airport grid-cells)	**Sensairp_36km** (airport+ background, 99 airport grid-cells)	**Airport emissions contribution**	**PVD airport emissions** (airport grid-cell)	**Sensairp_4km** (airport+ background ,airport grid-cell)	**Airport emissions contribution**
Formaldehyde	2214	24021	**9%**	3.41	6.70	**51%**
Acetaldehyde	689	9343	**7%**	1.06	2.11	**50%**
Acrolein	339	1498	**23%**	0.59	0.80	**74%**
Benzene	1068	46130	**2%**	0.40	8.54	**5%**
1,3-Butadiene	253	5243	**5%**	0.41	1.48	**27%**
Toluene	82	122118	**0%**	0.05	20.96	**0%**
Xylene	272	80448	**0%**	0.11	17.16	**1%**
Naphthalene	83	2479	**3%**	0.13	0.35	**37%**

Table A6: Breakdown of airport-level emissions at PVD airport by aircraft and other on-airport sources (taken from EDMS previous modeling work).

HAP	Aircraft	APU	GSE	Vehicles	Stationary	Total (tons/ year)	Contribution of aircraft to the total
Formaldehyde	10.49	0.11	0.27	0.31	0.006	11.18	94%
Acetaldehyde	5.28	0.01	0.08	0.17	0.004	5.55	95%
Benzene	4.35	0.10	0.57	0.99	0.004	6.02	72%
Toluene	1.50	0.04	0.78	N/A	0.002	2.31	65%
Acrolein	12.72	0.01	0.01	0.02	0.000	12.76	100%
1,3-Butadiene	2.16	N/A	0.10	0.13	0.000	2.40	90%
Xylene	1.53	0.02	0.73	N/A	0.001	2.28	67%
Naphthalene	0.71	0.01	N/A	N/A	0.000	0.72	99%

In Table A6 we present emissions from individual airport sources taken from a previous modeling study that used EDMS to estimate all emissions sources (Aircraft, APU, GSE, Stationary) at the PVD airport. We can clearly see that the aircraft emissions are the key contributor particularly for formaldehyde, acetaldehyde, acrolein, and 1,3-butadiene.

Table A7: Comparison of 36×36 km^2 (from EDMS) and 4×4 km^2 (from AEDT) PVD grid cell airport emissions.

Pollutant (tons/year)	36×36 km^2	4×4 km^2
Formaldehyde	5.27	3.41
Acetaldehyde	1.59	1.06
Acrolein	0.82	0.59
Benzene	0.66	0.40
1,3-Butadiene	0.62	0.41
Toluene	0.20	0.05
Xylene	0.17	0.11
Naphthalene	0.19	0.13

We also looked at monthly totals of aviation emissions to understand the seasonal variation in emissions during a year. We observed a 37% increase in daily total emissions in summer (not presented here) when comparing the highest day of emissions in the summer vs. the winter season. We didn't see significant differences between winter and summer season's monthly emission totals. Observation-based studies of aircraft engine exhaust (Timko et al., 2010) also indicated that emission rates from aircraft are temperature-dependent and relatively higher during low ambient temperatures. A recent study (Herndon et al., 2012) also found that the VOC emission indices for aircraft are twice as much during cold conditions than warm conditions. We did not observe any significant temperature dependency nature among emissions as pointed out in another study by Wood et al., 2008. This inability of not reflecting temperature dependency in the emission inventories can further introduce uncertainty in air quality model predictions. To improve the emission inventory, a comprehensive evaluation of aviation hydrocarbon profile at different parameters (temperature, aircraft thrust setting) and implementation of better hydrocarbon emission index at low thrusts in the emission inventory tool as observed in measurement studies is essential.

A.3. RESULTS:

A.3.1 HAPS 4 × 4 km^2 MODEL PERFORMANCE

Throughout this study we used Normalized mean bias (NMB) and Normalized mean error (NME) as model performance metrics. NMB calculates differences between modeled and observed values over the sum of observed values whereas NME calculates the absolute value of the NMB (Boylan et al., AE, 2006).

$$\text{NMB} = \frac{\sum_1^n (P-O)}{\sum_1^n (O)} * 100, where\ P = predicted\ and\ O = observed$$

$$\text{NME} = \frac{\sum_1^n |(P-O)|}{\sum_1^n (O)} * 100, where\ P = predicted\ and\ O = observed$$

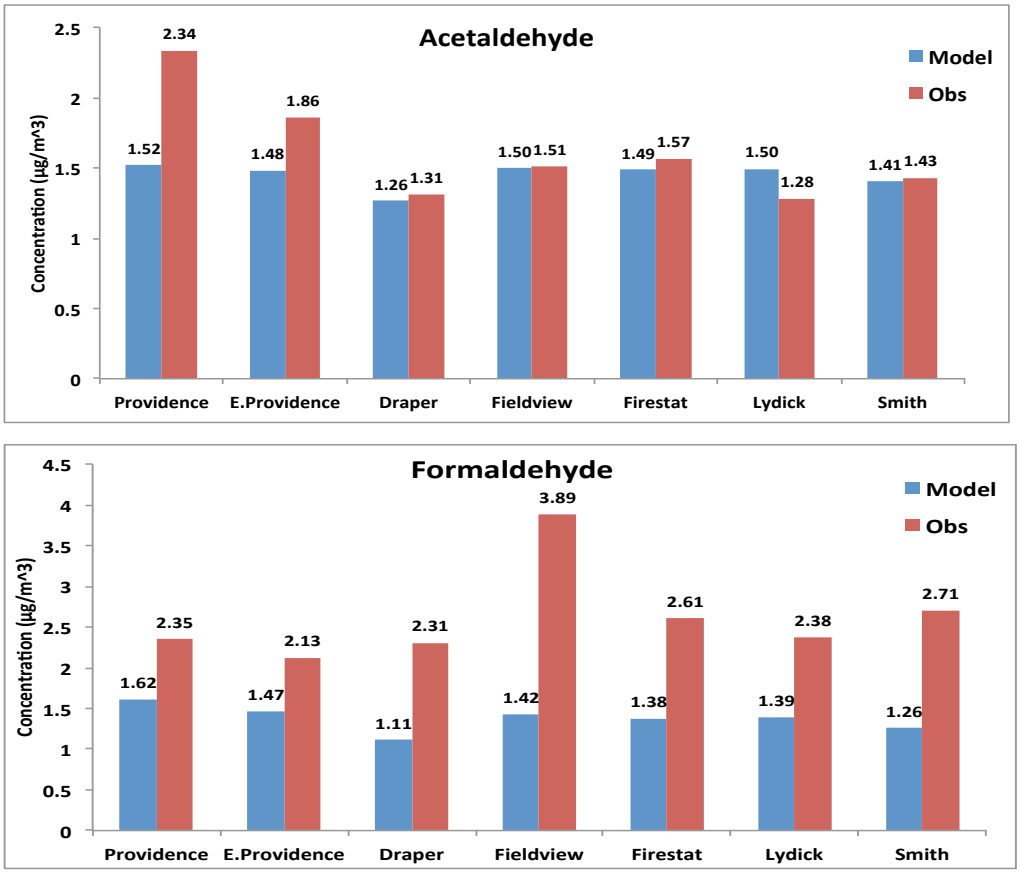

Figure A2: Bar plots comparing mean modeled values (all emissions sources) with observation data at RIDEM (5 sites) and AQS (2 sites).

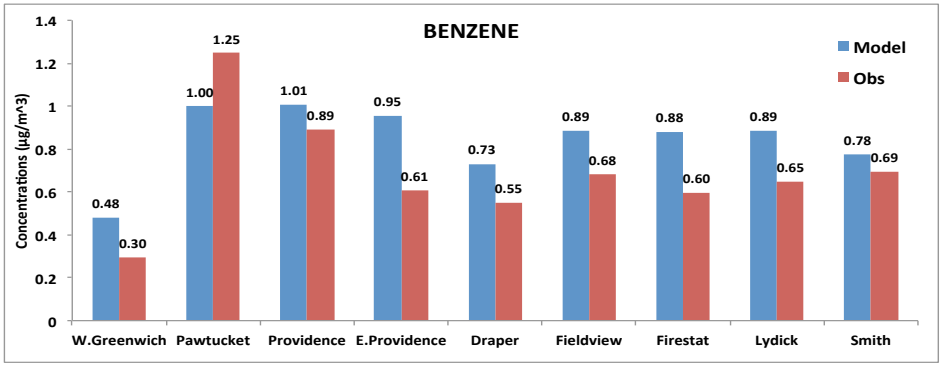

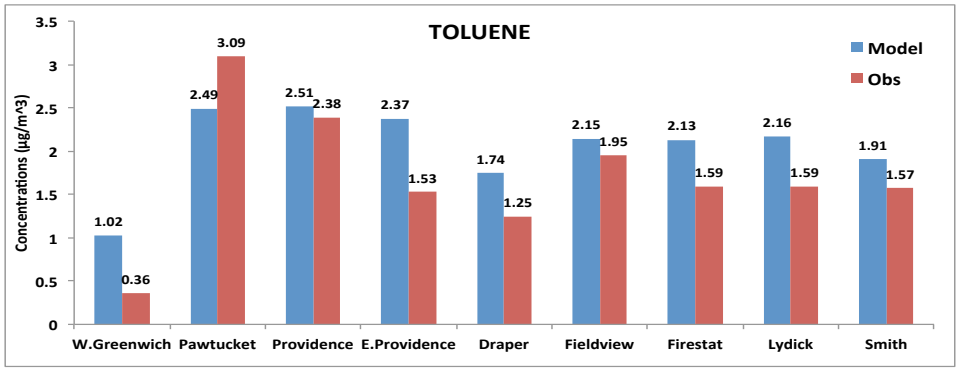

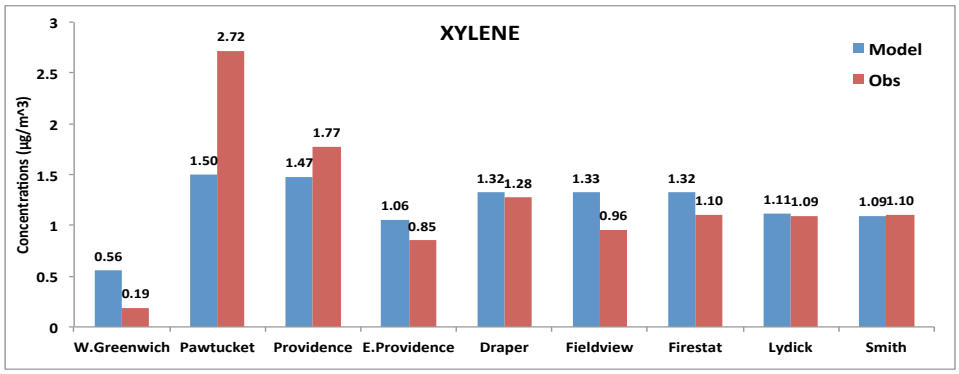

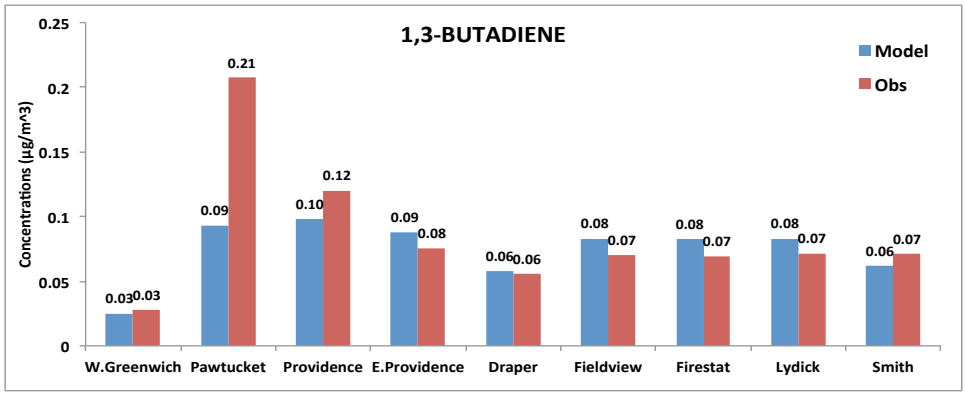

Figure A3: Bar plots comparing mean modeled values (all emissions sources) with observation data at RIDEM (5 sites) and AQS (4 sites).

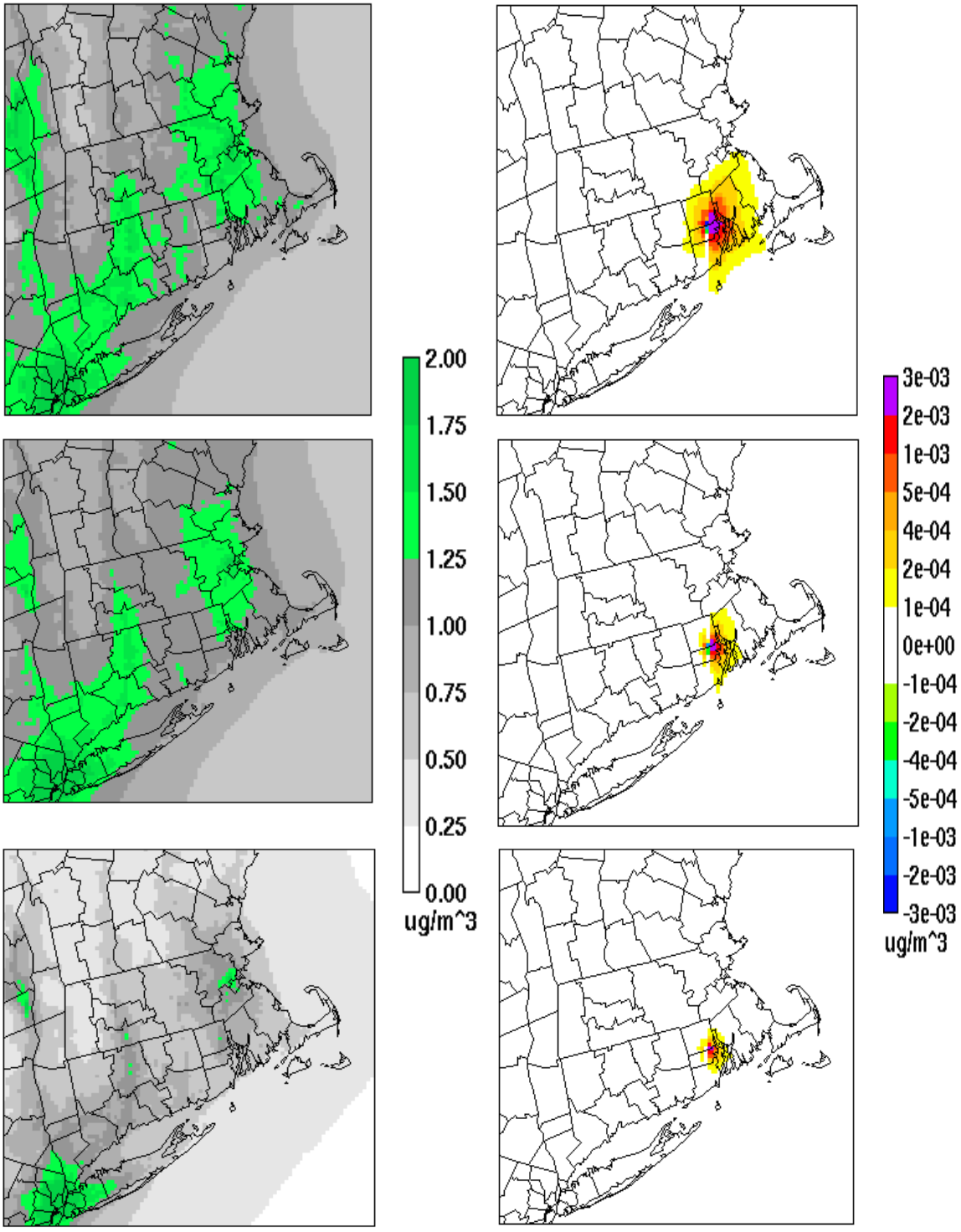

Figure A4a: Annual all source (sensairp_4km, left) and PVD airport-attributable (sensairp_4km minus base_4km, right) concentrations of formaldehyde (top), acetaldehyde (middle) and benzene (bottom).

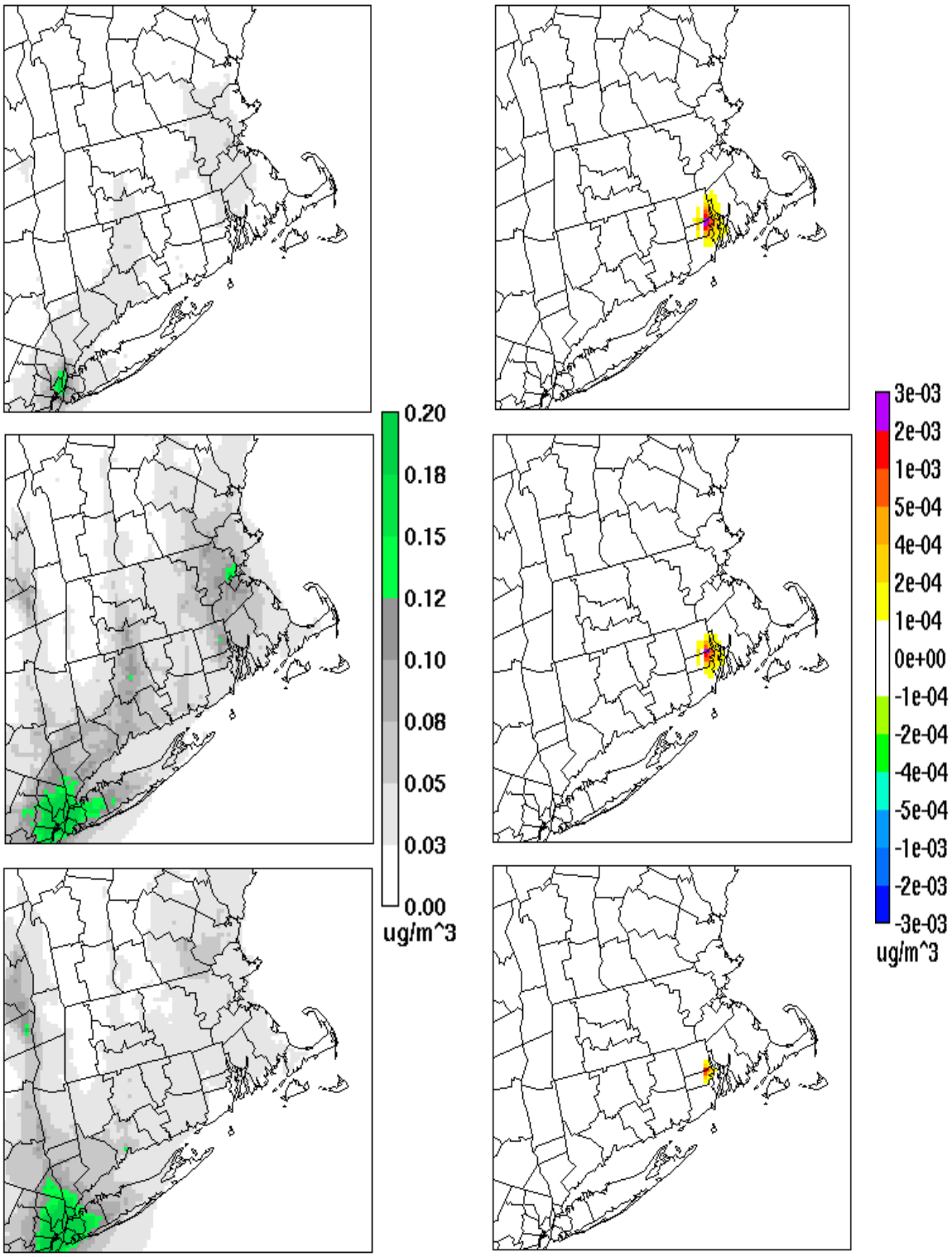

Figure A4b: Annual all source (sensairp_4km, left) and airport-attributable (sensairp_4km minus base_4km, right) concentrations of acrolein (top), 1,3-butadiene (middle) and naphthalene (bottom).

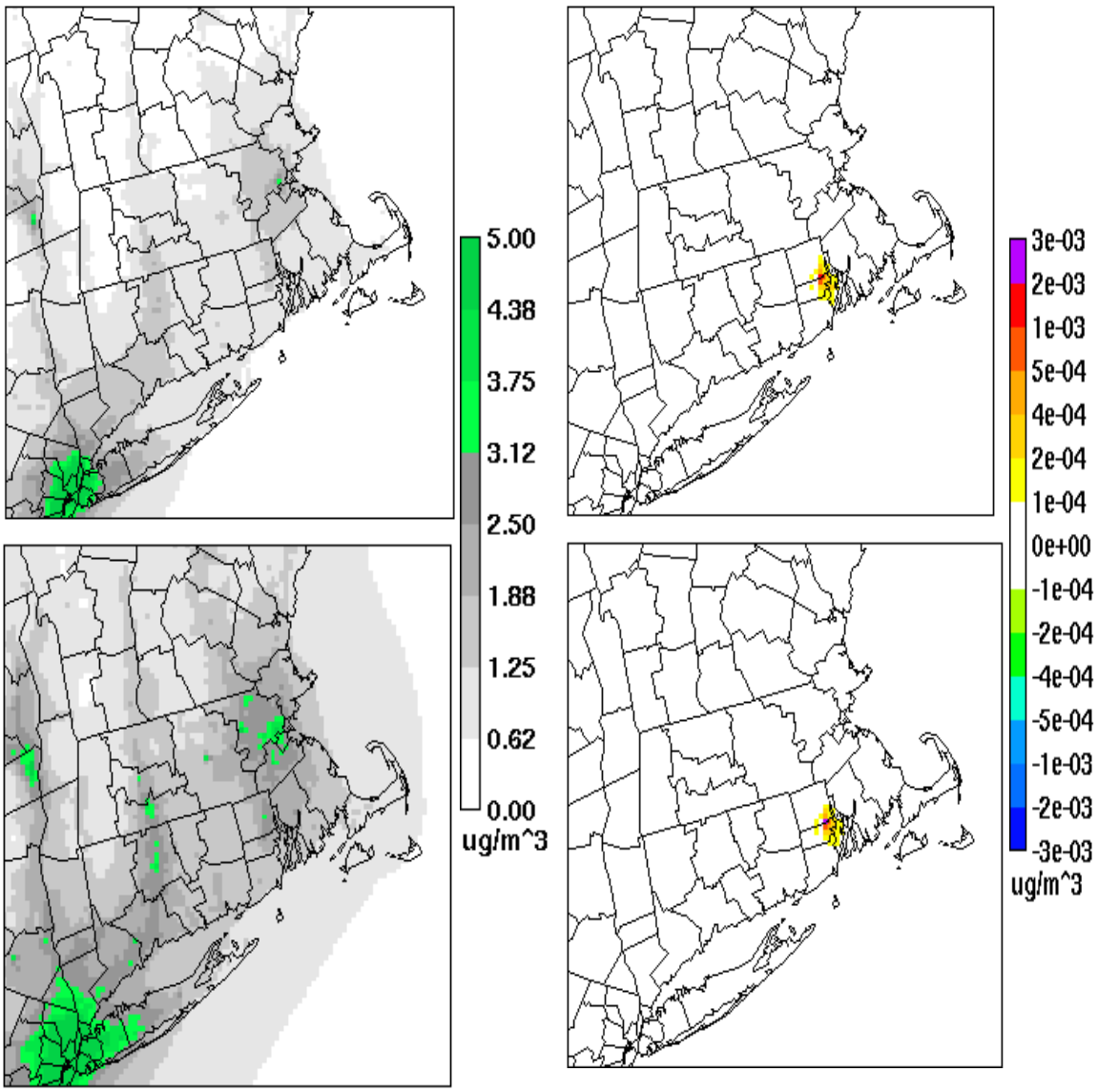

Figure A4c: Annual all source (sensairp_4km, left) and airport-attributable (sensairp_4km minus base_4km, right) concentrtions of xylene (top) and toluene (bottom).

Table A8: Predicted airport contribution in winter (January) and summer (July) months to the ambient concentrations in 4 × 4 km^2 PVD airport grid-cell.

HAPS	January (%)	July (%)
Formaldehyde	4.2	2.7
Acetaldehyde	1.7	0.7
Acrolein	19.8	28.7
1,3-Butadiene	4.3	9.5
Benzene	0.5	0.7
Naphthalene	4.3	9.0
Toluene	0.19	0.14
Xylene	0.18	0.18

A.3.2 HAPS 36 × 36 km^2 MODEL PERFORMANCE:

Figure A5 shows the location of major airports and collocated NATTS observational sites along with bar plots showing model performance of HAPs at each site. The NATTS network is a monitoring network started by U.S. EPA in 2003, which consists of long-term HAPs monitoring data for U.S. We used annual hourly model predictions and available observational data for year 2005 to calculate annual normalized mean bias (NMB) and normalized mean error (NME) metrics. Note that not all observational sites are located in the model grid cell of the airports, some are one or two grid cells away as shown in Table A4. Some of the largest U.S. airports such as ORD (O'Hare International Airport, Chicago), ATL (Hartsfield-Jackson Atlanta International Airport), BOS (Logan International airport, Boston), ROC (Greater Rochester International Airport, New York), SEA (Seattle-Tacoma International Airport, Seattle) are located in the same grid cells as the NATTS sites.

Overall we observe HAPs model performance throughout the U.S. near all NATTS sites as shown in Figure A5. There does not seem to be a specific trend spatially (such as overprediction or underprediction in one region vs. the other) in the NMB, as HAPs are locally emitted species and some are highly reactive. All the NATTS sites present in the map are urban sites except the one site located in Utah. At some urban counties such as Santa Clara County (San Jose, California), Harris County (Houston, Texas), Milwaukee County (Milwaukee,

Wisconsin) there was (NMB of -20 to -75%) underprediction of all HAPs. In the case of formaldehyde, except for the sites in Bronx County (New York) and King County (Seattle, Washington) that showed overprediction (42% and 75% respectively), all other sites showed underprediction (2–80%). High (NMB: 50–200%) overprediction of model results in Seattle area is comparable to the results reported in Tacoma and Seattle area air toxics evaluation (Air Toxics Study Report, 2010). Benzene concentrations are also highly overpredicted (NMB: 200%) near this site; as mentioned in the report this could be due to regulatory air toxics control actions, which reduced benzene concentrations in that area, whereas not updated in NEI. NMB in the range of ±70–90% was observed in the case of two highly reactive species, 1,3-butadiene and acrolein at majority of the sites. Overall at coarser resolution we observed moderate model performance (NMB: ~ ±50%) of HAPs near most sites, and poor model performance at some sites (NMB > ±50%).

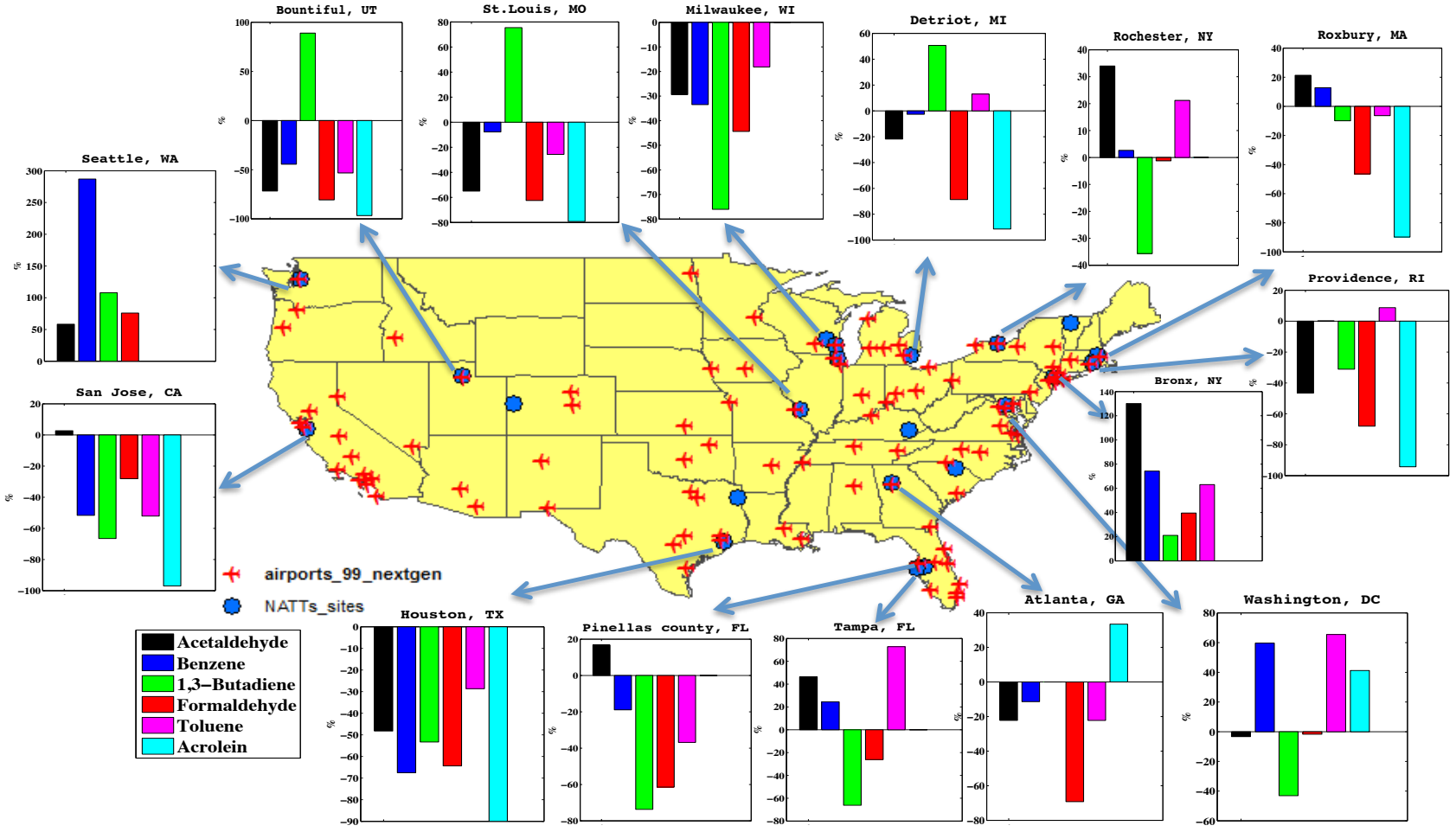

Figure A5: CMAQ 36 × 36 km^2 model performance near NATTS sites (blue dots) and 99 major airports (red aircraft), bar charts representing Normalized Mean Bias (NMB, %) for sensairp_36km.

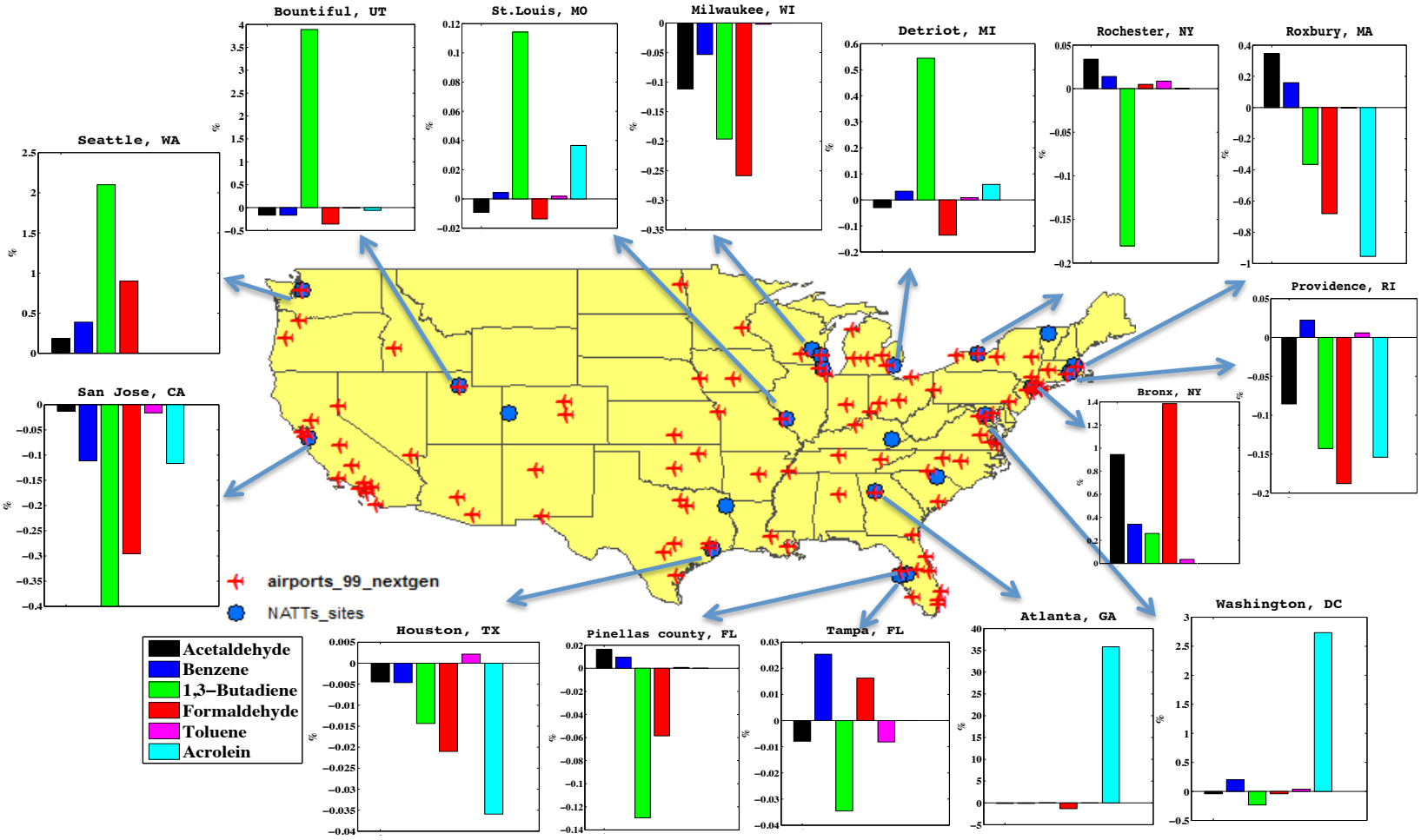

Figure A6: CMAQ 36 × 36 km^2 model performance near NATTS sites (blue dots) and 99 major airports (red aircraft), bar charts representing difference between sensairp_36km and base_36km normalized mean error (NME, %).

A.3.2.1 Comparison of base_36km and sensairp_36km model performance near airports

Figure A6 shows bar plots with the difference of normalized mean error (NME) between sensairp_36km minus base_36km cases. Negative values indicate an improvement in model performance after including airport emissions. We observed slight improvement (0.01–0.6%) in formaldehyde performance after considering airport emissions. Particularly in Georgia (DeKalb County) near Atlanta airport, model error decreased by about 1.5%. As Atlanta is one of the biggest and busiest airports in the world, due to its high traffic the taxi and idling time on an average is relatively higher (and thus leads to high unburned hydrocarbons) than compared to other mid-sized and smaller airports. However near two sites where formaldehyde is overpredicted (Figure A6) ((Bronx County (New York), King County (Seattle)) the model error increased even in sensairp_36km case.

A.3.3 NATA COMPARISON:

As the main focus of this paper is to study airport-based concentrations, we envisioned comparing HAPs concentrations due to airport emissions in CMAQ versus those from NATA. However, in NATA, airport concentrations were not reported separately, and instead combined with other non-road sources and collectively reported as non-road concentrations. Since there is no straightforward way to calculate the airport concentrations from NATA, we decided to calculate percent contribution of airport emissions in non–road NEI emissions and apply these numbers to NATA non-road concentrations to obtain NATA airport concentrations at county level. This approach might not give accurate values but nevertheless provides us with an approximate estimate of airport concentrations in non-road sector as reported by NATA.

The differences observed in total county-based concentrations are shown in Figure A7 (top panel). Also shown in Figure A7 (bottom panel) are the aircraft contributions in the Kent County. As mentioned before, we obtained NATA airport concentrations by applying aircraft emission factor to non-road concentrations in the Kent County. CMAQ concentrations are obtained by aggregating the grid-based concentrations in the county. In the case of total concentrations CMAQ is showing higher concentrations than NATA for all aromatic species (Toluene, Xylene, Benzene) and NATA is showing higher concentrations in the case of carbonyl species (Formaldehyde, Acetaldehyde, Acrolein). These carbonyl species higher concentrations

in NATA could be due to the double counting of the secondary formation concentrations. In the case of airport concentrations CMAQ is predicting lower concentrations than NATA due to two reasons: Not including other stationary and GSE emissions at the airport underpredict some of the concentrations in CMAQ, NATA airport concentrations could also be overpredicted as we are calculating them from the overall non-road county-based concentrations.

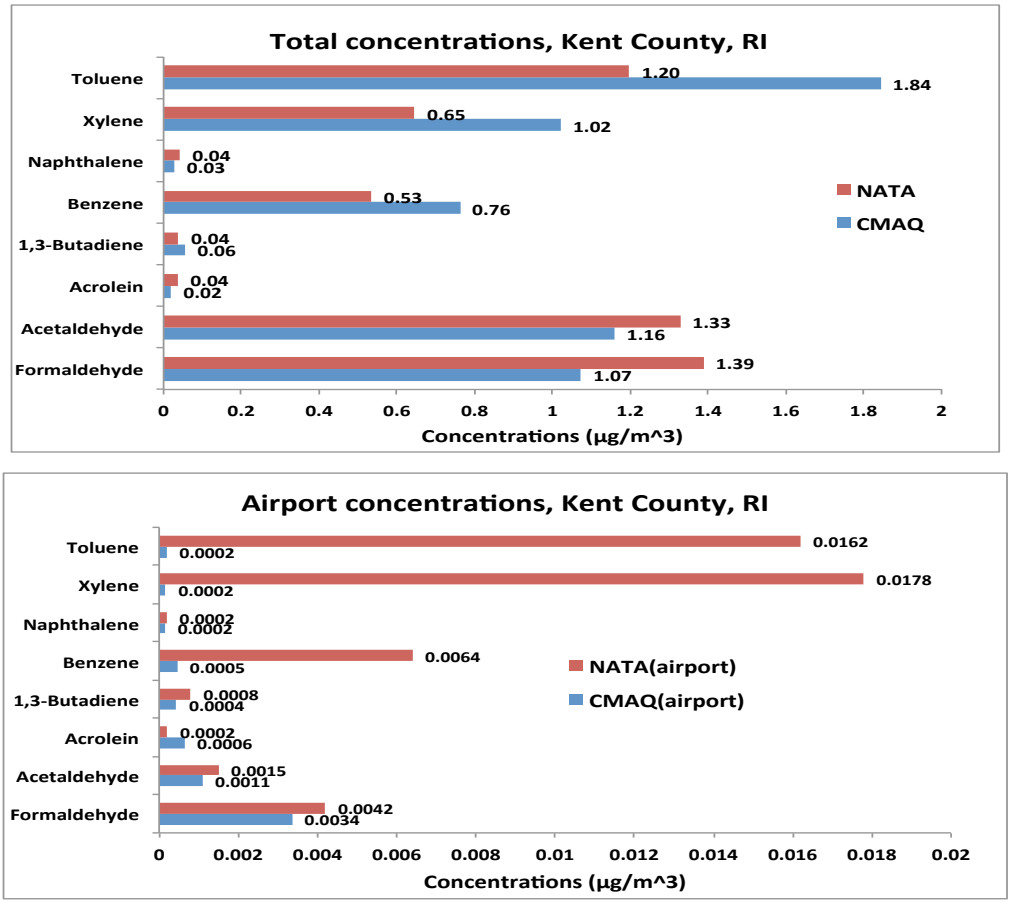

Figure A7: NATA and CMAQ total (all sources, top) and airport concentrations (bottom) in Kent county, Rhode Island (where PVD airport is located).

APPENDIX B: SUPPLEMENTAL MATERIAL: MODELED FULL-FLIGHT AIRCRAFT EMISSIONS IMPACTS ON AIR QUALITY AND THEIR SENSITIVITY TO GRID RESOLUTION

Table B1. Domain specifications used in WRF for CONUS and HEMI domains

WPS option	**CONUS domain**	**HEMI domain**
Horizontal Resolution	36 x 36 km	108 x 108 km
Domain Size (Grid Cells)	165 x 129	200 x 200
Map Projection	Lambert Conformal Conic	Polar Stereographic
Reference Latitude	40°N	90°N
Reference Longitude	97°W	-98°W
True Latitude 1	33°N	45°N
True Latitude 2	45°N	1°N
Standard Longitude	97°W	-98°W

Table B2: Vertical structure used in WRF meteorology modeling for two domains

WRF Layer	Sigma	Pressure (mb)	Height (m)
45	0	50	19314.2
44	0.0186	67.91	17814.9
43	0.0386	87.17	16525.9
42	0.0596	107.39	15400.9
41	0.0816	128.58	14393.2
40	0.1047	150.83	13470.8
39	0.1289	174.13	12616.3
38	0.1543	198.59	11813.6
37	0.181	224.3	11052.1
36	0.2089	251.17	10328.4
35	0.2383	279.48	9630.8
34	0.269	309.05	8960.7
33	0.3013	340.15	8309.9
32	0.3352	372.8	7676.6
31	0.3708	407.08	7058.3
30	0.4081	443	6454.1
29	0.4454	478.92	5888.3
28	0.4827	514.84	5355.9
27	0.52	550.76	4852.8
26	0.5573	586.68	4375.6
25	0.5946	622.6	3921.5
24	0.632	658.62	3487
23	0.6693	694.54	3072.4
22	0.7066	730.46	2674.9
21	0.7439	766.38	2292.8
20	0.7795	800.66	1941.5
19	0.8104	830.42	1646.3
18	0.8373	856.32	1396.3
17	0.8607	878.85	1183.7
16	0.881	898.4	1002.8
15	0.8987	915.45	847.6
14	0.9141	930.28	714.5
13	0.9275	943.18	600.1
12	0.9391	954.35	502.1
11	0.9492	964.08	417.4
10	0.958	972.55	344.3
9	0.9657	979.97	280.7
8	0.9723	986.32	226.5
7	0.9781	991.91	179.1
6	0.9831	996.73	138.4
5	0.9875	1000.96	102.8
4	0.9913	1004.62	72.1
3	0.9946	1007.8	45.4
2	0.9975	1010.59	22.2
1	1	1013.25	0

Table B3: Physical meteorology parameterization options used in WRF modeling

WRF Treatment	**Option**	**Notes**
Microphysics	Thompson	A scheme with ice, snow, and graupel processes suitable for high-resolution simulations.
Longwave Radiation	RRTMG	Rapid Radiative Transfer Model (RRTM) for GCMs includes random cloud overlap and improved efficiency over RRTM.
Shortwave Radiation	RRTMG	Same as above, but for shortwave radiation.
Land Surface Model (LSM)	NOAH	Four-layer scheme with vegetation and sub-grid tiling.
Planetary Boundary Layer (PBL) scheme	YSU	Yonsie University (Republic of Korea) Asymmetric Convective Model with non-local upward mixing and local downward mixing.
Cumulus parameterization	Kain-Fritsch	Kain-Fritsch modifications include representation of sub-grid clouds and radiation feedbacks
Analysis nudging	Nudging applied to winds, temperature and moisture	Nudging applied above PBL only
Initialization Dataset	MERRA reanalysis	0.5° deg. x 0.67° resolution

Table B4: WRF statistical evaluation using observational data (US region only) and comparison with other studies

	Temperature		Humidity		Wind Speed		Wind Direction	
	Bias	Error	Bias	Error	Bias	RMSE	Bias	Error
Benchmark - Simple Conditions (Emery et al., 2001)	≤ ±0.5 K	≤ 2.0 K	≤ ±0.5 g/kg	≤ 1.0 g/kg	≤ ±0.5 m/s	≤ 2.0 m/s	≤ ±5 deg	≤ 40 deg
Benchmark - Complex Conditions	≤ ±1.0 K	≤ 3.0 K	≤ ±1.0 g/kg	≤ 2.0 g/kg	≤ ±1.0 m/s	≤ 3.0 m/s	≤ ±10 deg	≤ 80 deg
EPA HEMI 108k - NCDC 's ISD Obs (Xing et al., 2015)	-0.4 K	N/A	N/A	N/A	0.4 m/s	N/A	-3 deg	N/A
HEMI 108km - MADIS Obs	-0.3 K	2.6 K	-0.4 g/kg	1.2 g/kg	0.1 m/s	2.0 m/s	7 deg	37 deg
CONUS 36km - MADIS Obs	-0.2 K	2.0 K	0.3 g/kg	1.0 g/kg	0.2 m/s	1.8 m/s	7 deg	33 deg

Table B5: Annual all sources and aviation emission totals (kilo tons/year) of key pollutants for whole HEMI domain (108km) and three sub regions (NA, EU, EA)

	Scenario (kilo tons/year)	**CO**	**NO**	**NO2**	**SO2**	**NH3**	**PM species**	**VOC**
All sources	HEMI	779896	98993	10999	115011	46120	106201	140956
	NA	79102	18878	2098	16318	5104	4176	17767
	EU	61951	18345	2038	18945	7998	6962	21913
	EA	150039	24365	2707	41939	11410	24755	30074
Aviation	HEMI	698	2426	274	226	_	45	117
	NA	311	705	81	72	_	12	53
	EU	166	534	63	51	_	8	25
	EA	81	397	45	33	_	6	13
Aviation (%)	HEMI	0.09	2.45	2.49	0.20	_	0.04	0.08
	NA	0.39	3.73	3.88	0.44	_	0.29	0.30
	EU	0.27	2.91	3.08	0.27	_	0.11	0.1
	EA	0.05	1.63	1.70	0.08	_	0.02	0.04

Table B6: Annual all sources and aviation emission totals (kilo tons/year) of key pollutants for CONUS domain (36 km).

Scenario (kilo tons/year)	CO	NO	NO2	SO2	NH3	PM species	VOC
CONUS (All sources)	122240	23724	2052	17836	4618	17612	47037
CONUS (Flight)	311.14	703.64	81.19	72.40		20.47	52.90
% Aviation	0.25	2.97	3.96	0.41	0.00	0.12	0.11

Table B7: Normalized Mean Error (%) averaged over a season in 2005 of hourly O_3 and $PM_{2.5}$ concentrations predicted by Airc36 (CONUS) and Airc108 (HEMI-NA) model scenarios in comparison with hourly AQS observations.

Seasons	O_3 (%)			$PM_{2.5}$ (%)		
	Airc36	Airc108	Diff (Airc108 – Airc36)	Airc36	Airc108	Diff (Airc108 – Airc36)
Winter	61	77	16	68	59.9	-8.4
Spring	33	36	3	59	55.4	-3.3
Summer	44	40	-5	57	66.2	9.5
Autumn	55	59	5	56	57.0	1.1

Table B8: NME (%) differences between Airc36, NoAirc36 and Airc108 model scenarios in comparison with INTEX observations for O_3, NO_2 and NO.

NME	O3 (%)		NO2 (%)		NO (%)	
Altitudes	**Airc36-NoAirc36**	**Airc36-Airc108**	**Airc36-NoAirc36**	**Airc36-Airc108**	**Airc36-NoAirc36**	**Airc36-Airc108**
92	0.30	-3.40	0.36	-28.50	0.00	-7.18
430	0.31	17.68	-0.32	-24.86	-0.09	-9.75
767	0.29	1.08	-0.46	4.44	-0.11	13.73
1104	0.30	-5.39	-0.45	-10.79	-0.10	-8.42
1441	0.31	-15.56	-0.58	13.24	-0.23	10.83
1778	-0.34	4.80	0.80	-56.95	-0.20	26.02
2116	-0.36	-18.81	-0.68	-0.35	-0.19	-3.90
2453	-0.36	-9.89	4.44	38.92	-1.52	-11.01
2790	-0.32	-10.42	-0.71	-16.26	-0.56	-8.79
3127	-0.31	-6.01	-1.74	-5.33	-0.73	-7.73
3464	-0.27	-3.55	-0.62	-5.00	-0.58	-13.95
3801	-0.42	-6.43	-1.33	-14.95	-0.52	-3.32
4139	-0.29	-7.95	-1.78	-15.82	-0.54	-7.20
4476	-0.55	-4.82	-1.74	-7.37	-0.39	-3.18
4813	-0.43	-9.78	-1.72	-26.73	-0.71	-10.59
5150	-0.75	-13.42	-2.62	-4.28	-0.76	-0.32
5487	-0.50	-7.75	-5.78	-46.32	-1.87	-12.39
5825	0.69	1.07	-8.42	-16.87	-2.74	-8.37
6162	-0.54	-8.55	5.17	-1.06	-1.32	-30.95
6499	-0.63	-10.81	-5.57	-41.93	-2.07	-16.11
6836	-0.80	-15.66	-3.28	-11.01	-1.20	-1.54
7173	-0.55	-2.59	-4.00	-16.01	-1.57	-7.24
7511	0.62	-20.41	-4.69	-23.11	-1.81	-8.20
8522	1.26	-0.64	-5.72	-10.76	-3.15	-6.04
8859	-0.80	-8.51	-5.65	-22.07	-3.40	-11.47
9196	-0.70	-9.29	-11.71	-15.42	-4.79	-7.03
9534	1.68	-1.08	-8.57	-14.32	-4.39	-13.18
9871	-1.30	-10.47	-9.39	-20.03	-5.55	-12.92
10208	1.49	-13.49	-6.89	-27.39	-4.74	-20.12
10545	-1.21	-7.52	-6.67	-22.08	-3.89	-16.13
10882	-0.38	-10.03	-4.32	-15.64	-3.88	-18.84
11220	-0.16	-2.41	-2.78	-31.55	-2.53	-24.29
11557	-0.72	-19.39	-1.08	-11.99	-3.14	-32.66
11894	0.96	-21.00	-1.86	-15.82	-3.63	-28.26
Max	**1.68**	**17.68**	**5.17**	**38.92**	**0.00**	**26.02**
Min	**-1.30**	**-21.00**	**-11.71**	**-56.95**	**-5.55**	**-32.66**
Average	**-0.18**	**-8.22**	**-3.16**	**-16.78**	**-1.95**	**-9.94**

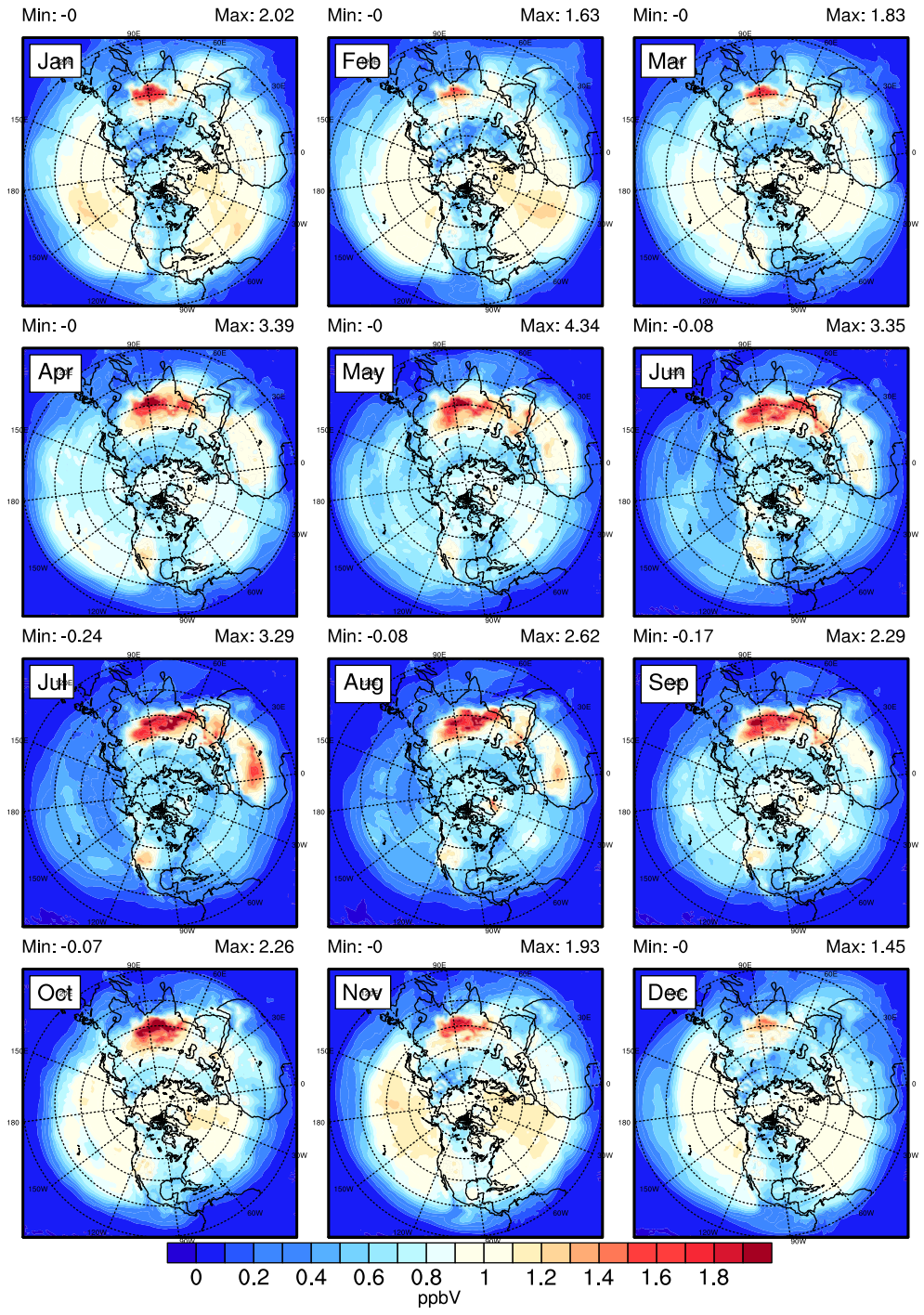

Figure B1: Monthly average aviation-attributable surface concentrations of O_3 in HEMI domain

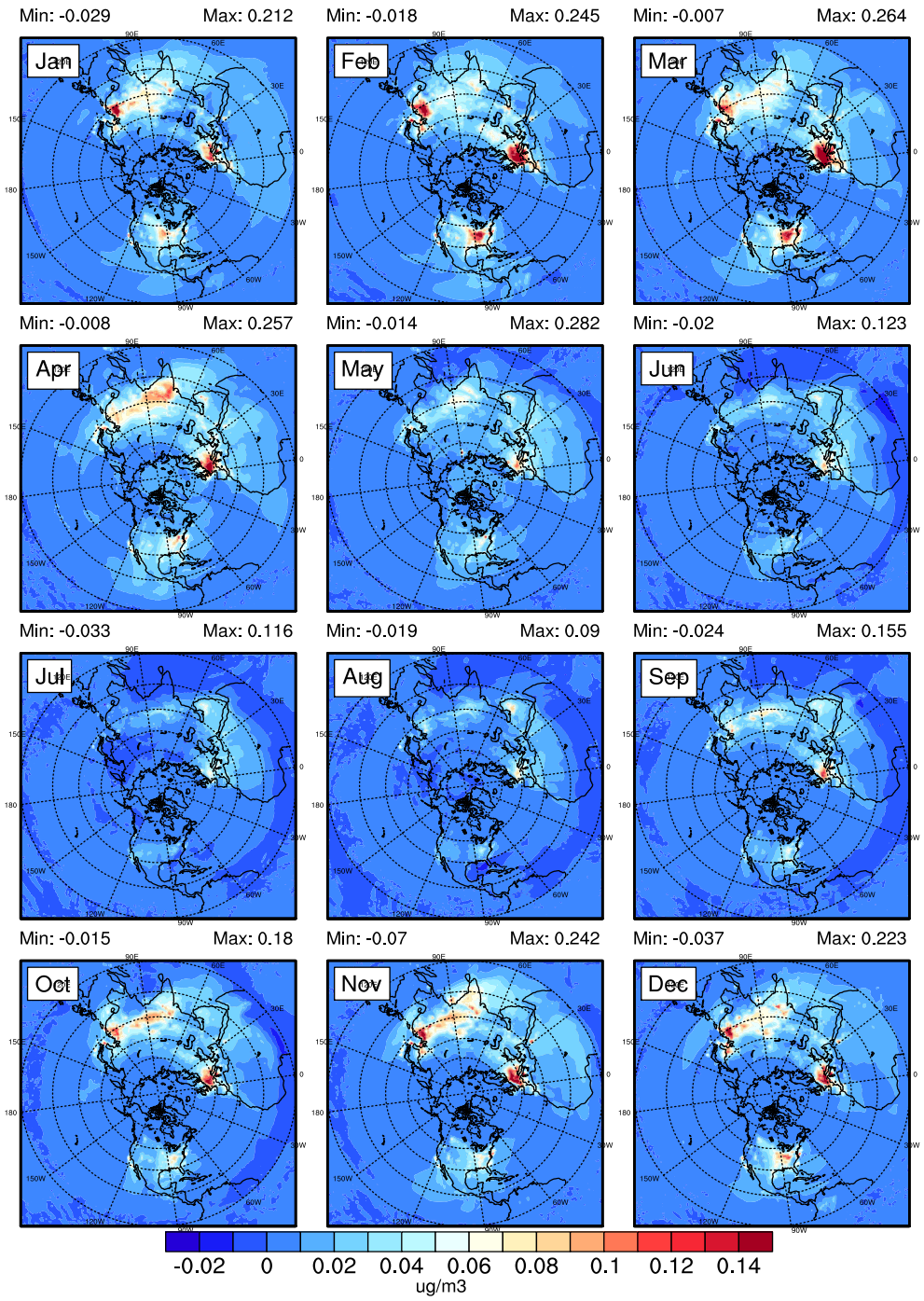

Figure B2: Monthly average aviation-attributable surface concentrations of $PM_{2.5}$ in HEMI domain

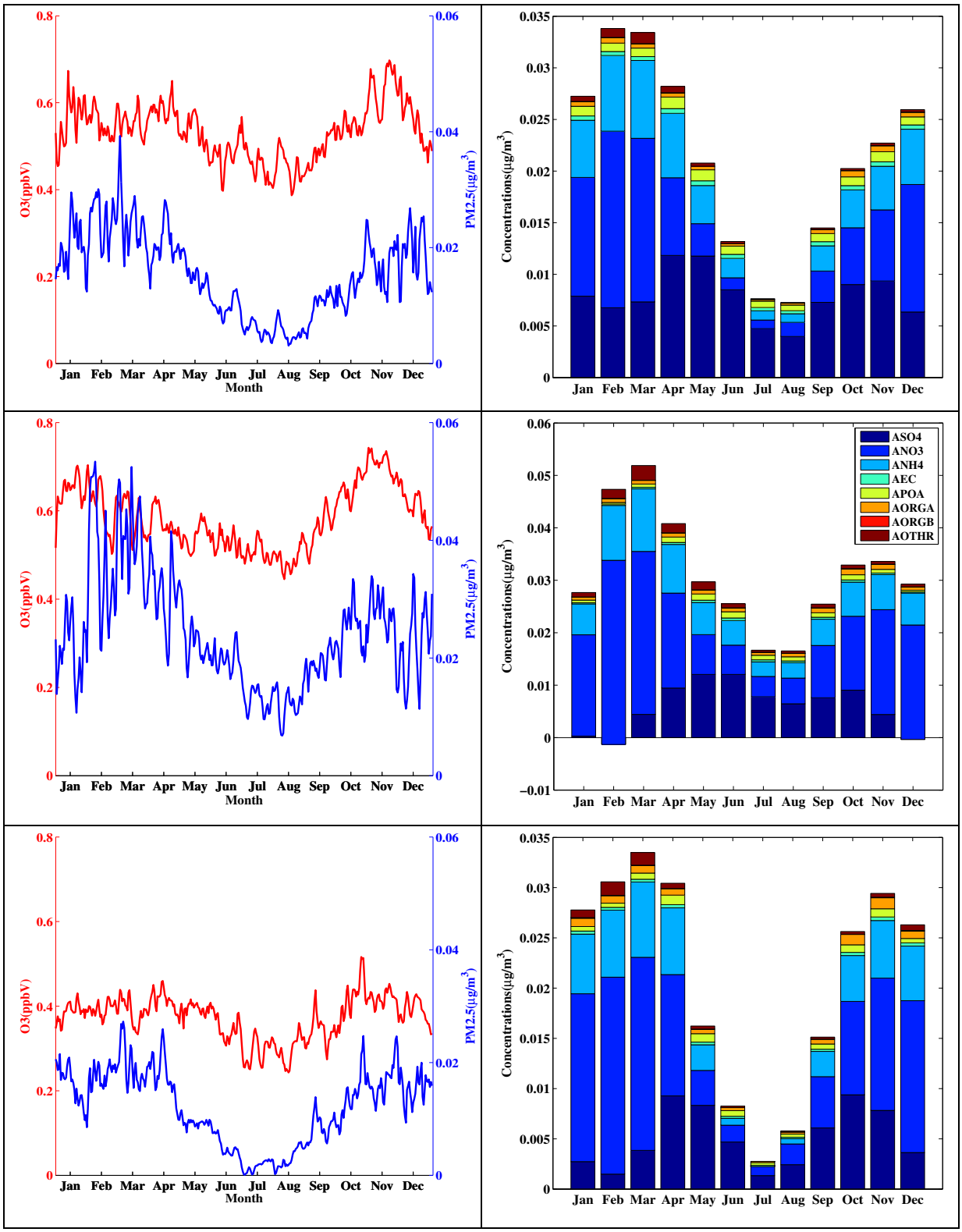

Figure B3: Daily domain-wide average AAC (left) of O_3 (red), $PM_{2.5}$ (blue) for NA (top), EU (middle) and EA (bottom) sub-regions from HEMI domain at the surface.

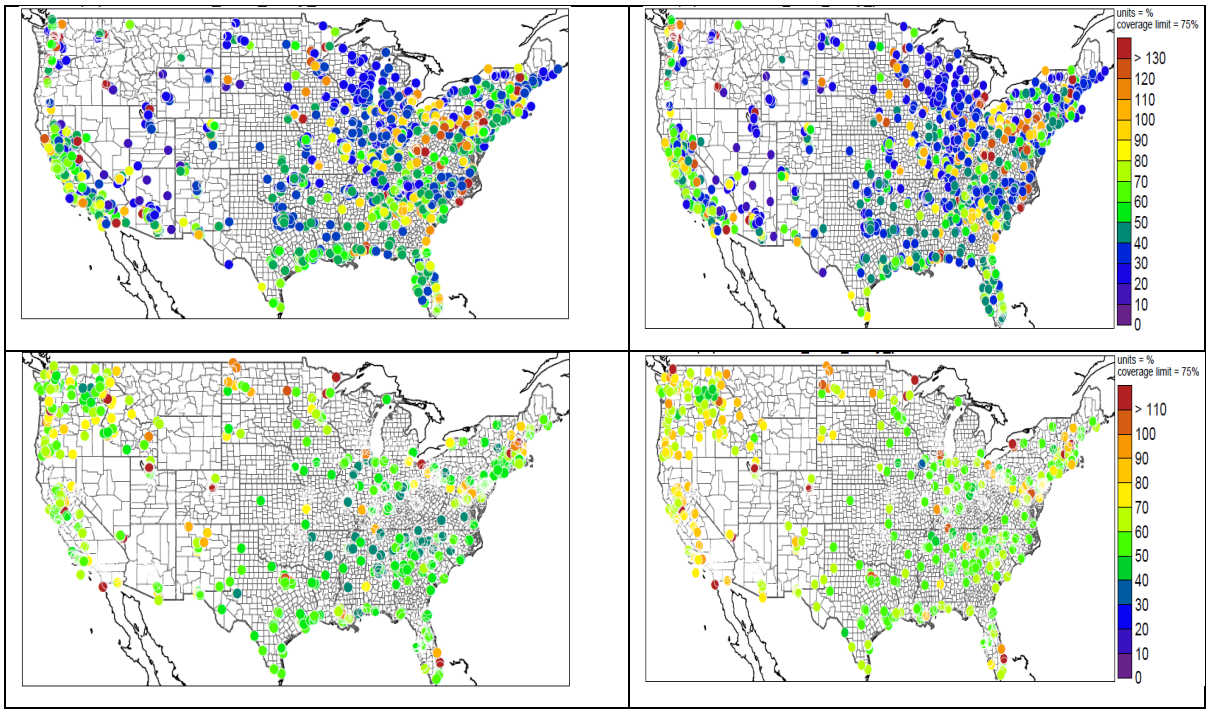

Figure B4: NME (%) spatial plots averaged over the year 2005 of hourly O_3 (top) and $PM_{2.5}$ (bottom) predicted by Airc36 (CONUS, left panel) and Airc108 (HEMI-NA, right panel) model scenarios in comparison with hourly AQS observations.

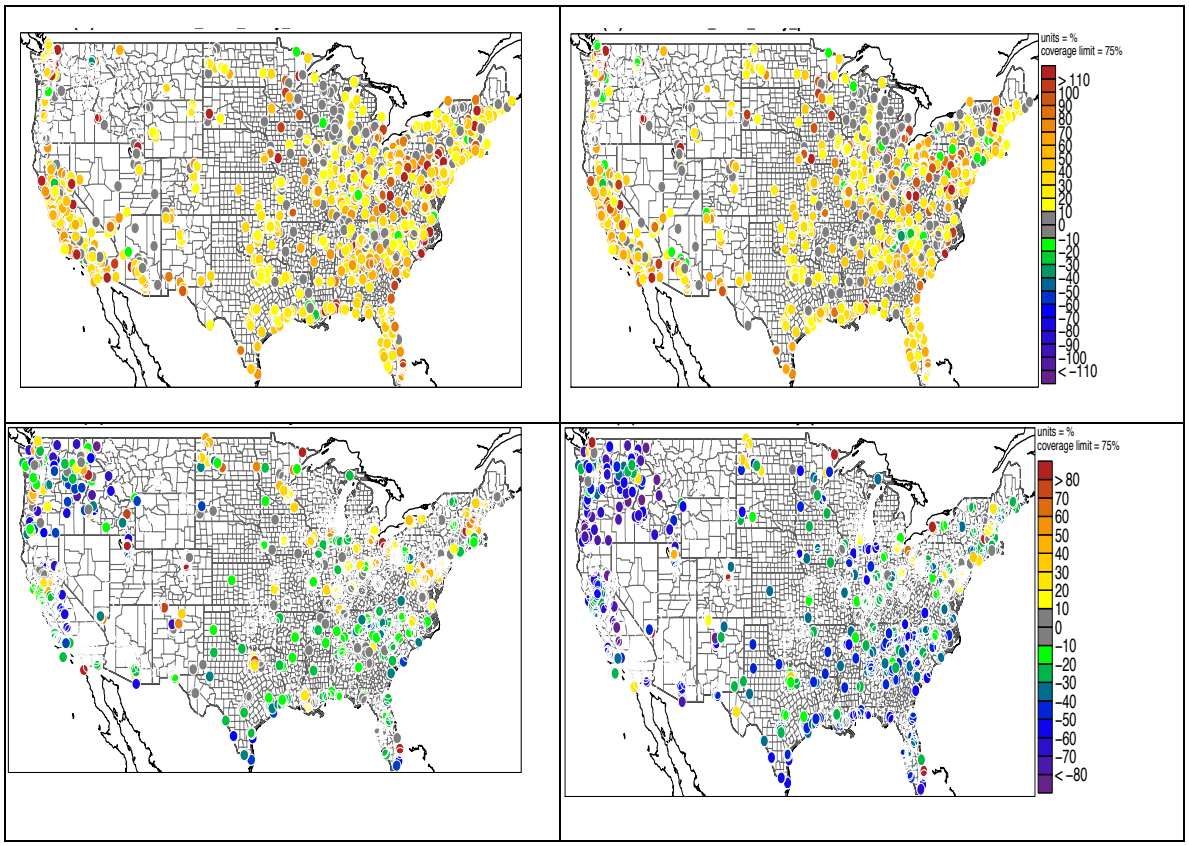

Figure B5: NMB (%) spatial plots averaged over the year 2005 of hourly O_3 (top) and $PM_{2.5}$ (bottom) predicted by Airc36 (CONUS, left panel) and Airc108 (HEMI-NA, right panel) model scenarios in comparison with hourly AQS observations.

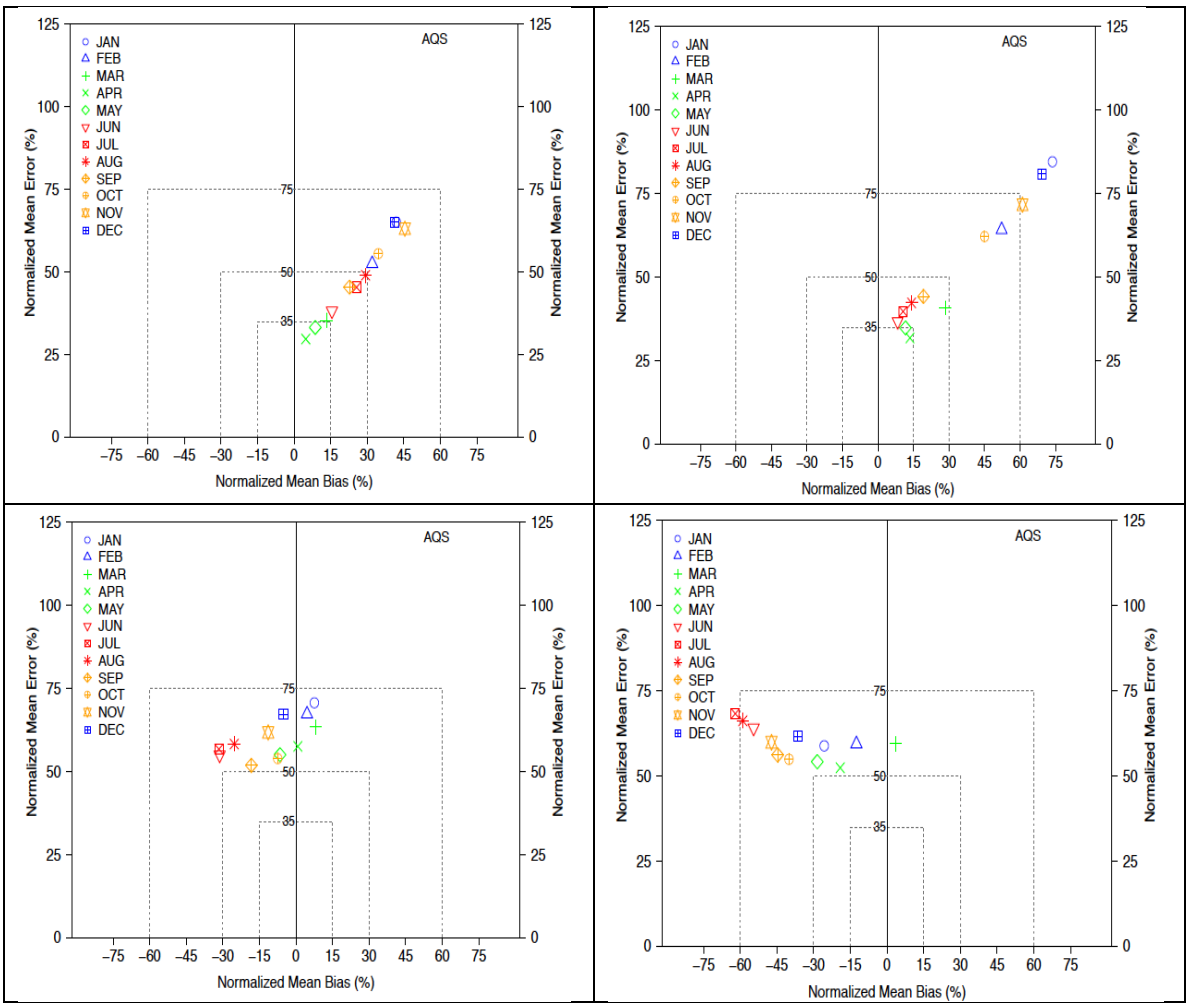

Figure B6: Monthly soccer plots of O_3 (top) and $PM_{2.5}$ (bottom) for Airc36 (CONUS, left panel) and Airc108 (HEMI-NA, right panel) model scenarios when compared with AQS observations.

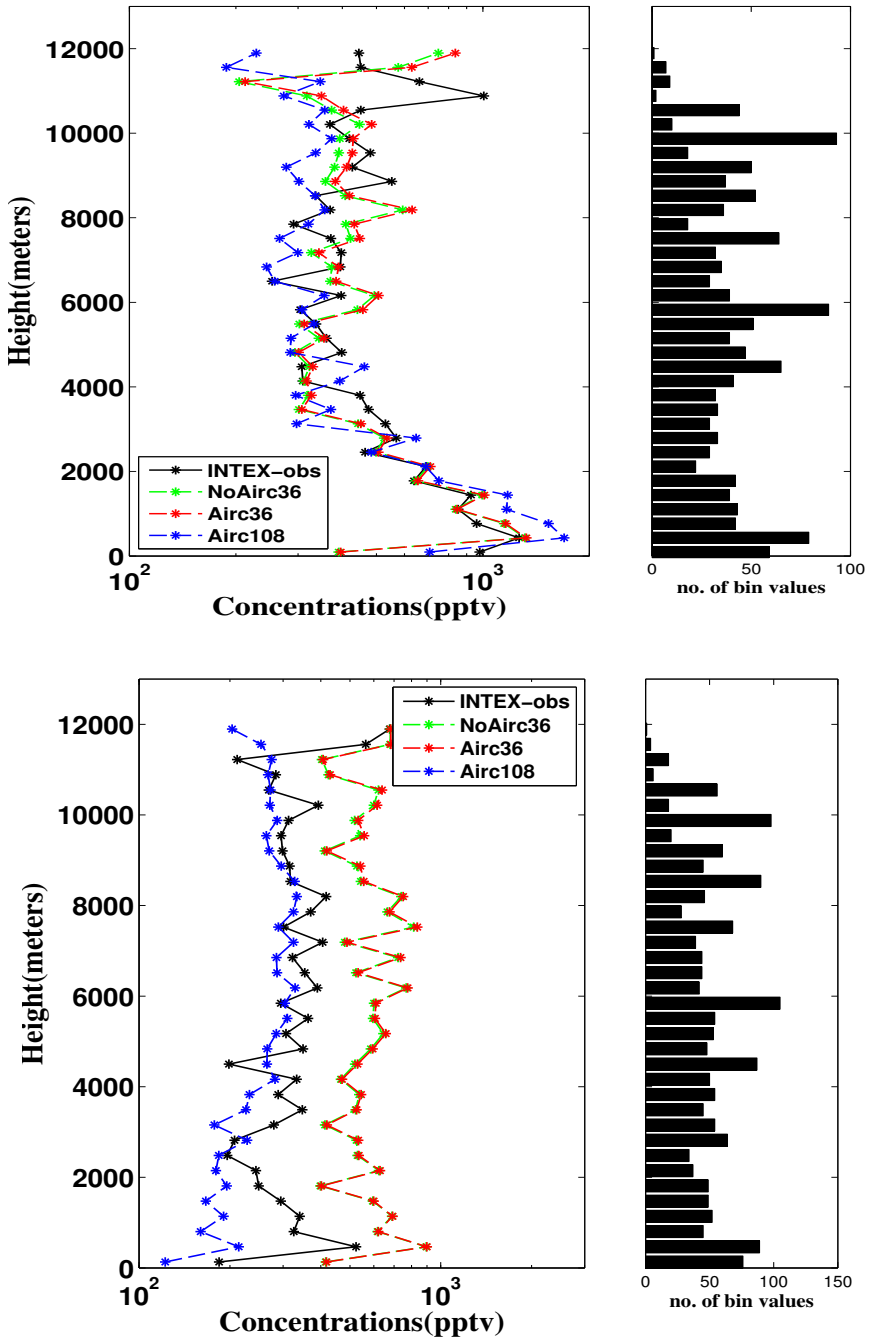

Figure B7: Comparison of modeled predictions of HNO_3 (top) and PAN (bottom) from scenarios NoAirc36 (green), Airc36 (red), Airc108 (blue) paired with INTEX-NA observations (black) and binned vertically. Each point represents the mean concentration value in a particular altitude bin of paired modeled and observations. The bar plot (right) shows the number of paired values in each bin.

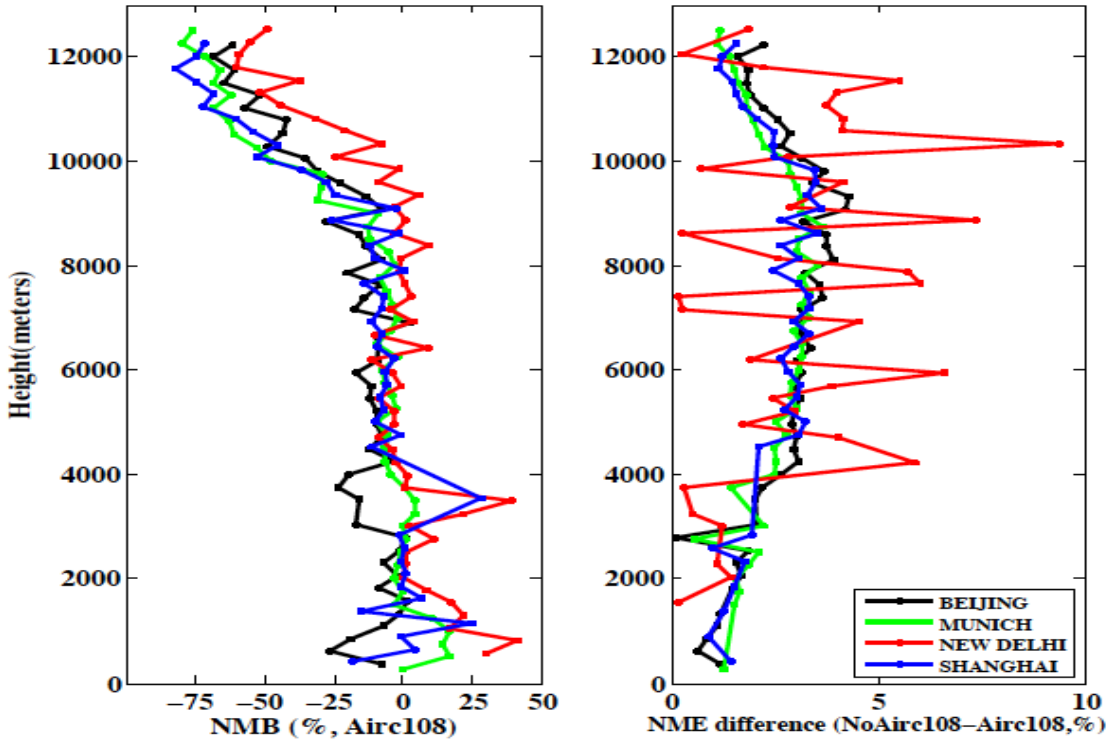

Figure B8: NMB (%) vertical profiles of hourly O_3 predicted by the Airc108 model scenarios when compared with MOZAIC in-situ aircraft observation data at four airports (Beijing, Munich, New Delhi, Shanghai). Also shown are the NME differences between NoAirc108 and Airc108 scenarios.

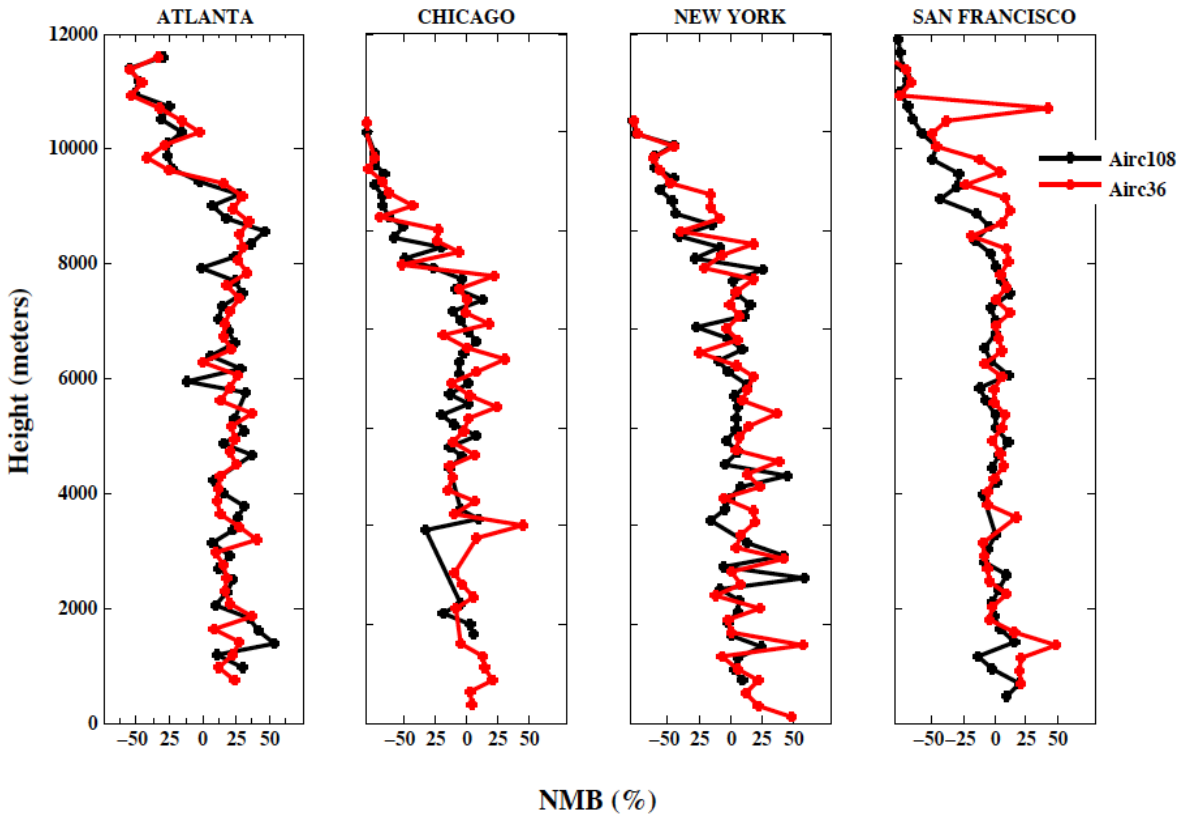

Figure B9: NMB (%) vertical profiles of hourly O_3 predicted by the Airc108 (black line) and Airc36 (red line) model scenarios when compared with MOZAIC in-situ aircraft observation data from four NA airports (Atlanta, Chicago, New York, San Francisco).

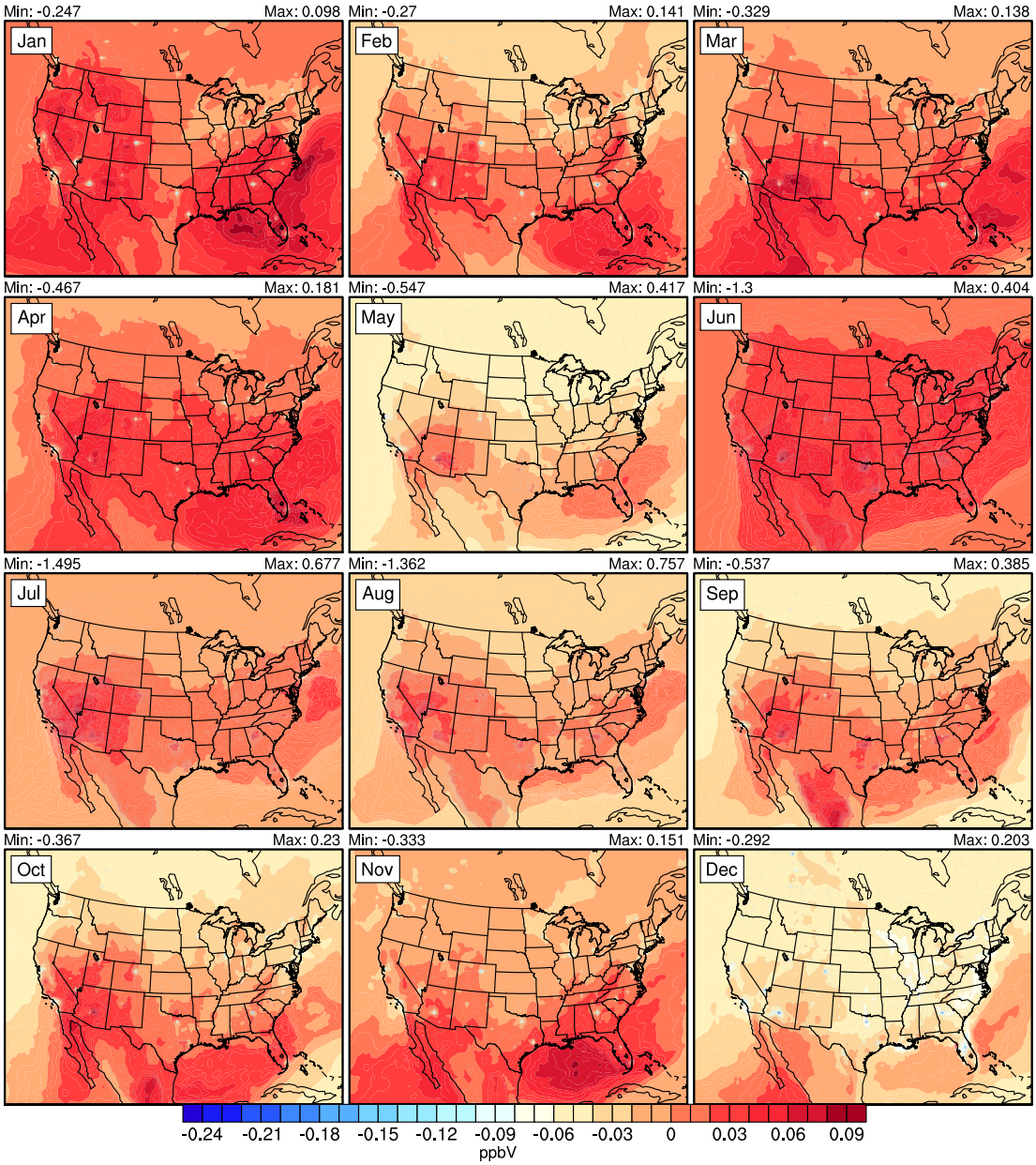

Figure B10: Monthly average aviation-attributable surface concentrations of O_3 in CONUS domain

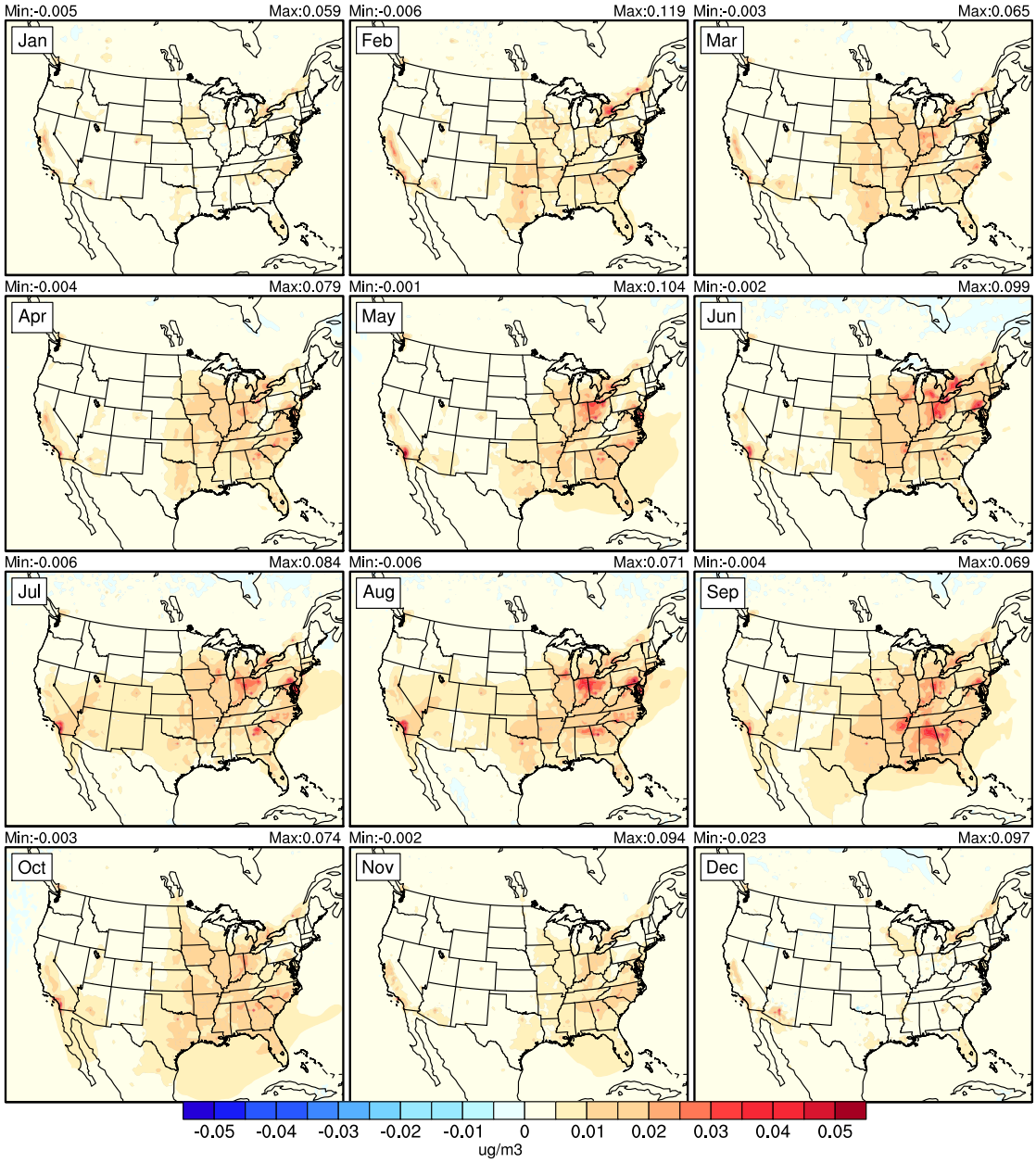

Figure B11: Monthly average aviation-attributable surface concentrations of $PM_{2.5}$ in CONUS domain at the surface.

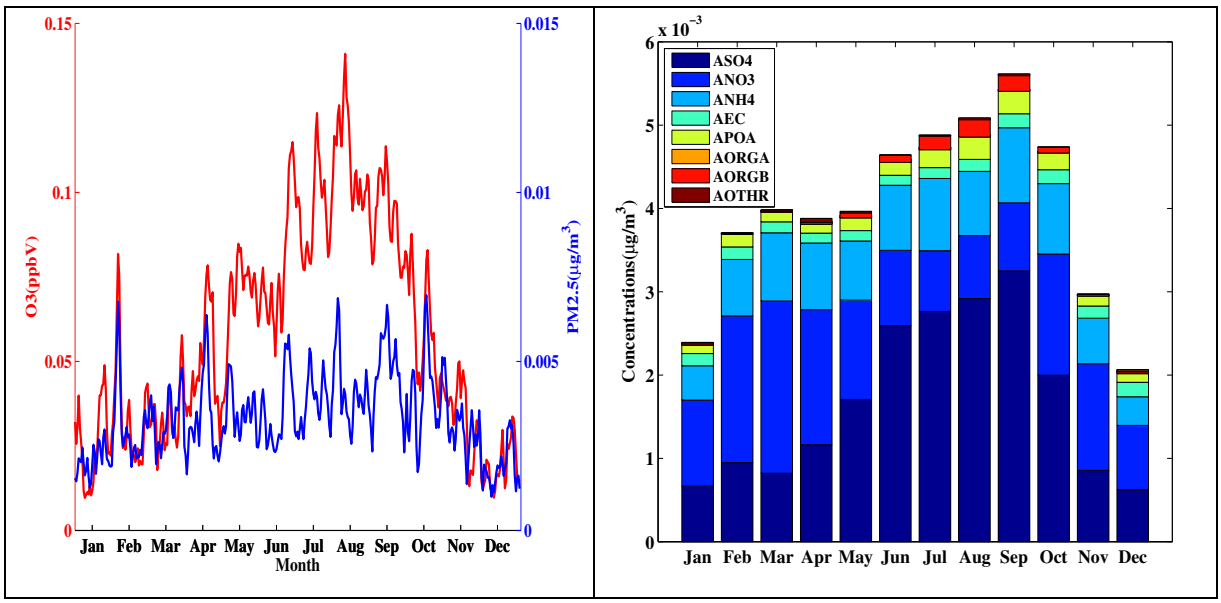

Figure B12: Daily domain-wide average AAC (left) of O_3 (red), $PM_{2.5}$ (blue) and monthly domain-wide average speciated $PM_{2.5}$ (right) AAC for CONUS domain (36 km) at the surface.

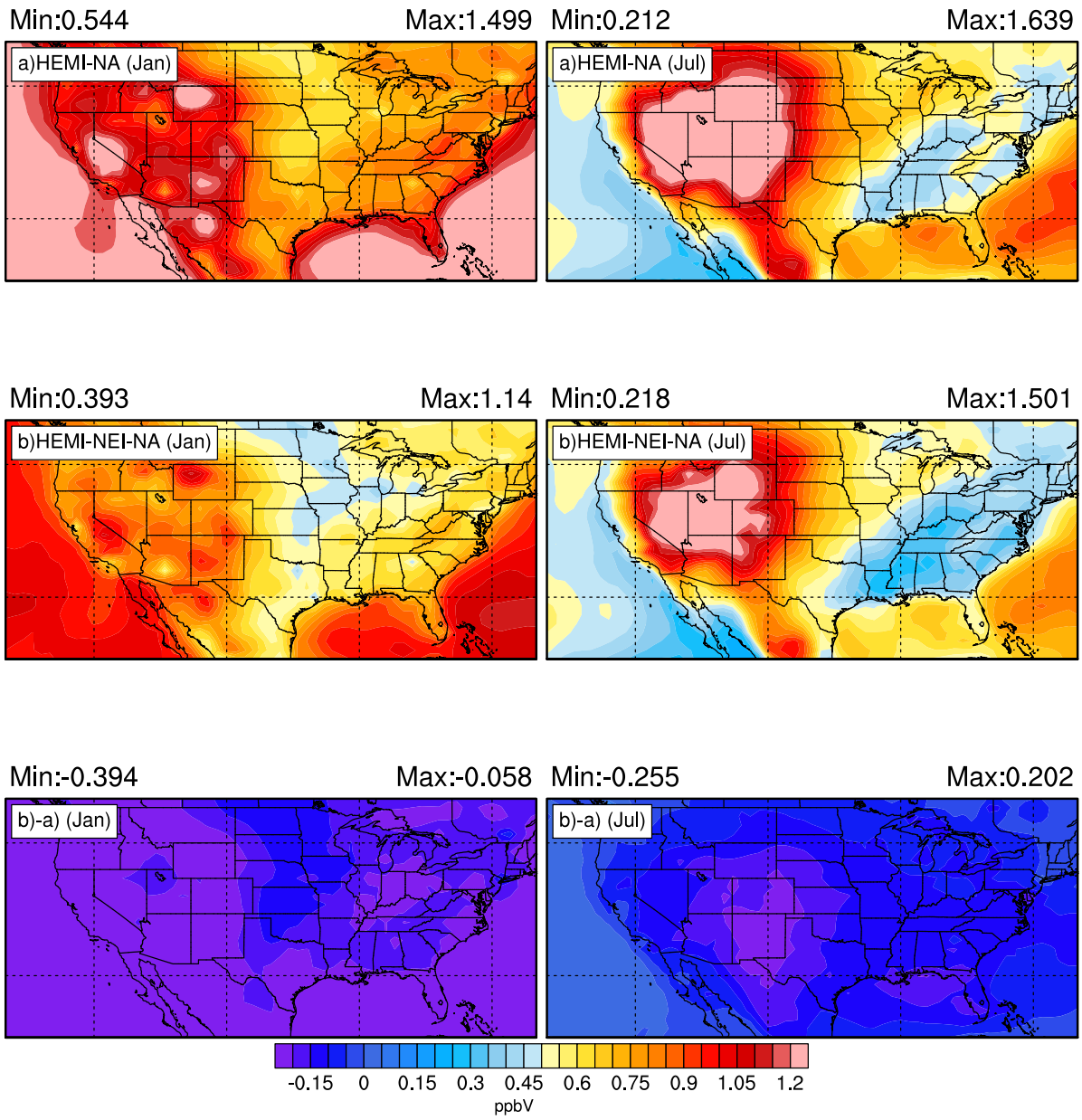

Figure B13: Monthly average ACC spatial plots of a) HEMI-NA (top), b) HEMI-NEI-NA (middle) and difference (b-a, bottom) in January (left) and July (right) for O_3.

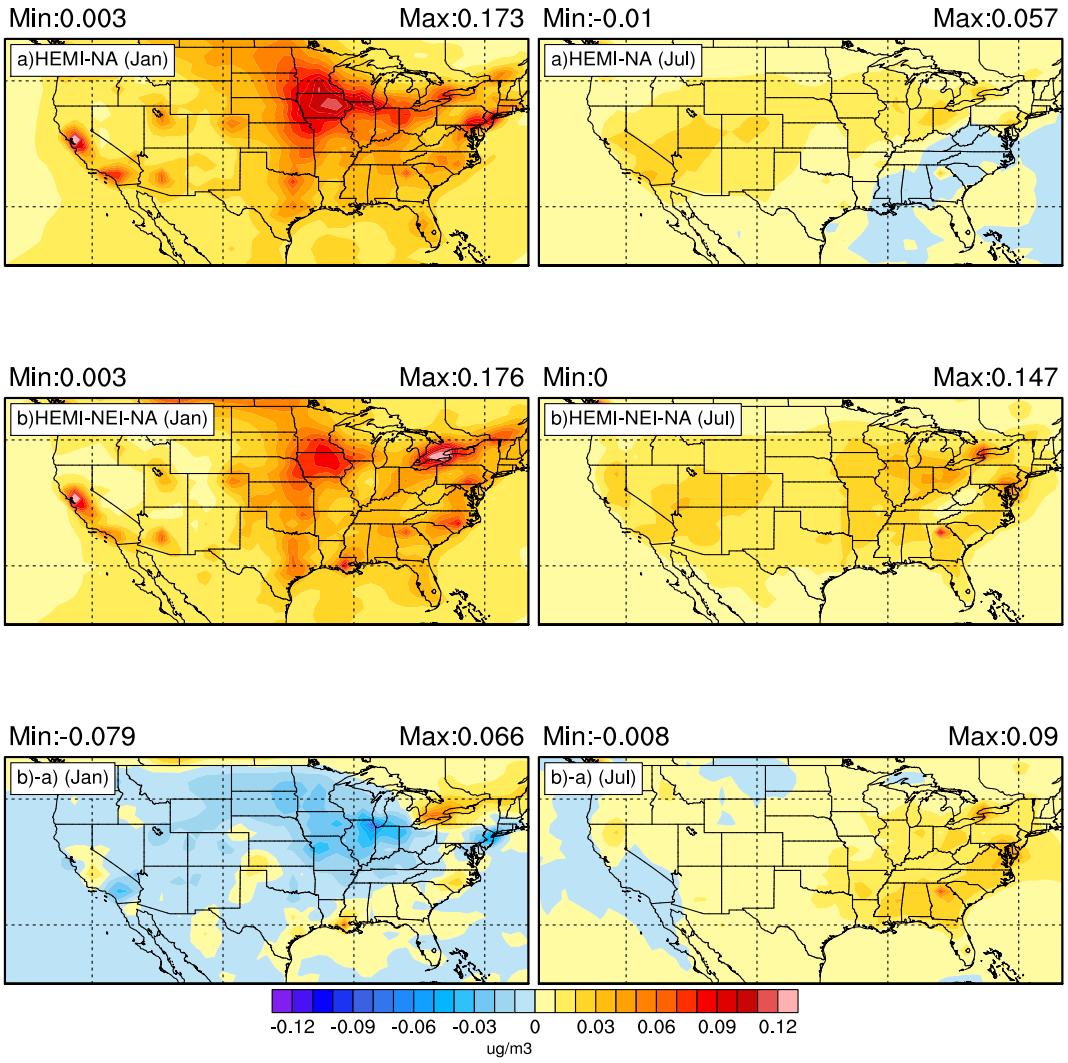

Figure B14: Monthly average AAC spatial plots of a) HEMI-NA (top), b) HEMI-NEI-NA (middle) and difference (b-a, bottom) in January (left) and July (right) for $PM_{2.5}$.

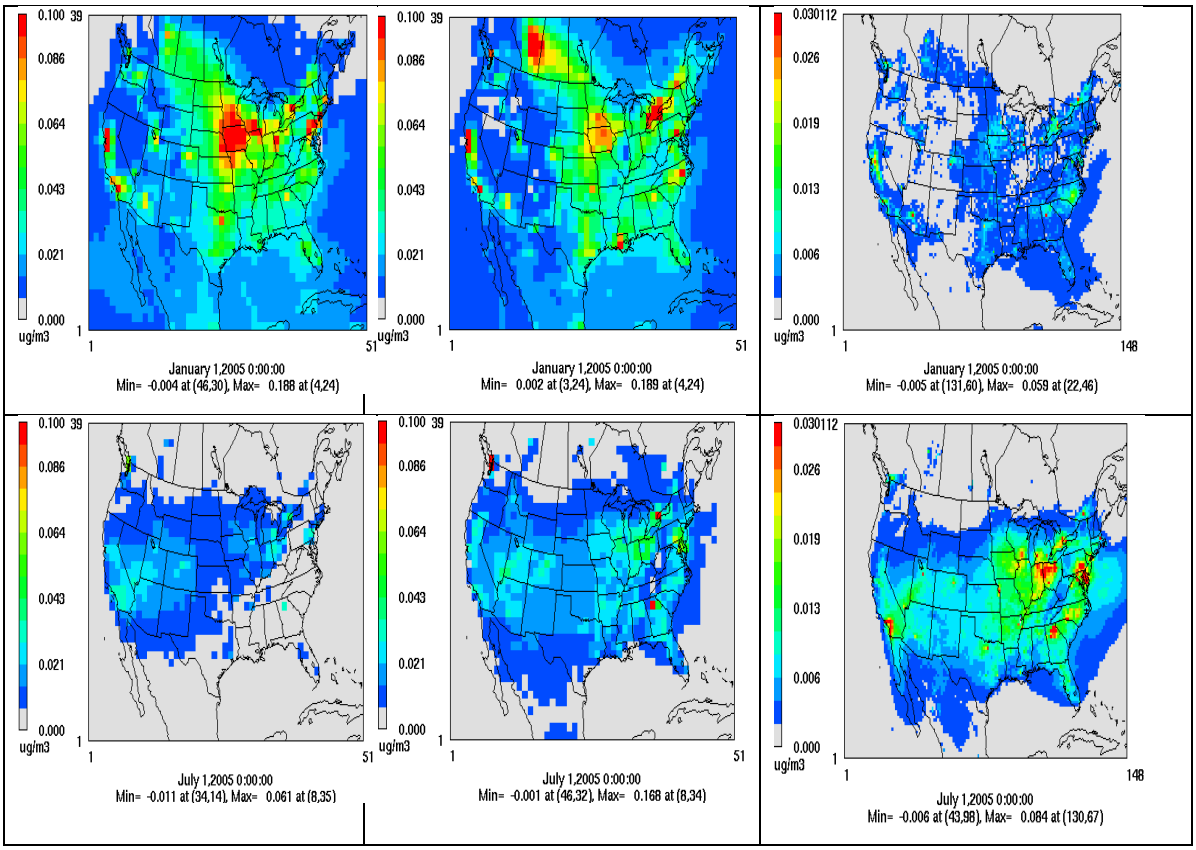

Figure B15: Comparison of monthly averages aviation-attributable $PM_{2.5}$ concentrations from three cases a) HEMI-NA (108km) (left) b) HEMI-NEI-NA (middle) c) CONUS (36km) (right) for January (top panel) and July (bottom panel) months The color bar limits are similar between a) and b) cases but for c) we used a lower limit to capture the spatial variation in CONUS.

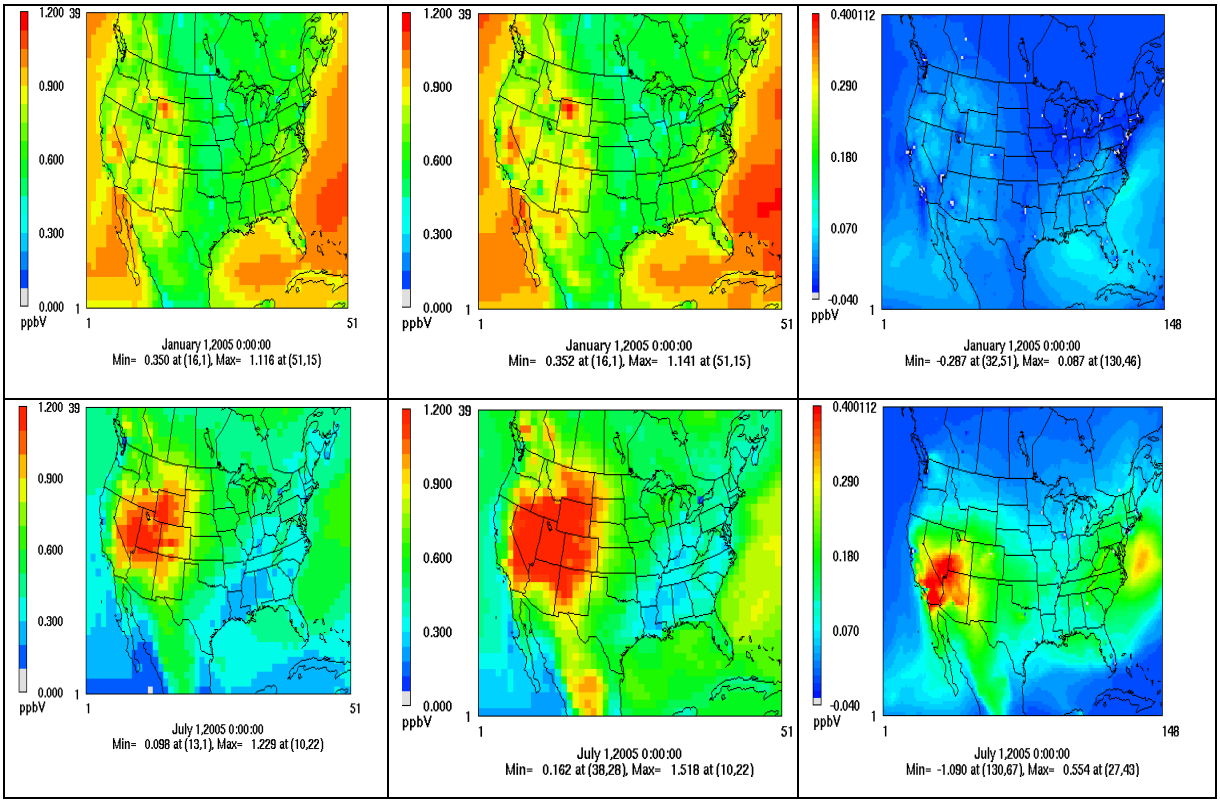

Figure B16: Comparison of monthly averages aviation-attributable O_3 concentrations from three cases a) HEMI-NA (108km) (left) b) HEMI-NEI-NA (middle) c) CONUS (right) (36km) for January (top panel) and July (bottom panel) months. The color bar limits are similar between a) and b) cases but for c) we used a lower limit to capture the spatial variation in CONUS.

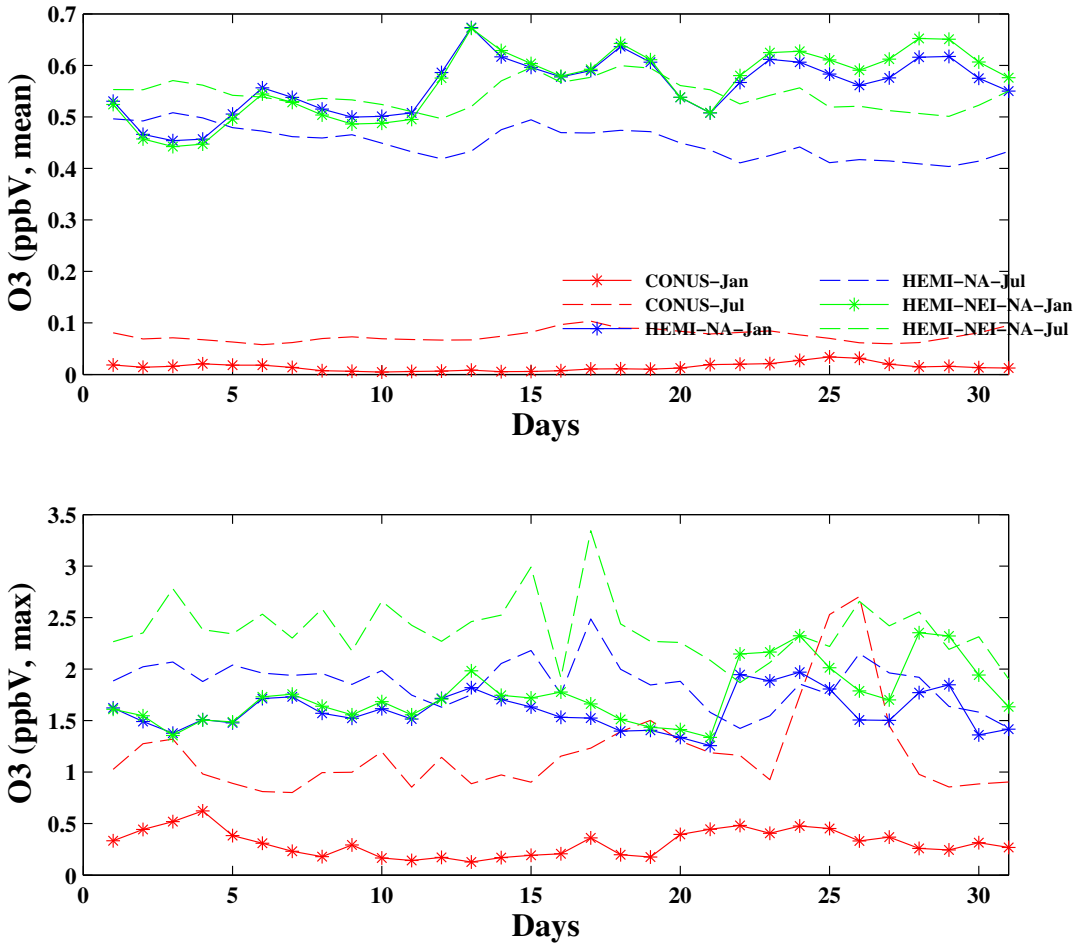

Figure B17: Mean (top) and Maximum (bottom) domain-wide daily aviation-attributable O_3 contributions for three cases (HEMI-NA, HEMI-NEI-NA, CONUS) for January and July months.

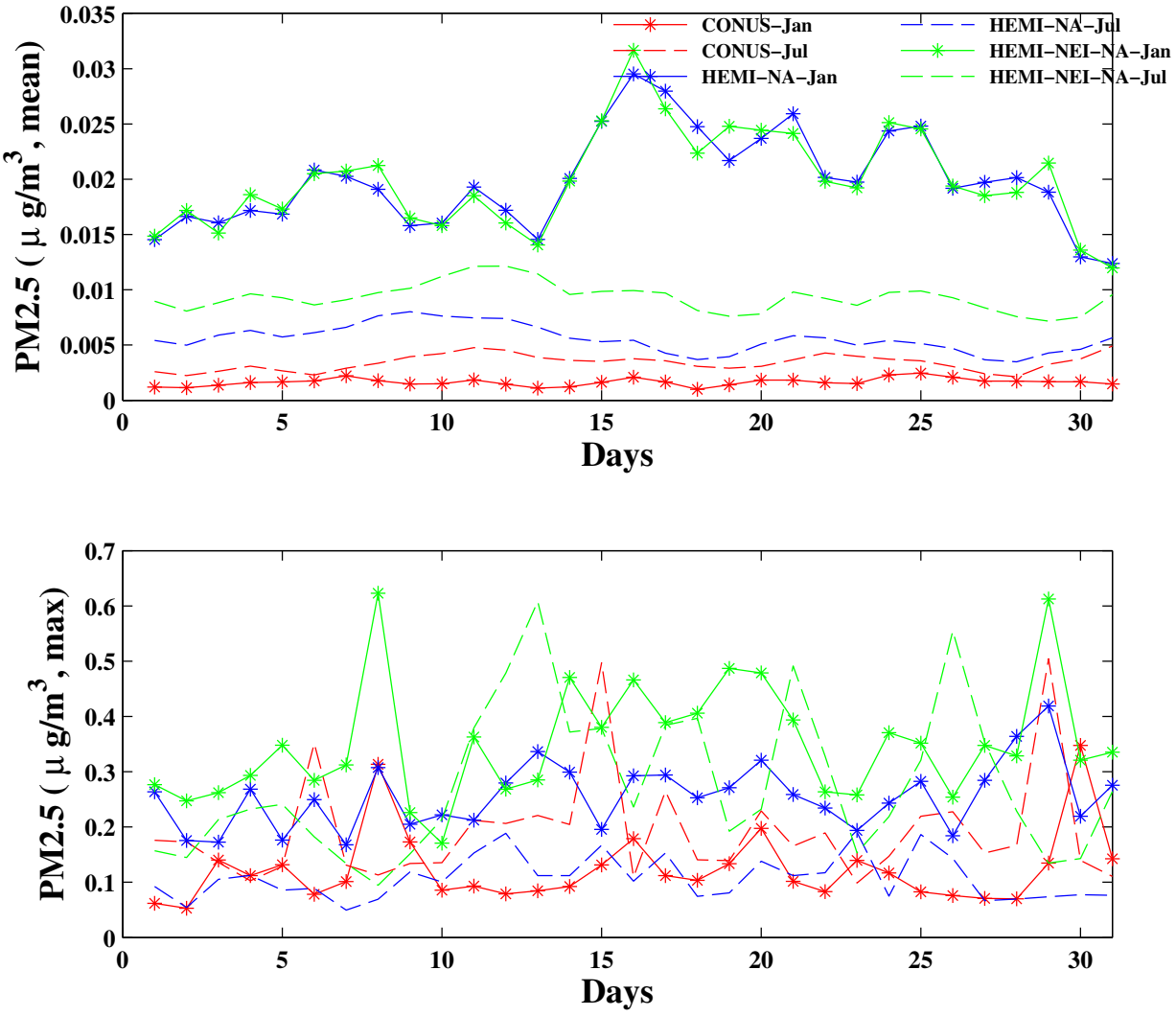

Figure B18: Mean (top) and Maximum (bottom) domain-wide daily aviation-attributable $PM_{2.5}$ contributions for three cases (HEMI-NA, HEMI-NEI-NA, CONUS) for January and July months.

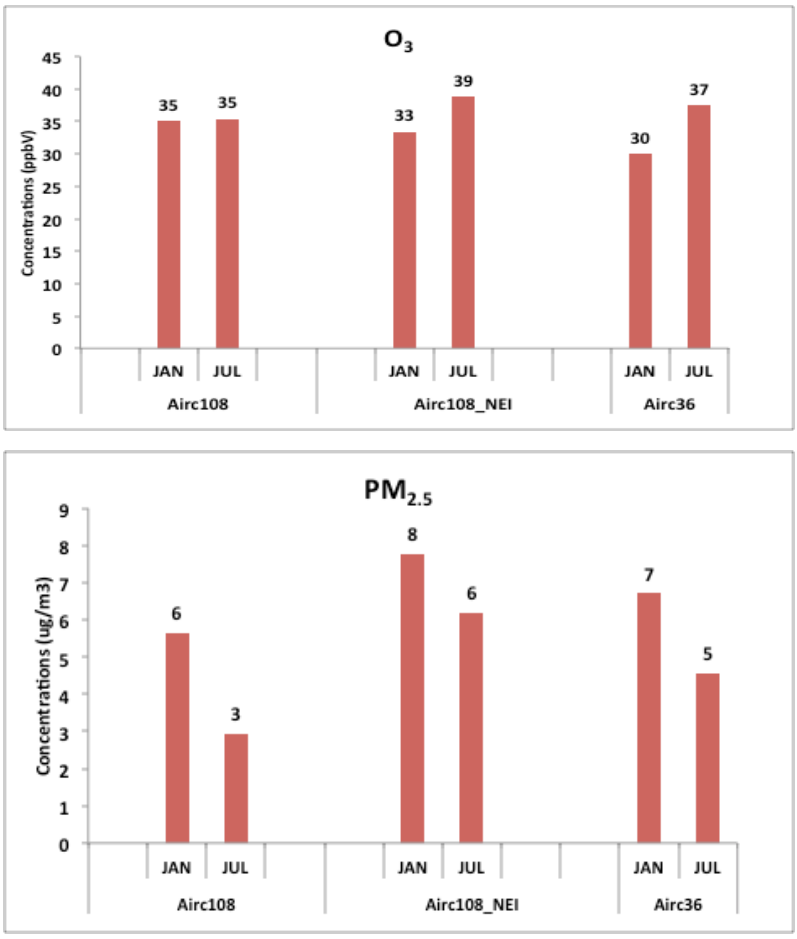

Figure B19: Domain-wide monthly average O_3 (top) and $PM_{2.5}$ (bottom) concentrations for three cases (Airc108, Airc108_NEI, Airc36) in January and July months.

REFERENCES

Akritidis, D., Pozzer, A., Zanis, P., Tyrlis, E., Škerlak, B., Sprenger, M., Lelieveld, J., 2016. On the role of tropopause folds in summertime tropospheric ozone over the eastern Mediterranean and the Middle East. Atmos. Chem. Phys. Discuss. 0, 1–24. doi:10.5194/acp-2016-547.

Alapaty, K., Mathur, R., 1998. Effects of Atmospheric Boundary Layer Mixing Representations on Vertical Distribution of Passive and Reactive Tracers. Meteorol. Atmsopheric Phys. 69, 101–118.

Allen, D., Pickering, K., Duncan, B., Damon, M., 2010. Impact of lightning NO emissions on North American photochemistry as determined using the Global Modeling Initiative (GMI) model. J. Geophys. Res. Atmos. 115, 1–24. doi:10.1029/2010JD014062

Allen, D.J., Pickering, K.E., Pinder, R.W., Henderson, B.H., Appel, K.W., Prados, a., 2012. Impact of lightning-NO on eastern United States photochemistry during the summer of 2006 as determined using the CMAQ model. Atmos. Chem. Phys. 12, 1737–1758. doi:10.5194/acp-12-1737-2012

Allen, J., Rood, R.B., Thompson, A.M., Hudson, D., 1996. Three-dimensional radon 222 calculations using assimilated meteorological data and a convective mixing algorithm Abstract . The distribution of 222Rn is simulated using a three-dimensional chemistry (PBL) to the upper troposphere CTM-calculated at Bermu. J. Geophys. Res. 101, 6871–6881.

Anderson, B.E., Chen, G., Blake, D.R., 2006. Hydrocarbon emissions from a modern commercial airliner. Atmos. Environ. 40, 3601–3612. doi:10.1016/j.atmosenv.2005.09.072

Anenberg, S.C., West, I.J., Fiore, A.M., Jaffe, D. a, Prather, M.J., Bergmann, D., Cuvelier, K., Dentener, F.J., Duncan, B.N., Gauss, M., Hess, P., Jonson, J.E., Lupu, A., Mackenzie, I. a, Marmer, E., Park, R.J., Sanderson, M.G., Schultz, M., Shindell, D.T., Szopa, S., Vivanco, M.G., Wild, O., Zeng, G., 2009. Intercontinental impacts of ozone pollution on human mortality. Environ. Sci. Technol. 43, 6482–6487.

Arunachalam, S., Wang, B., Davis, N., Baek, B.H., Levy, J.I., 2011. Effect of chemistry-transport model scale and resolution on population exposure to PM2.5 from aircraft emissions during landing and takeoff. Atmos. Environ. 45, 3294–3300. doi:10.1016/j.atmosenv.2011.03.029

Baek, B.H., Arunachalam, S., Woody, M., Vennam, L.P., Omary, M., Binkowski, F., Fleming, G., 2012a. A New Interface to Model Global Commercial Aircraft Emissions from the FAA Aviation Environmental Design Tool (AEDT) in Air Quality Models, in: CMAS.

Baek, B.H., Arunachalam, S., Woody, M., Vennam, L.P., Omary, M., Binkowski, F., Fleming, G., 2012b. A New Interface to Model Global Commercial Aircraft Emissions from the FAA

Aviation Environmental Design Tool (AEDT) in Air Quality Models. Annual CMAS Conference, 15–17 October, 2012., Chapel Hill, NC.

Barbara J. Finlayson-Pitts and James N. Pitts Jr, 2000. CHAPTER 2 - The Atmospheric System, In Chemistry of the Upper and Lower Atmosphere. Academic Press, San Diego, pp. 15–42.

Barrett, S.R.H., Britter, R.E., Waitz, I.A., 2010. Global mortality attributable to aircraft cruise emissions. Environ. Sci. Technol. 44, 7736–7742. doi:10.1021/es101325r

Beck, J.P., Reeves, C.E., de Leeuw, F.A.A.M., Penkett, S.A., 1992. The effect of aircraft emissions on tropospheric ozone in the northern hemisphere. Atmos. Environ. Part A. Gen. Top. 26, 17–29. doi:10.1016/0960-1686(92)90257-L

Beyersdorf, A.J., Thornhill, K.L., Winstead, E.L., Ziemba, L.D., Blake, D.R., Timko, M.T., Anderson, B.E., 2012. Power-dependent speciation of volatile organic compounds in aircraft exhaust. Atmos. Environ. 61, 275–282. doi:10.1016/j.atmosenv.2012.07.027

Beyersdorf, A.J., Timko, M.T., Ziemba, L.D., Bulzan, D., Corporan, E., Herndon, S.C., Howard, R., Miake-Lye, R., Thornhill, K.L., Winstead, E., Wey, C., Yu, Z., Anderson, B.E., 2014. Reductions in aircraft particulate emissions due to the use of Fischer-Tropsch fuels. Atmos. Chem. Phys. 14, 11–23. doi:10.5194/acp-14-11-2014

Brunelle-Yeung, E., Masek, T., Rojo, J.J., Levy, J.I., Arunachalam, S., Miller, S.M., Barrett, S.R.H., Kuhn, S.R., Waitz, I.A., 2014. Assessing the impact of aviation environmental policies on public health. Transp. Policy 34, 21–28. doi:10.1016/j.tranpol.2014.02.015

Byun, D.W., Schere, K., 2006. Review of the governing equations, computational algorithms, and other components of the models-3 Community Multiscale Air Quality (CMAQ) modeling system. Appl.Mech.Rev 51–57.

Cahill, T.M., 2014. Ambient acrolein concentrations in coastal, remote, and urban regions in California. Environ. Sci. Technol. 48, 8507–8513. doi:10.1021/es5014533

Caiazzo, F., Ashok, A., Waitz, I. a., Yim, S.H.L., Barrett, S.R.H., 2013. Air pollution and early deaths in the United States. Part I: Quantifying the impact of major sectors in 2005. Atmos. Environ. 79, 198–208. doi:10.1016/j.atmosenv.2013.05.081

Clark, A.I., McIntyre, a. E., Perry, R., Lester, J.N., 1983. Air quality measurement in the vicinity of airports. Environ. Pollut. Ser. B Chem. Phys. 6, 245–261. doi:10.1016/0143-148X(83)90012-5

CMAS, 2015. CMAQv5.1. http://www.airqualitymodeling.org/cmaqwiki/index.php?title=CMAQ_version_5.1_(September_2015_beta_release)_Technical_Documentation#Gas_and_AerosolChemistry (accessed 7.12.15).

CMAS, 2014. CMAQv5.0.2 release notes. http://www.airqualitymodeling.org/cmaqwiki/index.php?title=CMAQv5.0.2_gas-phase_chemistry (accessed 1.21.15).

Cooper, O.R., Oltmans, S.J., Johnson, B.J., Brioude, J., Angevine, W., Trainer, M., Parrish, D.D., Ryerson, T.R., Pollack, I., Cullis, P.D., Ives, M. a., Tarasick, D.W., Al-Saadi, J., Stajner, I., 2011. Measurement of western U.S. baseline ozone from the surface to the tropopause and assessment of downwind impact regions. J. Geophys. Res. 116, D00V03. doi:10.1029/2011JD016095

Dentener, F., Keating, T., and Akimoto, H., 2010. Hemispheric Transport of 2010 Part a : Ozone and Particulate Matter. Air Pollut. Stud., vol. 17, United Nations, New York.

Dessens, O., Köhler, M.O., Rogers, H.L., Jones, R.L., Pyle, J.A., 2014. Aviation and climate change. Transp. Policy 34, 14–20. doi:10.1016/j.tranpol.2014.02.014

Dodson, R.E., Houseman, E.A., Morin, B., Levy, J.I., 2009. An analysis of continuous black carbon concentrations in proximity to an airport and major roadways. Atmos. Environ. 43, 3764–3773. doi:10.1016/j.atmosenv.2009.04.014

Eastham, S.D., Weisenstein, D.K., Barrett, S.R.H., 2014. Development and evaluation of the unified tropospheric–stratospheric chemistry extension (UCX) for the global chemistry-transport model GEOS-Chem. Atmos. Environ. 89, 52–63. doi:10.1016/j.atmosenv.2014.02.001

European Commission, J.R.C. (JRC)/Netherlands E.A.A. (PBL):, 2016. Emission Database for Global Atmospheric Research (EDGAR). http://edgar.jrc.ec.europa.eu (accessed 3.1.16).

Eyers, C.J., Norman, P., Middel, J., Plohr, M., Michot, S., Atkinson, K., 2004. AERO2k Global Aviation Emissions Inventories for 2002 and 2025.

FAA, 2011. FAA National forecast FY 2011-2031.

FAA, 2010. FAA Aerospace Forecast Fiscal Years 2010-2030.

FAA, 2009. Guidance for quantifying speciated organic gas emissions from airport sources.

Fang, Y., Fiore, A.M., Horowitz, L.W., Levy, H., Hu, Y., Russell, A.G., 2010. Sensitivity of the NOy budget over the United States to anthropogenic and lightning NOx in summer. J. Geophys. Res. 115, D18312. doi:10.1029/2010JD014079

Federal Aviation Administration, 2010. FAA aerospace forecast fiscal years 2010 – 2030.

Federal Aviation Administration, 2005. Aviation & Emissions A Primer.

Forster, C., Stohl, A., James, P., 2003. The residence times of aircraft emissions in the stratosphere using a mean emission inventory and emissions along actual flight tracks. J. Geophys. Res. 108. doi:10.1029/2002JD002515

Friedfeld, S., Fraser, M., Ensor, K., Tribble, S., Rehle, D., Leleux, D., Tittel, F., 2002. Statistical analysis of primary and secondary atmospheric formaldehyde. Atmos. Environ. 36, 4767–4775. doi:10.1016/S1352-2310(02)00558-7

Gan, C.M., Hogrefe, C., Mathur, R., Pleim, J., Xing, J., Wong, D., Gilliam, R., Pouliot, G., Wei, C., 2016. Assessment of the effects of horizontal grid resolution on long-term air quality trends using coupled WRF-CMAQ simulations. Atmos. Environ. 132, 207–216. doi:10.1016/j.atmosenv.2016.02.036

Gantt, B., Kelly, J.T., Bash, J.O., 2015. Updating sea spray aerosol emissions in the Community Multiscale Air Quality (CMAQ) model version 5.0.2. Geosci. Model Dev. 8, 3733–3746. doi:10.5194/gmd-8-3733-2015

Gardner, R.M., Adams, K., Cook, T., Deidewig, F., Ernedal, S., Falk, R., Fleuti, E., Herms, E., Johnson, C.E., Lecht, M., Newon, P., Shmitt, A., Vanderbergh, C., van Drimmelen, R., 1997. The ANCAT/EC Global Inventory of NOx Emissions from Aircraft. Atmos. Environ. 31, 1751–1766.

Gauss, M., Isaksen, I.S.A., Lee, D.S., Søvde, O.A., 2006. Impact of aircraft NOx emissions on the atmosphere - Tradeoffs to reduce the impact. Atmos. Chem. Phys. 6, 1529–1548. doi:10.5194/acp-6-1529-2006

Gerbig, C., Körner, S., Lin, J.C., 2008. Vertical mixing in atmospheric tracer transport models: error characterization and propagation. Atmos. Chem. Phys. 8, 591–602. doi:10.5194/acp-8-591-2008

Grell, G.., Dudhia, J., Stauffer, D.R., 1994. A description of the fifth generation Penn State/NCAR mesoscale model (MM5).

Hauglustaine, D. a., Koffi, B., 2012. Boundary layer ozone pollution caused by future aircraft emissions. Geophys. Res. Lett. 39, L13808. doi:10.1029/2012GL052008

Henderson, B.H., Akhtar, F., Pye, H.O.T., Napelenok, S.L., Hutzell, W.T., 2014. A database and tool for boundary conditions for regional air quality modeling: Description and evaluation. Geosci. Model Dev. 7, 339–360. doi:10.5194/gmd-7-339-2014

Henderson, B.H., Pinder, R.W., Crooks, J., Cohen, R.C., Hutzell, W.T., Sarwar, G., Goliff, W.S., Stockwell, W.R., Fahr, A., Mathur, R., Carlton, A.G., Vizuete, W., 2011. Evaluation of simulated photochemical partitioning of oxidized nitrogen in the upper troposphere. Atmos. Chem. Phys. 11, 275–291. doi:10.5194/acp-11-275-2011

Herndon, S., Wood, E., Franklin, J., Miake-Lye, R., Knighton, W.B., Babb, M., Nakahara, A., Reynolds, T., Balakrishnan, H., 2012. Measurement of Gaseous HAP Emissions from Idling Aircraft as a Function of Engine and Ambient Conditions.

Herndon, S.C., Rogers, T., Dunlea, E.J., Jayne, J.T., Miake-Lye, R., Knighton, B., 2006. Hydrocarbon emissions from in-use commercial aircraft during airport operations. Environ. Sci. Technol. 40, 4406–13.

Holliday, K.M., Avery, C.L., Poole, C., McGraw, K., Williams, R., Liao, D., Smith, R.L., Whitsel, E. a, 2014. Estimating personal exposures from ambient air pollution measures: using meta-analysis to assess measurement error. Epidemiology 25, 35–43. doi:10.1097/EDE.0000000000000006

Holloway, T., Fiore, A., Hastings, M.G., 2003. Intercontinental transport of air pollution: Will emerging science lead to a new hemispheric treaty? Environ. Sci. Technol. 37, 4535–4542. doi:10.1021/es034031g

Houyoux, M.R., Vukovich, J.M., Jr., C.J.C., Wheeler, N.J.M., Kasibhatla, P.S., 2000. Emission inventory development and processing for the Seasonal Model for Regional Air Quality (SMRAQ) project. J. Geophys. Res. Atmos. 105, 9079–9090.

Hu, Y., Talat Odman, M., Russell, A.G., 2006. Mass conservation in the Community Multiscale Air Quality model. Atmos. Environ. 40, 1199–1204. doi:10.1016/j.atmosenv.2005.10.038

ICAO, 2016. ICAO CO2 Standard for New Aircraft.

Jacob, D.J., Logan, J.A., Murti, P.P., 1999. Effect of rising asian emissions on surface ozone in the united states. Geophys. Res. Lett. 26, 2175–2178.

Jacobson, M.Z., Wilkerson, J.T., Naiman, A.D., Lele, S.K., 2011. The effects of aircraft on climate and pollution. Part I: Numerical methods for treating the subgrid evolution of discrete size- and composition-resolved contrails from all commercial flights worldwide. J. Comput. Phys. 230, 5115–5132. doi:10.1016/j.jcp.2011.03.031

Jaegle, L., 2007. Pumping up surface air. Science. 315, 772–773. doi:10.1126/science.1138988

Jaffe, D., Anderson, T., Covert, D., Kotchenruther, R., Trost, B., Danielson, J., Simpson, W., Berntsen, T., Karlsdottir, S., Blake, D., Harris, J., Carmichael, G., Uno, I., 1999. Transport of Asian Air Pollution to North America. Geophys. Res. Lett. 26, 711–714.

Jiao, C., Flanner, M.G., 2016. Changing black carbon transport to the Arctic from present day to the end of 21st century. J. Geophys. Res. Atmos. 121, 4734–4750. doi:10.1002/2015JD023964

Kentarchos, A.S., Roelofs, G.J., 2002. Impact of aircraft NO x emissions on tropospheric ozone calculated with a chemistry-general circulation model : Sensitivity to higher hydrocarbon chemistry. J. Geophys. Res. 107, 1–12.

Klich, C.A., Fuelberg, H.E., 2014. The role of horizontal model resolution in assessing the transport of CO in a middle latitude cyclone using WRF-Chem. Atmos. Chem. Phys. 14, 609–627. doi:10.5194/acp-14-609-2014

Koch, D.M., Jacob, J., Graustein, C., 1996. Vertical transport of tropospheric aerosols as indicated by Be and Pb in a chemical tracer model. J. Geophys. Res. 101, 18651–18666.

Koo, J., Wang, Q., Henze, D.K., Waitz, I.A., Barrett, S.R.H., 2013. Spatial sensitivities of human health risk to intercontinental and high-altitude pollution. Atmos. Environ. 71, 140–147. doi:10.1016/j.atmosenv.2013.01.025

Lam, Y.F., Fu, J.S., 2009. A novel downscaling technique for the linkage of global and regional air quality modeling. Atmos. Chem. Phys. 9, 9169–9185.

Lamarque, J.-F., Emmons, Hess, P.G., Kinnison, D.E., Tilmes, S., Vitt, F., Heald, C.L., Holland, E.A., Lauritzen, P.H., Neu, J., Orlando, J.J., Rasch, P.J., Tyndall, G.K., 2012. CAM-chem : description and evaluation of interactive atmospheric chemistry in the Community Earth System Model. Geosci. Model Dev. 5, 369–411. doi:10.5194/gmd-5-369-2012

Land, C., Feichter, J., Sausen, R., 2002. Impact of vertical resolution on the transport of passive tracers in the ECHAM4 model. Tellus, Ser. B Chem. Phys. Meteorol. 54, 344–360. doi:10.1034/j.1600-0889.2002.201367.x

Laurent, A., Hauschild, M.Z., 2014. Impacts of NMVOC emissions on human health in European countries for 2000–2010: Use of sector-specific substance profiles. Atmos. Environ. 85, 247–255. doi:10.1016/j.atmosenv.2013.11.060

Lee, H., Olsen, S.C., Wuebbles, D.J., Youn, D., 2013. Impacts of aircraft emissions on the air quality near the ground. Atmos. Chem. Phys. 13, 5505–5522. doi:10.5194/acp-13-5505-2013

Leibensperger, E.M., Mickley, L.J., Jacob, D.J., Barrett, S.R.H., 2011. Intercontinental influence of NOx and CO emissions on particulate matter air quality. Atmos. Environ. 45, 3318–3324. doi:10.1016/j.atmosenv.2011.02.023

Levy, J.I., Hsu, H., Melly, S., 2008. High-Priority Compounds Associated with Aircraft Emissions.

Levy, J.I., Woody, M., Baek, B.H., Shankar, U., Arunachalam, S., 2012. Current and Future Particulate-Matter-Related Mortality Risks in the United States from Aviation Emissions During Landing and Takeoff. Risk Anal. 32, 237–249. doi:10.1111/j.1539-6924.2011.01660.x

Li, Y., Chang, J.S., 1996. A three-dimensional global episodic tracer transport model: 1. Evaluation of its transport processes by radon 222 simulations. J. Geophys. Res. 101, 25931–25947. doi:10.1029/96JD02209

Liang, Q., Douglass, A.R., Duncan, B.N., Stolarski, R.S., Witte, J.C., 2009. The governing processes and timescales of stratosphere-to-troposphere transport and its contribution to ozone in the Arctic troposphere. Atmos. Chem. Phys. 3011–3025.

Lim, S.S., Vos, T., Flaxman, A.D., Danaei, G., Shibuya, K., Adair-Rohani, H., Amann, M., Anderson, H.R., Andrews, K.G., Aryee, M., Atkinson, C., Bacchus, L.J., Bahalim, A.N., Balakrishnan, K., Balmes, J., Barker-Collo, S., Baxter, A., Bell, M.L., Blore, J.D., Blyth, F., Bonner, C., Borges, G., Bourne, R., Boussinesq, M., Brauer, M., Brooks, P., Bruce, N.G., Brunekreef, B., Bryan-Hancock, C., Bucello, C., Buchbinder, R., Bull, F., Burnett, R.T., Byers, T.E., Calabria, B., Carapetis, J., Carnahan, E., Chafe, Z., Charlson, F., Chen, H., Chen, J.S., Cheng, A.T.-A., Child, J.C., Cohen, A., Colson, K.E., Cowie, B.C., Darby, S., Darling, S., Davis, A., Degenhardt, L., Dentener, F., Des Jarlais, D.C., Devries, K., Dherani, M., Ding, E.L., Dorsey, E.R., Driscoll, T., Edmond, K., Ali, S.E., Engell, R.E., Erwin, P.J., Fahimi, S., Falder, G., Farzadfar, F., Ferrari, A., Finucane, M.M., Flaxman, S., Fowkes, F.G.R., Freedman, G., Freeman, M.K., Gakidou, E., Ghosh, S., Giovannucci, E., Gmel, G., Graham, K., Grainger, R., Grant, B., Gunnell, D., Gutierrez, H.R., Hall, W., Hoek, H.W., Hogan, A., Hosgood, H.D., Hoy, D., Hu, H., Hubbell, B.J., Hutchings, S.J., Ibeanusi, S.E., Jacklyn, G.L., Jasrasaria, R., Jonas, J.B., Kan, H., Kanis, J. a, Kassebaum, N., Kawakami, N., Khang, Y.-H., Khatibzadeh, S., Khoo, J.-P., Kok, C., Laden, F., Lalloo, R., Lan, Q., Lathlean, T., Leasher, J.L., Leigh, J., Li, Y., Lin, J.K., Lipshultz, S.E., London, S., Lozano, R., Lu, Y., Mak, J., Malekzadeh, R., Mallinger, L., Marcenes, W., March, L., Marks, R., Martin, R., McGale, P., McGrath, J., Mehta, S., Mensah, G. a, Merriman, T.R., Micha, R., Michaud, C., Mishra, V., Mohd Hanafiah, K., Mokdad, A. a, Morawska, L., Mozaffarian, D., Murphy, T., Naghavi, M., Neal, B., Nelson, P.K., Nolla, J.M., Norman, R., Olives, C., Omer, S.B., Orchard, J., Osborne, R., Ostro, B., Page, A., Pandey, K.D., Parry, C.D.H., Passmore, E., Patra, J., Pearce, N., Pelizzari, P.M., Petzold, M., Phillips, M.R., Pope, D., Pope, C.A., Powles, J., Rao, M., Razavi, H., Rehfuess, E. a, Rehm, J.T., Ritz, B., Rivara, F.P., Roberts, T., Robinson, C., Rodriguez-Portales, J. a, Romieu, I., Room, R., Rosenfeld, L.C., Roy, A., Rushton, L., Salomon, J. a, Sampson, U., Sanchez-Riera, L., Sanman, E., Sapkota, A., Seedat, S., Shi, P., Shield, K., Shivakoti, R., Singh, G.M., Sleet, D. a, Smith, E., Smith, K.R., Stapelberg, N.J.C., Steenland, K., Stöckl, H., Stovner, L.J., Straif, K., Straney, L., Thurston, G.D., Tran, J.H., Van Dingenen, R., van Donkelaar, A., Veerman, J.L., Vijayakumar, L., Weintraub, R., Weissman, M.M., White, R. a, Whiteford, H., Wiersma, S.T., Wilkinson, J.D., Williams, H.C., Williams, W., Wilson, N., Woolf, A.D., Yip, P., Zielinski, J.M., Lopez, A.D., Murray, C.J.L., Ezzati, M., AlMazroa, M. a, Memish, Z. a, 2012. A comparative risk assessment of burden of disease and injury attributable to 67 risk factors and risk factor clusters in 21 regions, 1990-2010: a systematic analysis for the Global Burden of Disease Study 2010. Lancet 380, 2224–60. doi:10.1016/S0140-6736(12)61766-8

Lin, C., Jacob, D.J., Munger, J.W., Fiore, A.M., 2000. Increasing background ozone in surface air over the United States. Geophys. Res. Lett. 27, 3465–3468. doi:10.1029/2000GL011762

Lin, J., Pan, D., Davis, S.J., Zhang, Q., He, K., Wang, C., Streets, D.G., Wuebbles, D.J., Guan, D., 2014. Chinas International trade and air pollution in US. PNAS 111, 1736–1741. doi:10.1073/pnas.1312860111

Lin, M., Fiore, A.M., Cooper, O.R., Horowitz, L.W., Langford, A.O., Levy, H., Johnson, B.J., Naik, V., Oltmans, S.J., Senff, C.J., 2012. Springtime high surface ozone events over the western United States: Quantifying the role of stratospheric intrusions. J. Geophys. Res. Atmos. 117, 1–20. doi:10.1029/2012JD018151

Lobo, P., Condevaux, J., Yu, Z., Kuhlmann, J., Hagen, D.E., Miake-Lye, R.C., Whitefield, P.D., Raper, D.W., 2016. Demonstration of a Regulatory Method for Aircraft Engine Nonvolatile PM Emissions Measurements with Conventional and Isoparaffinic Kerosene fuels. Energy & Fuels acs.energyfuels.6b01581. doi:10.1021/acs.energyfuels.6b01581

Luecken, D.J., Hutzell, W.T., Gipson, G.L., 2006. Development and analysis of air quality modeling simulations for hazardous air pollutants. Atmos. Environ. 40, 5087–5096. doi:10.1016/j.atmosenv.2005.12.044

Luecken, D.J., Hutzell, W.T., Strum, M.L., Pouliot, G.A., 2012. Regional sources of atmospheric formaldehyde and acetaldehyde, and implications for atmospheric modeling. Atmos. Environ. 47, 477–490. doi:10.1016/j.atmosenv.2011.10.005

Ma, P.L., Rasch, P.J., Fast, J.D., Easter, R.C., Gustafson, W.I., Liu, X., Ghan, S.J., Singh, B., 2014. Assessing the CAM5 physics suite in the WRF-Chem model: Implementation, resolution sensitivity, and a first evaluation for a regional case study. Geosci. Model Dev. 7, 755–778. doi:10.5194/gmd-7-755-2014

Ma, P.L., Rasch, P.J., Wang, M., Wang, H., Ghan, S.J., Easter, R.C., Gustafson, W.I., Liu, X., Zhang, Y., Ma H.-Y, 2015. How does increasing horizontal resolution in a global climate model improve the simulation of aerosol-cloud interactions? Geophys. Res. Lett. 42, 1–8. doi:10.1002/2015GL064183

Masiol, M., Harrison, R.M., 2014. Aircraft engine exhaust emissions and other airport-related contributions to ambient air pollution: A review. Atmos. Environ. 95, 409–455. doi:10.1016/j.atmosenv.2014.05.070

Mathur, R., Gilliam, R., Bullock Jr, O.R., Roselle, S., Pleim, J., Wong, D., Binkowski, F., Streets, D., 2012. Extending the applicability of the community multiscale air quality model to hemispheric scales: motivation, challenges, and progress, in: Air Pollution Modeling and Its Application XXI. pp. 175–179.

Mazaheri, M., Johnson, G.R., Morawska, L., 2009. Particle and gaseous emissions from commercial aircraft at each stage of the landing and takeoff cycle. Environ. Sci. Technol. 43, 441–6.

Mazraati, M., 2010. World aviation fuel demand outlook. OPEC Energy Rev. 34, 42–72. doi:10.1111/j.1753-0237.2010.00174.x

Morita, H., Yang, S., Unger, N., Kinney, P.L., 2014. Global health impacts of future aviation emissions under alternative control scenarios. Environ. Sci. Technol. 48, 14659–14667. doi:10.1021/es5055379

Nazelle, A. De, Arunachalam, S., Marc, S.L., 2010. Bayesian Maximum Entropy Integration of Ozone Observations and Model Predictions: An Application for Attainment Demonstration in North Carolina. Environ. Sci. Technol. 44, 5707–5713. doi:10.1021/es100228w

Nikoleris, T., Gupta, G., Kistler, M., 2011. Detailed estimation of fuel consumption and emissions during aircraft taxi operations at Dallas/Fort Worth International Airport. Transp. Res. Part D Transp. Environ. 16, 302–308. doi:10.1016/j.trd.2011.01.007

Olsen, S.C., Wuebbles, D.J., Owen, B., 2013. Comparison of global 3-D aviation emissions datasets. Atmos. Chem. Phys. 13, 429–441. doi:10.5194/acp-13-429-2013

Ott, L.E., Pickering, K.E., Stenchikov, G.L., Allen, D.J., DeCaria, A.J., Ridley, B., Lin, R.F., Lang, S., Tao, W.K., 2010. Production of lightning NOx and its vertical distribution calculated from three-dimensional cloud-scale chemical transport model simulations. J. Geophys. Res. Atmos. 115, 1–19. doi:10.1029/2009JD011880

Parrish, D.D., Aikin, K.C., Oltmans, S.J., Johnson, B.J., Ives, M., Sweeny, C., 2010. Impact of transported background ozone inflow on summertime air quality in a California ozone exceedance area. Atmos. Chem. Phys. 10, 10093–10109. doi:10.5194/acp-10-10093-2010

Parrish, D.D., Dunlea, E.J., Atlas, E.L., Schauffler, S., Donnelly, S., Stroud, V., Goldstein, A.H., Millet, D.B., McKay, M., Jaffe, D.A., Price, H.U., Hess, P.G., Flocke, F., Roberts, J.M., 2004. Changes in the photochemical environment of the temperate North Pacific troposphere in response to increased Asian emissions. J. Geophys. Res. 109, D23S18. doi:10.1029/2004JD004978

Pickering, K.E., Wang, Y., Tao, W.-K., Price, C., Müller, J.-F., 1993. Vertical distributions of lightning NO_x for use in regional and global chemical transport models. J. Geophys. Res. 103, 31203–31216. doi:10.1029/98JD02651

Pleim, J.E., 2007a. A Combined Local and Nonlocal Closure Model for the Atmospheric Boundary Layer. Part I: Model Description and Testing. J. Appl. Meteorol. Climatol. 46, 1383–1395. doi:10.1175/JAM2539.1

Pleim, J.E., 2007b. A Combined Local and Nonlocal Closure Model for the Atmospheric Boundary Layer. Part II: Application and Evaluation in a Mesoscale Meteorological Model. J. Appl. Meteorol. Climatol. 46, 1396–1409. doi:10.1175/JAM2534.1

Ratliff, G., Sequeira, C., Waitz, I., Ohsfeldt, M., Michael, T.T., Thompson, G.T., 2009. Aircraft Impacts on Local and Regional Air Quality in the United States.

Rauscher, S.A., Coppola, E., Piani, C., Giorgi, F., 2010. Resolution effects on regional climate model simulations of seasonal precipitation over Europe. Clim. Dyn. 35, 685–711. doi:10.1007/s00382-009-0607-7

Reidmiller, D.R., Fiore, A.M., Jaffe, D.A., Bergmann, D., Cuvelier, C., Dentener, F.J., Duncan, B.N., Folberth, G., Gauss, M., Gong, S., Hess, P., Jonson, J.E., Keating, T., Lupu, A., Marmer, E., Park, R., Schultz, M.G., Shindell, D.T., Szopa, S., Vivanco, M.G., Wild, O., Zuber, A., 2009. The influence of foreign vs. North American emissions on surface ozone in the US. Atmos. Chem. Phys. 9, 5027–5042. doi:10.5194/acp-9-5027-2009

Rienecker, M.M., Suarez, M.J., Gelaro, R., Todling, R., Bacmeister, J., Liu, E., Bosilovich, M.G., Schubert, S.D., Takacs, L., Kim, G.K., Bloom, S., Chen, J., Collins, D., Conaty, A., Da Silva, A., Gu, W., Joiner, J., Koster, R.D., Lucchesi, R., Molod, A., Owens, T., Pawson, S., Pegion, P., Redder, C.R., Reichle, R., Robertson, F.R., Ruddick, A.G., Sienkiewicz, M., Woollen, J., 2011. MERRA: NASA's modern-era retrospective analysis for research and applications. J. Clim. 24, 3624–3648. doi:10.1175/JCLI-D-11-00015.1

Roof, C., Hansen, A., Fleming, G., Thrasher, T., Nguyen, A., Hall, C., Dinges, E., Bea, R., Grandi, F., Kim, B., Usdrowski, S., Hollingsworth, P., 2007. Aviation Environmental Design Tool (AEDT).

Runde, T., Dameris, M., Garny, H., Kinnison, D., 2016. Classification of stratospheric extreme events according to their downward propagation to the troposphere. Geophys. Res. Lett. 1–8. doi:10.1002/2016GL069569

Sarwar, G., Appel, K.W., Carlton, A.G., Mathur, R., Schere, K., Zhang, R., Majeed, M.A., 2011. Impact of a new condensed toluene mechanism on air quality model predictions in the US. Geosci. Model Dev. 4, 183–193. doi:10.5194/gmd-4-183-2011

Sarwar, G., Simon, H., Xing, J., Mathur, R., 2014. Importance of tropospheric ClNO2 chemistry across the Northern Hemisphere. Geophys. Res. Lett. 41, 4050–4058. doi:10.1002/2014GL059962

Schäfer, A.W., Waitz, I. a., 2014. Air transportation and the environment. Transp. Policy 1–4. doi:10.1016/j.tranpol.2014.02.012

Schoeberl, M.R., Morris, G.A., 2000. A Lagrangian simulation of supersonic and subsonic aircraft exhaust emissions. J. Geophys. Res. 105, 11833–11839.

Schumann, U., 1997. The impact of nitrogen oxides emissions from aircraft upon the atmosphere at flight altitudes - Results from the AERONOX project. Atmos. Environ. 31, 1723–1733.

Schürmann, G., Schäfer, K., Jahn, C., Hoffmann, H., Bauerfeind, M., Fleuti, E., Rappenglück, B., 2007. The impact of NOx, CO and VOC emissions on the air quality of Zurich airport. Atmos. Environ. 41, 103–118. doi:10.1016/j.atmosenv.2006.07.030

Seaman, V.Y., Bennett, D.H., Cahill, T.M., 2009. Indoor acrolein emission and decay rates resulting from domestic cooking events. Atmos. Environ. 43, 6199–6204. doi:10.1016/j.atmosenv.2009.08.043

Simon, H., Beck, L., Bhave, P. V, Divita, F., Hsu, Y., Luecken, D., Mobley, J.D., Pouliot, G.A., Reff, A., Sarwar, G., Strum, M., 2010. The development and uses of EPA's SPECIATE database. Atmos. Pollut. Res. 1, 196–206. doi:10.5094/apr.2010.026

Singh, H.B., Brune, W.H., Crawford, J.H., Jacob, D.J., Russell, P.B., 2006. Overview of the summer 2004 Intercontinental Chemical Transport Experiment-North America (INTEX-A). J. Geophys. Res. Atmos. 111. doi:10.1029/2006JD007905

Skamarock, W.C., Klemp, J.B., Dudhi, J., Gill, D.O., Barker, D.M., Duda, M.G., Huang, X.-Y., Wang, W., Powers, J.G., 2008. A Description of the Advanced Research WRF Version 3. Tech. Rep. 113. doi:10.5065/D6DZ069T

Speth, R.L., Rojo, C., Malina, R., Barrett, S.R.H., 2015. Black carbon emissions reductions from combustion of alternative jet fuels. Atmos. Environ. 105, 37–42. doi:10.1016/j.atmosenv.2015.01.040

Spicer, C.W., Buxton, B.E., Holdren, M.W., Smith, D.L., Kelly, T.J., Rust, S.W., Pate, A.D., Sverdrup, G.M., Chuang, J.C., 1996. Variability of hazardous air pollutants in an urban area. Atmos. Environ. 30, 3443–3456. doi:Doi 10.1016/1352-2310(95)00200-6

Stettler, M.E.J., Eastham, S., Barrett, S.R.H., 2011. Air quality and public health impacts of UK airports. Part I: Emissions. Atmos. Environ. 45, 5415–5424. doi:10.1016/j.atmosenv.2011.07.012

Stohl, A., Eckhardt, S., Forster, C., James, P., Spichtinger, N., 2002. On the pathways and timescales of intercontinental air pollution transport. J. Geophys. Res. 107, 4684. doi:10.1029/2001JD001396

Tang, W., Cohan, D.S., Morris, G. a., Byun, D.W., Luke, W.T., 2011. Influence of vertical mixing uncertainties on ozone simulation in CMAQ. Atmos. Environ. 45, 2898–2909. doi:10.1016/j.atmosenv.2011.01.057

Tarrason, L., Jonson, J.E., Berntsen, T.K., Rypdal, K., 2002. Study on air quality impacts of non-LTO emissions from aviation.

Thouret, V., Cammas, J.-P., Sauvage, B., Athier, G., Zbinden, R., Nédélec, P., Simon, P., Karcher, F., 2005. Tropopause referenced ozone climatology and inter-annual variability (1994–2003) from the MOZAIC programme. Atmos. Chem. Phys. 6, 1033–1051. doi:10.5194/acp-6-1033-2006

Timko, M.T., Herndon, S.C., Wood, E.C., Onasch, T.B., Northway, M.J., J.T, J., Canagaratna, M.R., Miake-Lye, R.C., 2010. Gas Turbine Engine Emissions – Part I: Volatile Organic Compounds and Nitrogen Oxides. J. Eng. Gas Turbines Power 132. doi:doi:10.1115/1.4000131

Toohey, D., McConnell, J., Avallone, L., Evans, W., 2010. Aviation and Chemistry and Transport Processes in the Upper Troposphere and Lower Stratosphere. Bull. Am. Meteorol. Soc. 91, 485–490. doi:10.1175/2009BAMS2841.1

Turgut, E.T., Rosen, M.A., 2010. Assessment of emissions at busy airports. Int. J. Energy Res. 34, 800–814. doi:10.1002/er

U.S EPA, 2016. Finding That Greenhouse Gas Emissions From Aircraft Cause or Contribute to Air Pollution That May Reasonably Be Anticipated To Endanger Public Health and Welfare; Final Rule.

U.S EPA, 2007. 2005 National Emission Inventory.

Unal, A., Hu, Y., Chang, M.E., Talat Odman, M., Russell, A.G., 2005. Airport related emissions and impacts on air quality: Application to the Atlanta International Airport. Atmos. Environ. 39, 5787–5798. doi:10.1016/j.atmosenv.2005.05.051

US EPA, 2014. EPA sets Tier 3 Motor Vehicle Emission and Fuel Standards.

US EPA, 2011. An Overview of Methods for EPA's National-Scale Air Toxics Assessment.

US EPA, 2009. Technical Assistance Document for the National Air Toxics Trends Stations Program.

US EPA, 2007. 2005 National Emission Inventory.

Van Velthoven, P.F.J., Sausen, R., Johnson, C.E., Kelder, H., Köhler, I., Kraus, A.B., Ramaroson, R., Rohrer, F., Stevenson, D., Strand, A., Wauben, W.M.F., 1997. The passive transport of NO(x) emissions from aircraft studied with a hierarchy of models. Atmos. Environ. 31, 1783–1799. doi:10.1016/S1352-2310(96)00330-5

Vennam, L.P., Vizuete, W., Arunachalam, S., 2015. Evaluation of model-predicted hazardous air pollutants (HAPs) near a mid-sized U.S. airport. Atmos. Environ. 119, 107–117. doi:10.1016/j.atmosenv.2015.08.015

Wang, H., Rasch, P., Easter, R., Singh, B., Zhang, R., Ma, P.-L., Qian, Y., Ghan, S., Beagley, N., 2014. Using an explicit emission tagging method in global modeling of source-receptor relationships for black carbon in the Arctic: Variations, sources, and transport pathways. J. Geophys. Res. Atmos. 119, 1–22. doi:10.1002/2014JD022297

Wasiuk, D.K., Khan, M.A.H., Shallcross, D.E., Lowenberg, M.H., 2016. A commercial aircraft fuel burn and emissions inventory for 2005-2011. Atmosphere (Basel). 7, 1–14. doi:10.3390/atmos7060078

Wauben, W.M.F., Velthoven, P.F.J.V., Kelder, H., 1997. A 3D chemistry transport model study of changes in atmospheric ozone due to aircraft NOx emissions. Atmos. Environ. 31, 1819–1836. doi:10.1016/S1352-2310(96)00332-9

Wayson, R. L., Fleming, G. G., and Iovinelli, R., 2009. Methodology to estimate particulate matter emissions from certified commercial aircraft engines. J. Air Waste Manage. Assoc. 59, 91–100.

West, J.J., Naik, V., Horowitz, L.W., Fiore, A.M., 2009. Effect of regional precursor emission controls on long-range ozone transport – Part 2: steady-state changes in ozone air quality and impacts on human mortality. Atmos. Chem. Phys. 9, 6095–6107. doi:10.5194/acp-9-6095-2009

Whitt, D.B., Jacobson, M.Z., Wilkerson, J.T., Naiman, A.D., Lele, S.K., 2011. Vertical mixing of commercial aviation emissions from cruise altitude to the surface. J. Geophys. Res. 116, D14109. doi:10.1029/2010JD015532

Whitten, G.Z., Heo, G., Kimura, Y., McDonald-Buller, E., Allen, D.T., Carter, W.P.L., Yarwood, G., 2010. A new condensed toluene mechanism for Carbon Bond: CB05-TU. Atmos. Environ. 44, 5346–5355. doi:10.1016/j.atmosenv.2009.12.029

Wild, O., Akimoto, H., 2001. Intercontinental transport of ozone and its precursors in a three-dimensional global CTM. J. Geophys. Res. 106, 27,729-27,744.

Wilkerson, J.T., Jacobson, M.Z., Malwitz, a., Balasubramanian, S., Wayson, R., Fleming, G., Naiman, a. D., Lele, S.K., 2010. Analysis of emission data from global commercial aviation: 2004 and 2006. Atmos. Chem. Phys. 10, 6391–6408. doi:10.5194/acp-10-6391-2010

Wood, E., Herndon, S., Miake-Lye, R., Nelson, D., Seeley, M., 2008. Aircraft and Airport-Related Hazardous Air Pollutants: Research Needs and Analysis.

Wood, E.C., Herndon, S.C., Timko, M.T., Yelvington, P.E., Miake-Lye, R.C., 2008. Speciation and chemical evolution of nitrogen oxides in aircraft exhaust near airports. Environ. Sci. Technol. 42, 1884–1891. doi:10.1021/es072050a

Woody, M., Haeng Baek, B., Adelman, Z., Omary, M., Fat Lam, Y., Jason West, J., Arunachalam, S., 2011. An assessment of Aviation's contribution to current and future fine particulate matter in the United States. Atmos. Environ. 45, 3424–3433. doi:10.1016/j.atmosenv.2011.03.041

Xing, J., Mathur, R., Pleim, J., Hogrefe, C., Gan, C.-M., Wong, D.C., Wei, C., Gilliam, R., Pouliot, G., 2015. Observations and modeling of air quality trends over 1990–2010 across the Northern Hemisphere: China, the United States and Europe. Atmos. Chem. Phys. 15, 2723–2747. doi:10.5194/acp-15-2723-2015

Xing, J., Mathur, R., Pleim, J., Hogrefe, C., Wang, J., Gan, C.-M., Sarwar, G., Wong, D.C., McKeen, S., 2016. Representing the effects of stratosphere-troposphere exchange on 3-D O3 distributions in chemistry transport models using a potential vorticity based parameterization. Atmos. Chem. Phys. 16, 10865–10877. doi:10.5194/acp-16-10865-2016

Yan, Y., Lin, J., Chen, J., Hu, L., 2016. Improved simulation of tropospheric ozone by a global-multi-regional two-way coupling model system. Atmos. Chem. Phys. 16, 2381–2400. doi:10.5194/acp-16-2381-2016

Yang, H., Chen, G., Tang, Q., Hess, P., 2016. Quantifying isentropic stratosphere-troposphere exchange of ozone. J. Geophys. Res. Atmos. 1–16. doi:10.1002/2015JD024180

Yarwood, G., Rao, S., Yocke, M., Whitten, G.Z., 2005. Updates to the Carbob Bond Chemical Mechanism:CB05.

Yim, S.H.L., Lee, G.L., Lee, I.H., Allroggen, F., Ashok, A., Caiazzo, F., Eastham, S.D., Malina, R., Barrett, S.R.H., 2015a. Global, regional and local health impacts of civil aviation emissions. Environ. Res. Lett. 10, 34001. doi:10.1088/1748-9326/10/3/034001

Yim, S.H.L., Lee, G.L., Lee, I.H., Allroggen, F., Ashok, A., Caiazzo, F., Eastham, S.D., Malina, R., Barrett, S.R.H., 2015b. Global, regional and local health impacts of civil aviation emissions. Environ. Res. Lett. 10, 34001. doi:10.1088/1748-9326/10/3/034001

Zhu, Y., Fanning, E., Yu, R.C., Zhang, Q., Froines, J.R., 2011. Aircraft emissions and local air quality impacts from takeoff activities at a large International Airport. Atmos. Environ. 45, 6526–6533. doi:10.1016/j.atmosenv.2011.08.062

Zyryanov, D., Foret, G., Eremenko, M., Beekmann, M., Cammas, J.P., D'Isidoro, M., Elbern, H., Flemming, J., Friese, E., Kioutsioutkis, I., Maurizi, A., Melas, D., Meleux, F., Menut, L., Moinat, P., Peuch, V.H., Poupkou, A., Razinger, M., Schultz, M., Stein, O., Suttie, A.M., Valdebenito, A., Zerefos, C., Dufour, G., Bergametti, G., Flaud, J.M., 2012. 3-D evaluation of tropospheric ozone simulations by an ensemble of regional Chemistry Transport Model. Atmos. Chem. Phys. 12, 3219–3240. doi:10.5194/acp-12-3219-2012